AD-A046 010 PENNSYLVANIA STATE UNIV UNIVERSITY PARK MATERIALS RE--ETC F/G 9/1
CERAMIC PIEZOELECTRIC TRANSDUCERS.(U)
JUL 77 L E CROSS, J V BIGGERS, R E NEWNHAM N00014-76-C-0515

UNCLASSIFIED NL

1 OF 2
ADA 046010

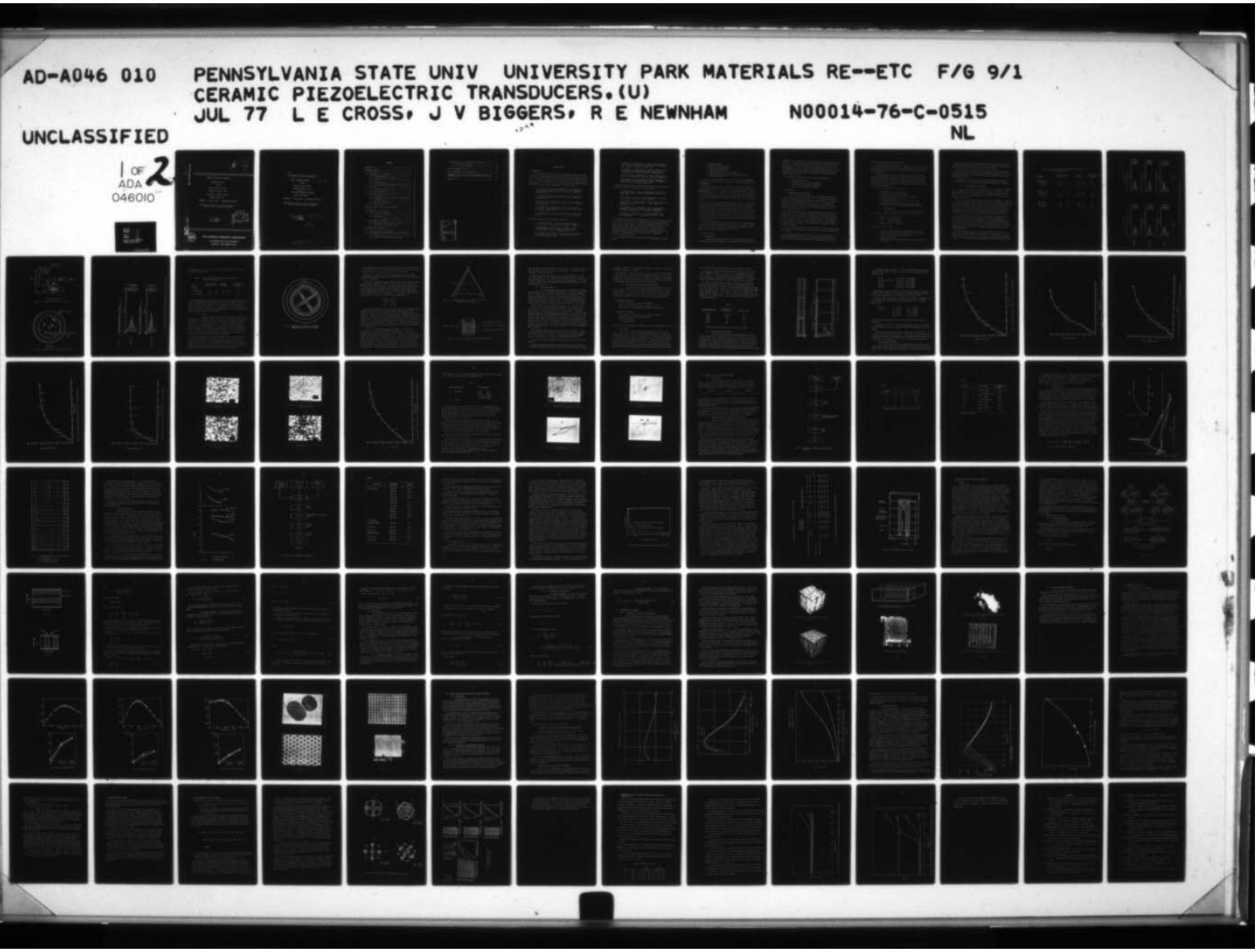

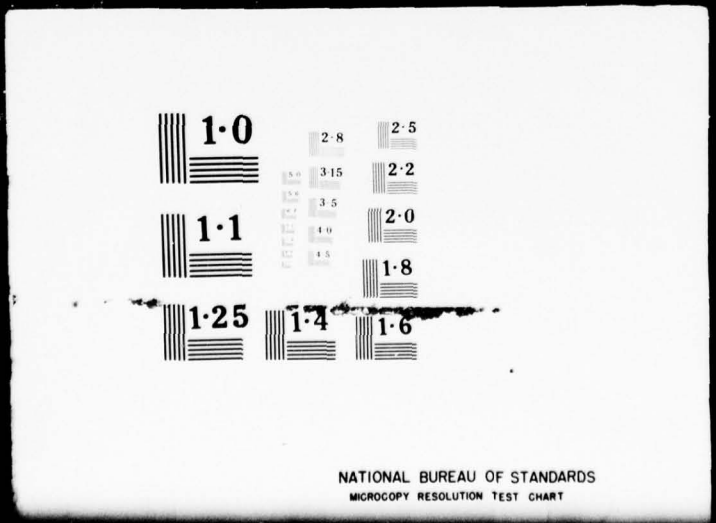

CERAMIC PIEZOELECTRIC TRANSDUCERS

Semi-Annual Report

to the

Office of Naval Research

Arlington, Virginia 22217

Contract No. N00014-76-C-0515

January to July 1977

APPROVED FOR PUBLIC RELEASE: DISTRIBUTION UNLIMITED

L. E. Cross
J. V. Biggers
R. E. Newnham

THE MATERIALS RESEARCH LABORATORY

THE PENNSYLVANIA STATE UNIVERSITY

UNIVERSITY PARK, PENNSYLVANIA

(6) CERAMIC PIEZOELECTRIC TRANSDUCERS.

(9) Semi-Annual Report. Jan - Jul 77

to the

Office of Naval Research

Arlington, Virginia 22217

Contract No. (15) N00014-76-C-0515

January to July 1977

APPROVED FOR PUBLIC RELEASE: DISTRIBUTION UNLIMITED

(10) L. E./Cross
J. V./Biggers
R. E./Newnham

(11) Jul 77

(12) 97p.

220 750

AB

CONTENTS

PROGRESS REPORT

1. INTRODUCTION

The present studies under this contract on piezoelectric ceramics have been in progress since January 1976 and have been running at full strength since March 1976. Progress up to December 1976 was described in the annual report No. N00014-76-C-0515. The present document is a semi-annual report covering progress up to and including July 1977. Over this period, work upon the contract has contributed substantially to the following presentations at scientific meetings.

L. E. Cross, H. A. McKinstry. A Computer Graphic Presentation of the Polarization Surfaces of Constant Elastic Gibbs Free Energy in Perovskite Type Ferroelectrics. Amer. Ceram. Soc. Meeting, Chicago, May 1977.

R. E. Newnham, J. Kramer, A. SaNeto and T. Cline. Second Harmonic Generation by Ceramic Materials. Amer. Ceram. Soc. Meeting, Chicago, May 1977.

W. A. Schulze, J. V. Biggers and L. E. Cross. Aging of Dielectric Dispersion in PLZT Relaxor Ceramics. Amer. Ceram. Soc. Meeting, Chicago, May 1977.

D. A. Skinner, R. E. Newnham and L. E. Cross. Dielectric and Piezoelectric Studies on Layer Structure Titanates. Amer. Ceram. Soc. Meeting, Chicago, May 1977.

R. C. Pohanka and L. E. Cross. Inorganic Glass and Glass Ceramic Ferroelectric Dielectrics. Amer. Ceram. Soc. Meeting, Chicago, May 1977.

The following papers have been accepted for presentation.

L. E. Cross and A. Bhalla. Domain Decoration in $Gd_2(MoO_4)_3$. Intl. Meeting on Ferroelectrics, IMF4, Leningrad, September 1977.

S. Venkataramani, L. J. Tarhay and J. V. Biggers. Role of Chemically Prepared ZrO_2 on the Properties of PZT Ceramics. Fall Meeting Amer. Ceram. Soc., Montreal, September 1977.

K. A. Klicker and J. V. Biggers. Control of the Lead Atmosphere During Sintering of PZT Ceramics. Fall Meeting Amer. Ceram. Soc., Montreal, September 1977.

T. Shrout, W. A. Schulze and J. V. Biggers. Processing Effects on the Microstructure of Tape Cast PZT Ceramics. Fall Meeting Amer. Ceram. Soc., Montreal, September 1977.

D. L. Hankey, L. J. Tarhay and J. V. Biggers. Commercial Powder Characteristics of ZrO_2 and Their Effects on PZT Processing. Fall Meeting Amer. Ceram. Soc., Montreal, September 1977.

D. P. Skinner, R. E. Newnham and L. E. Cross. Diphasic Transducers. Fall Meeting Amer. Ceram. Soc., Montreal, September 1977.

W. A. Schulze, L. E. Cross and W. R. Buessem. Degradation of $BaTiO_3$ Ceramics Under High AC Electric Fields. Fall Meeting Amer. Ceram. Soc., Montreal, September 1977.

The following papers published or submitted for publication over the contract period have received partial support from contract funds.

A. S. Bhalla and L. E. Cross. A Simple Technique for Decorating Ferroelectric Domains in Gadolinium Molybdate. J. Mat. Sci. Sept. 1977

S. T. Liu and L. E. Cross. Primary Pyroelectricity in Strontium Barium Niobate. Phys. Stat. Sol. 41, K83,1977.

W. A. Schulze, J. V. Biggers and L. E. Cross. Aging of Dielectric Dispersion in PLZT Relaxor Ceramics. J. Amer. Ceram. Soc. Accepted, July 1977.

P. J. Cressman, L. B. Schein and L. E. Cross. Electrostatic Measurements of Primary, Secondary and Tertiary Pyroelectricity in Partially Clamped $LiNbO_3$. J. Appl. Phys. Submitted.

T. Cline, L. E. Cross and S. T. Liu. Dielectric Behavior of Strontium Barium Niobate ($Sr_{0.5}Ba_{0.5}Nb_2O_6$) Crystals. J. Appl. Phys. Submitted.

It is evident from the papers being presented that a number of the topics initiated in 1976 are now bearing fruit. In the published output, because of the longer time constants we expect the major output to being towards the end of this year. However, several highly productive joint studies with Honeywell Research Center and Xerox Central Laboratories upon topics of close relevance to our program objectives have been completed and are now published or in process of publication. These perhaps provide some measure of the excellent cooperation and high interest from industry.

The studies which will be reported here fall effectively under six topical titles:

1. Processing Studies
2. Diphasic Transducer Structures
3. Electrostriction Transducers
4. Poling and Property Studies
5. Basic Phenomenology for PZT Perovskites
6. Fundamental Studies of Amorphous and Micro-crystalline High T_c Ferroelectrics

It should be stressed, however, that these are not separate independent studies, but, as we hope to show in this report, are closely interconnected and interdependent.

Underpinning the whole effort to prepare new combinations of materials in closely interconnected microstructures is the basic work on ceramic processing. ~~We believe that~~ this work can contribute to a better understanding, and thus to better reproducibility of conventional PZT bodies, but its major thrust must be to provide the foundation of electroceramic competence necessary for processing the more sophisticated diphasic systems which are the major hope for significant advance.

Significant progress has been made particularly in the tape casting studies and a number of the lamellar heterogeneous structures originally proposed have now been successfully fabricated. Also in the diphasic area a theoretical evaluation of the bounds of possible piezoelectric and pyroelectric properties which could be achieved for some of the simpler types of connectivity in linear elasto-electric materials has been accomplished. This is an essential first step toward the more general consideration of non-linear ferroic systems, where 'self-bias prestressing' may be further exploited to modify possible properties in connected systems.

A major advance has been the successful fabrication of three-dimensionally connected ceramic:plastic structures which can be poled to saturation remanence, then partially crushed to give highly flexible bodies with excellent piezoelectric g-coefficients and high hydrostatic sensitivity.

2. PROCESSING STUDIES

2.1. Introduction

There has been considerable work in the past two decades upon the preparation and processing of piezoelectric ceramics; however, in many cases the

reproducibility still leaves much to be desired and there are obvious unanswered questions. The experimental work described in this section of the report has been designed in part to provide additional information to help answer some of these questions. We believe, however, that the more important goal is to allow us to develop the expertise in processing PZT and related systems necessary to fabricate the more complex multiphase systems which are the major emphasis of the whole contract effort.

In this section, the work which is in progress on the topics of:

1. The reactivity of ZrO_2
2. Preparation of high surface area powders
3. Tape casting of piezoelectric formulations
4. Hot isostatic pressing of piezoceramics

will be discussed.

2.2. The Reactivity of ZrO_2 Powders

Among the more important factors which are believed to contribute to the variation in properties of PZT ceramics are: raw material characteristics (composition and particle morphology), material mixing, calcining conditions, and control of the PbO atmosphere during firing (1-3). It is frequently suggested, both in the US and by off-shore suppliers, that variations in the commercial ZrO_2 powders are a major cause of inconsistent results in the properties of finished ceramics (4,5).

Whilst much proprietary work has clearly been done on the characterization of ZrO_2 powders and on the influence the powders have upon processing, there appears to be no general consensus as to the nature of the difference between the so-called 'good' and 'bad' lots of ZrO_2 which are referred to. Rosolowskii et al. (6) have found as much as 1.3 wt% of unreacted ZrO_2 in a 'good' commercial PZT powder, which they attribute to hard agglomerates in the original powders which remain unreacted.

It is our feeling also that some of the differences in ZrO_2 are indeed related to the agglomerate nature, which will effect reactivity both during calcining and on final firing.

In the work described here we will attempt to show that the differences in the nature of agglomeration in ZrO_2 is a significant cause of variability and further, that by the construction and use of 'calcining diagrams' much of the

variability can be reduced in final properties.

The ZrO_2 problem has provided us with a valuable entry point for our processing studies and the opportunity to develop 'standardized' processing techniques which permit proper evaluation of the alternative processing methods required for the newer systems.

The general experimental plan is to produce a number of sets of ceramic discs for microstructural and property evaluations. Each set is being produced using identical processing with regard to oxide mixing, pressing, calcining, firing and poling. The variables in the experiment are the sources of ZrO_2 powder and the different pre-treatments of these powders which have been introduced to break-up agglomerates.

The following specific areas will be described:

1. Characterization of commercial ZrO_2
2. Pre-treatment to break-up agglomerates
3. Calcining studies to follow the reactions occurring between the mixed oxides
4. Firing studies which will enable us to produce dense, stoichiometric ceramics
5. Microstructural and piezoelectric evaluation of ceramics produced from different ZrO_2 sources and process variations

2.2.1. Characterization

Commercial ZrO_2 powders chosen for the study include lots characterized as 'good' and 'bad' by industrial users (4). They are:

1. Harshaw: Lots #5-76 and #1-75
2. Tizon: Lots #367 and #317
3. Tam: Type 7, Lot #3009
4. Magnesium Electron: Lot #10522

Characterization plans include:

1. Optical emission spectrographic determination of impurities
2. Wet chemical analysis and x-ray diffraction for major elements
3. Particle size and shape using automated SEM
4. Surface areas using BET
5. Surface composition using Auger (AES) and Ion scattering spectroscopy (ISS).

Most of the particle characterization work has not been assigned high priority and to date only the surface area and particle size measurements have been made. Some typical results are shown in Table 1 and Figures 1 and 2.

The AES and ISS work has been started but charging difficulties associated with the non-conductive ZrO_2 powders have precluded generation of any useful data. Experimental techniques - gold grid and mixing of gold powders with ZrO_2 - are being tried at present.

The major effort on characterization will be made after our experimental work on evaluation of microstructure and piezoelectric properties is completed.

2.2.2. Pre-Treatment of ZrO_2 Powders

Assuming that some of the disparity in ZrO_2 behavior is attributable to agglomerates formed during processing (calcining) by the supplier, two deagglomeration techniques have been chosen in an attempt to modify this characteristic. The first is high energy milling using a 4" jet mill (Fluid Energy Products Co., Hatfield, Pa.).

Figures 3 and 4 show schematic diagrams of the jet mill operation. In principle, high velocity manifold air keeps the largest particles near the outside of the mill causing particle-particle impact. Fine particles migrate to the center of the mill and exit with the effluent air stream into a cloth filter bag. The fineness of the product is controlled by the manifold pressure and feed rate of the material. A comparatively narrow size range can be obtained with minimal contamination. Some of the data given in Table 1 and Figures 1 and 2 is from jet milled ZrO_2.

From the average particle size as well as the particle distribution data it appears that jet milling effectively reduces the larger sizes (agglomerates). The surface area data confirms this assumption. If the agglomerates were actually single crystallite particles there would be a dramatic increase in surface area. However, since the agglomerates are made up of many smaller particles, surface area as measured by the BET technique is not greatly increased even if they are completely broken apart.

Additional support of this theory is derived from jet milling results on a commercially calcined PZT powder, Ultrasonics 501A. Size reduction of the larger classes (see Figure 5 and Table 2) was associated with a near three-fold increase in surface area. Assuming that these larger particles are initially typical single

Table 1. Data on ZrO_2 Powders From Automated SEM Image Analysis and Surface Area Analysis.

ZrO_2 Sample:	Average Diameter Mean (m)	σ	Min/Max Mean (m)	σ	Surface Area (BET) (m^2/gm)
Harshaw Lot 5-76					
As-Received	0.80	0.5	0.44	0.18	14.6
3 Jet Mills	0.69	0.4	0.51	0.17	15.5
Harshaw Lot 1-75					
As-Received	0.72	0.5	0.53	0.17	13.5
3 Jet Mills	0.62	0.3	0.49	0.17	14.6
TIZON 367m					
As-Received	0.69	0.5	0.47	0.17	18.4
3 Jet Mills	0.59	0.5	0.50	0.18	18.7

As Received

AVERAGE DIAMETER DISTRIBUTION (# PERCENT)

Harshaw Lot 5-76

CLASS LIMIT	CLASS X	NO.
0.10	0.00	0
0.16	0.06	5
0.25	3.01	58
0.40	14.02	270
0.63	27.67	533
1.00	32.19	620
1.60	16.51	318
2.50	4.83	93
4.00	1.04	20
6.30	0.47	9

AVERAGE DIAMETER DISTRIBUTION (# PERCENT)

Harshaw Lot 1-75

CLASS LIMIT	CLASS X	NO.
0.10	0.00	0
0.16	0.09	2
0.25	3.31	74
0.40	16.35	365
0.63	38.24	854
1.00	26.02	581
1.60	10.39	232
2.50	4.08	91
4.00	1.25	28
6.30	0.22	5
10.00	0.04	1

AVERAGE DIAMETER DISTRIBUTION (# PERCENT)

Tizon 367 m

CLASS LIMIT	CLASS X	NO.
0.10	0.00	0
0.16	0.39	8
0.25	6.49	133
0.40	21.62	440
0.63	28.75	585
1.00	26.68	543
1.60	11.89	242
2.50	2.65	54
4.00	1.18	24
6.30	0.29	6
10.00	0.05	1

Figure 1

Three Jet Mills

AVERAGE DIAMETER DISTRIBUTION (# PERCENT)

CLASS LIMIT	CLASS X	NO.
0.10	0.00	0
0.16	0.10	2
0.25	4.31	85
0.40	18.24	360
0.63	32.88	649
1.00	25.53	504
1.60	15.55	307
2.50	3.24	64
4.00	0.15	3

AVERAGE DIAMETER DISTRIBUTION (# PERCENT)

CLASS LIMIT	CLASS X	NO.
0.10	0.00	0
0.16	0.24	5
0.25	4.18	88
0.40	20.02	421
0.63	36.04	758
1.00	29.01	610
1.60	9.56	201
2.50	0.95	20

AVERAGE DIAMETER DISTRIBUTION (# PERCENT)

CLASS LIMIT	CLASS X	NO.
0.10	0.00	0
0.16	0.77	15
0.25	8.78	172
0.40	28.78	564
0.63	33.27	652
1.00	17.70	347
1.60	7.50	147
2.50	2.24	44
4.00	0.56	11
6.30	0.31	6
10.00	0.10	2

Figure 2

Particle size distributions from automated SEM image analysis.

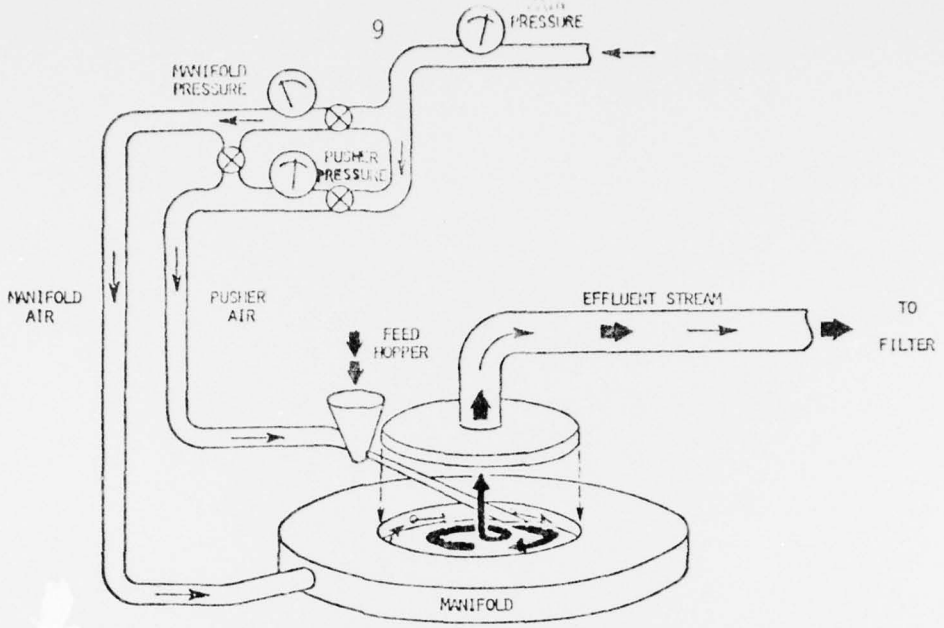

Figure 3. Representation of air flow in jet mill

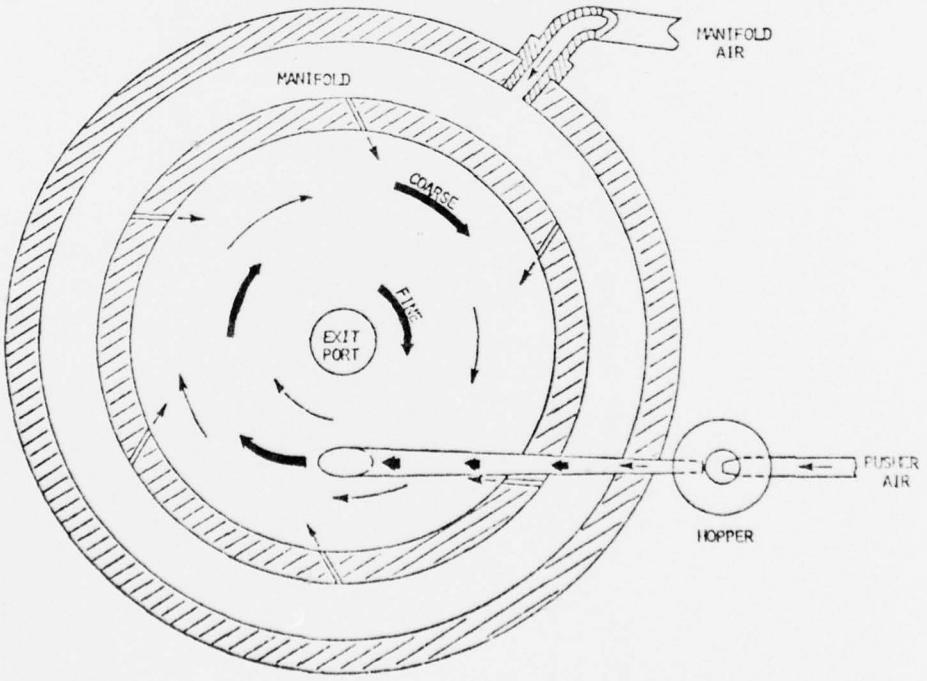

Figure 4. Horizontal cross-section of mill chamber

PZT 501A

AVERAGE DIAMETER DISTRIBUTION (# PERCENT)

As Received

CLASS LIMIT	CLASS % 0 1 2 3 4 5 6 7 8 9 10	CLASS %	NO.
0.25	[	0.00	0
0.40	[	0.26	7
0.63	[**	4.64	127
1.00	[**********	20.77	569
1.60	[******************	34.32	940
2.50	[************	24.97	684
4.00	[******	11.65	319
6.30	[*	2.92	80
10.00	[	0.47	13

AVERAGE DIAMETER DISTRIBUTION (# PERCENT)

Three Jet Mills

CLASS LIMIT	CLASS % 0 1 2 3 4 5 6 7 8 9 10	CLASS %	NO.
0.25	[	0.00	0
0.40	[*	2.02	47
0.63	[**********	19.22	446
1.00	[**********************	46.45	1078
1.60	[***************	29.94	695
2.50	[*	2.02	47
4.00	[	0.26	6
6.30	[	0.09	2

Fig. 5. Particle size distributions from automated SEM image analysis for PZT 501A

crystallite particles, a reduction in size would subsequently be associated with an increase in surface area.

Table II. Data on PZT 501A from Automated SEM Image Analysis and Surface Area Analyses.

Sample	Average Diameter Mean (1 μm)	σ	Min/Max Mean (μm)	σ	Surface Area (BET) (m^2/gm)
PZT-501A					
As-Received	1.66	1.0	0.58	0.15	0.71
3 Jet Mills	0.89	0.3	0.57	0.15	1.92

The second deagglomeration technique used was an "attritor" type mill that consists of a stationary polyurethane lined jar mill in which rotating impeller imparts energy to the ball charge. Currently, work is underway for optimizing milling conditions and minimizing contamination. Zirconia balls, 3/8 inch in diameter, are being used exclusively in the ZrO_2 powder deagglomeration study. Figure 6 shows a schematic drawing of the "Attritor" type mill.

2.2.3. Firing

To prepare ceramic specimens for microstructural and electrical measurements it is absolutely essential to have close control of the firing process. The important firing variables are time, temperature and atmosphere. With todays electronics it is a relatively easy matter to reproduce any reasonable furnace profile. With a few simple exceptions it is not an easy matter to control the furnace atmosphere. PZT ceramics are a good example of systems that should be processed in a carefully controlled atmosphere because any loss or gain of PbO, the only volatile species, will lead to creation of defects and/or new phases which can have a deleterious effect on piezoelectric properties.

Ideally, the PZT ceramics should be formulated exactly on stoichiometry and processed in an atmosphere that has the equilibrium p_{PbO} for the particular composition. This practice is seldom followed either in the laboratory or on a commercial scale. The typical firing processes are based on control of the kinetics of PbO loss or gain which is usually difficult to obtain and presumably leads to variations in properties because of off-stoichiometric compositions.

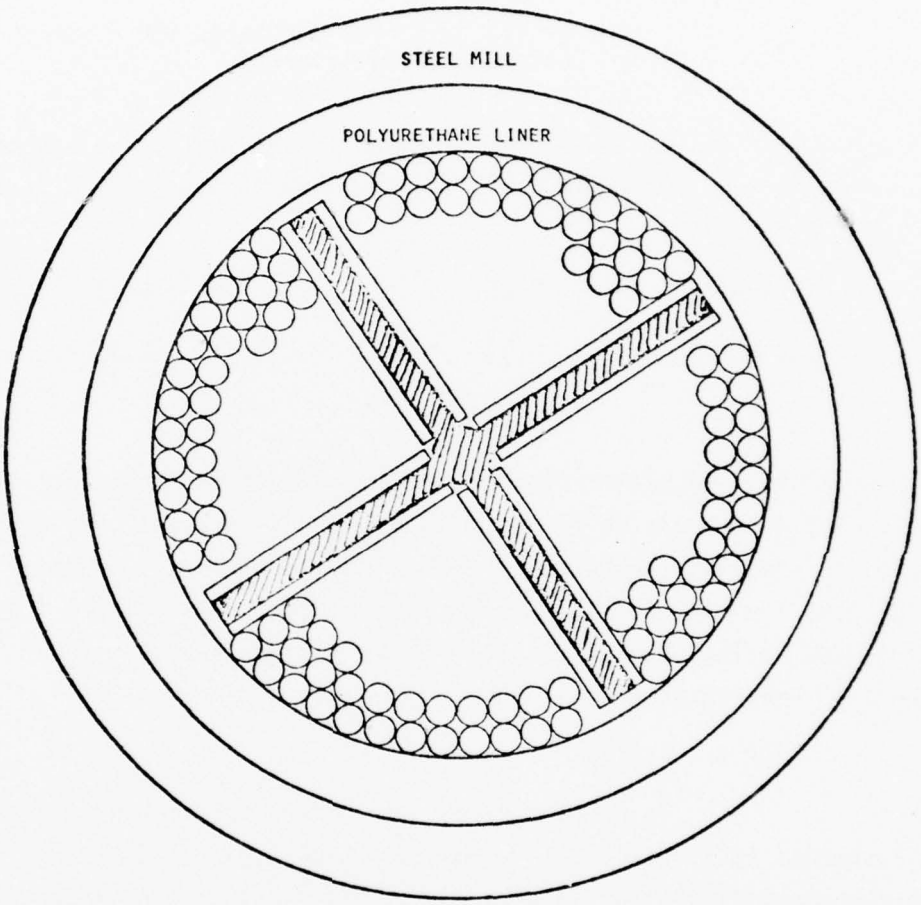

Figure 6. ATTRITOR MILLING: SHOWING IMPELLER AND UNIFORM DISTRIBUTION OF MEDIA ALONG MILL CIRCUMFERENCE.

One common technique is to batch the composition with a PbO excess to make up for vaporization during firing. The PbO excess compositions are calcined, formed into parts and fired in closed containers with little free volume.

Variations of this method use a packing powder of the same (or sometimes different) composition or pressed pellets of $PbZrO_3$ which will have a higher p_{PbO} than any PZT composition.

In the past six months we have been conducting firing experiments to determine the best method of reproducibly firing the large number of discs that are to be used in the ZrO_2 reactivity studies. The technique that we have developed uses a source pellet that has a composition in the liquid-PZT region as shown in the ternary isothermal section (Figure 7A). This diagram was constructed using the lower temperature work of Fushimi and Ikeda (7). The liquid in equilibrium with a $PZ_{.55}T_{.45}$ has the composition (in terms of the psuedoternary) of:

$PbZrO_3$ - .067 m/o

$PbTiO_3$ - .553 m/o

PbO - .380 m/o

Source pellets were made by mixing pre-reacted oxides of the calculated liquid composition and the mixed oxides of the 55/45 Zr/Ti PZT composition. X-ray diffraction studies of the pre-reacted liquid composition showed presence of PbO and $PbTiO_3$. It was presumed that pre-reacting the liquid compositions would promote formation of proper liquid and provide a better distribution of the liquid phase during firing. Firing tests at 1330°C for 1.5 hours showed that 91 w/o PZT - 9 w/o liquid was a workable combination of components. Less liquid lead to entrance into the single phase region and variable p_{PbO} and more liquid caused phase separation and refractory attack.

The specific firing procedure developed from this work is as follows: $PbZr_{.55}Ti_{.45}O_3$ is pressed into 40 gm, 2-inch diameter discs. These discs are sintered in an alumina crucible at 1330°C. These PZT pellets (5/8" diameter) are weighed and placed on the sintered two-inch discs. PZT pieces are used as separators between the two-inch setters so that the setters can be stacked. After mixing of the PZT and pre-reacting, two, forty gram, two-inch pellets are pressed at the source composition. A source pellet is placed both on top of and on the bottom of the stack of setters. The entire stack of pellets is set upon an alumina plate, an alumina tube is slipped over the stack of setters and an alumina plate is set on

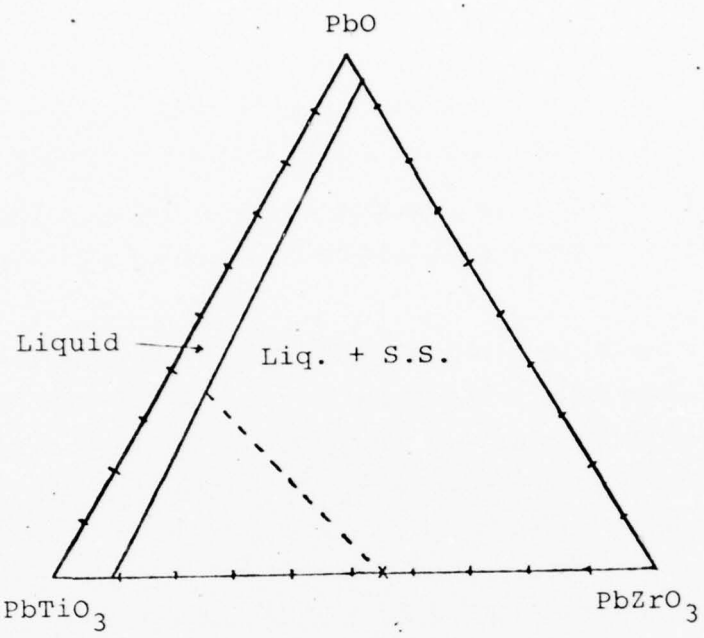

Fig. 7A. Proposed ternary for 1330°C. Tie line is shown for $PbZr_{.55}Ti_{.45}O_3$.

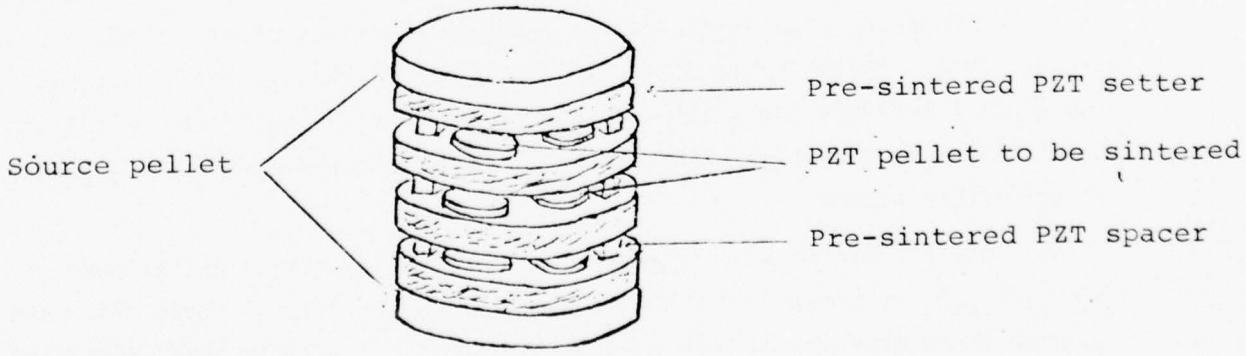

Fig. 7B. Stacking technique for firing PZT pellets.

top. The length of the alumina tube is such that there is as little free space as possible between the top plate and the top source pellet. A schematic of this arrangement is shown in Figure 7B.

If the source pellets are large and free volume of the container is small and if the container is tightly sealed, the discs should sinter in a p_{PbO} that is of the equilibrium value. The results to date are most encouraging - 1-1/2 hour firings at 1330°C, we have produced ceramics with minimal weight gains (∿.2 Wo/o) and good densities (> 7.6).

2.2.4. Calcining Studies

It is our present belief that calcining operation may compound the non-reproducibility in the PZT processing sequence. The work of Matsuo and Sasaki (8) clearly shows that there are several possible combinations of phases that can be present after calcining. Slight changes in reactivity of any of the oxide phase could produce a calcine with a different phase assemblage (both in relative amounts and specific phases present). It is quite possible that these differences would then affect the sintering and final properties of the ceramic.

In order to test this hypothesis we are preparing "calcining maps" of the type shown in Figure 8 (taken from Matsuo and Sasaki (9)), as part of the ZrO_2 reactivity study. We have selected two specific compositions for this work $PbZr_{0.55}Ti_{0.45}O_3$ and $Pb_{0.991}Nb_{0.018}Zr_{0.9329}Ti_{0.0491}O_3$ (10,11). These two compositions were chosen as being representative of the range of commercial PZTs. Large batches of these compositions are being prepared using the 6 as-received lots of zirconia already listed. Additional batches of powders are being prepared using the jet milled and " ttritor" milled powders. A majority of the powders are being pressed into discs for use in the studies to determine microstructural and piezoelectric property differences. A portion of each batch will be used to determine the calcining maps.

The experimental procedure that we are using entails calcining 10 - 15 gms of each powder contained in small 99.9 alumina crucibles at temperatures between 550° - 950° and times of 0 - 16 hours. A large resistance heated programmable furnace with controlled air circulation is being used for the calcining.

All of the sample lots are being calcined together for each set of calcining conditions.

The phases present after calcining are determined by x-ray diffraction and the amounts of unreacted PbO and ZrO_2 + TiO_2 by a wet chemical technique developed

by Robinson and Joyce (8). (The method is described in more detail in the section on chemical preparation of powders).

With completion of the calcining maps we will select the most interesting calcining conditions for further study. Larger batches of powders will be calcined and the results of the initial work will be checked. Disc samples of the calcined powders will be prepared and microstructural and piezoelectric properties checked using techniques developed during the ZrO_2 reactivity studies.

2.2.5. Microstructural and Piezoelectric Evaluation

The ZrO_2 reactivity study will require the evaluation of a large number of ceramic samples. Our initial characterization of the matrix of samples will be designed as to screen out the interersting variations (if any) for more detailed study. To accomplish this task we will make the following measurements on representative numbers of discs ($\sim$10) from all the process variations.

Microstructural Properties

Density - Geometrical and mercury displacement
Grain size - intercept techniques using optical and SEM
Phases present - X-ray diffraction, optical microscopy and SEM

Piezoelectric Properties

Permittivity - 1 KHz weak field as a function of temperature
Hysteresis behavior - 60 Hz room temperature
Poling characteristics
d_{33} - room temperature

In addition for 95/5 compositions: Remanant polarization and hydrostatic depoling.

2.3. Tape Casting

Tape casting or doctor blading has long been used to fabricate thin ceramic sheets (13). It is possible to manipulate these sheets in different ways to produce devices with different configurations i.e., multilayers with internal electrodes, multilayers with different compositions etc., which cannot be achieved by pressing or other more common forming methods. In addition to the ability to fabricate unusual configurations, it is also likely (using multilayer capacitor dielectrics as a case in point) that the ceramic produced from the tapes will have somewhat different firing temperatures and as a result, different microstructures

and electrical properties when compared to ceramics produced by pressing.

In the past six month period, we have constructed a small continuous tape caster diagrammed in Figure 9. The tape is cast on tempered glass plates 3" x 6" x 0.25". A variable speed drive moves the plates past a hopper and doctor blade based on a description by Runk and Andrejco(14). This design minimizes casting difficulties due to slip head variations and surface tension.

In initial work with the new caster we have elected to use a commercial organic system (Cladan B62) and four commercial PZT formulations (UP1, 401, 401 - 888, USH32 and 501A). Casting slips were prepared by techniques described in the last report. Typical viscosities and densities for different organic/powder ratios are shown in Table 4. For casting a rate of ∿.4 in/sec was used. The doctor blade set height was 0.025". The room containing the casting unit was maintained at 22 ± 1°C during casting. Tapes prepared in this way were used in two studies described below.

Table 4

Organic/Powder Ratio	Viscosity (cps) 22°C, 100 rpm,	Green ρ - g/cc
26/74	2250 cps	4.1
35/65	330	4.05
50/50	175	3.5
66/34	115	2.7
*26/74	1010	3.7

*used jet milled 135-401 with specific surface = 1.23 m^2/g.

2.3.1. Densification of Green Tapes

The green density of untreated cast tapes depends markedly on the organic/powder ratio in the starting slip, but to maintain correct viscosity for casting this ratio is limited by the characteristics of the powder, primarily its surface area. Finding the lowest organic/powder ratio which will give proper reproducible casting can be most time consuming. Since in the present program a wide range of powders with very different characteristics must be processed, a technique for pressure densifying the green tape after casting has been investigated.

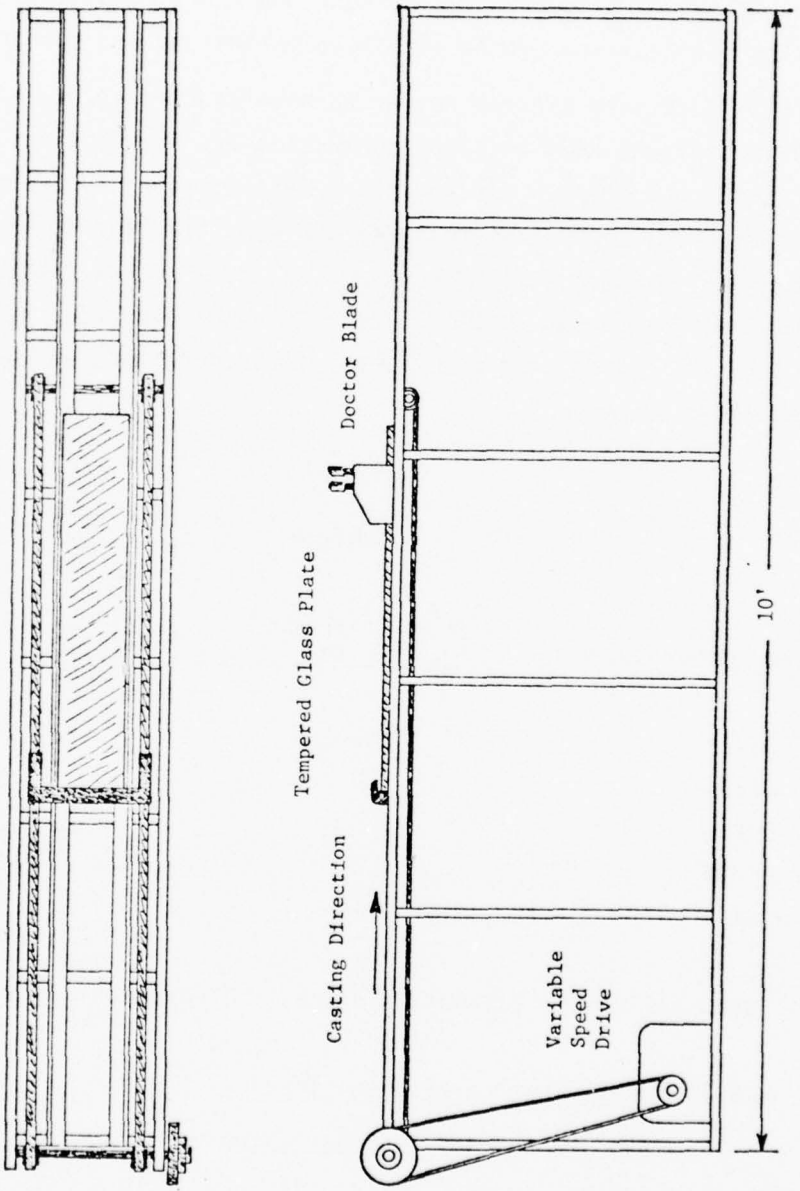

Figure 9. Tape casting machine.

For these tape compacting studies UPI 401 PZT formulation was used with the Cladan B62 binder system. In the initial study the following organic/401 powder ratios were used:

PZT 401	26 wt% B62 : 74 wt% powder
PZT 401 (jet milled)	26 wt% B62 : 74 wt% powder
PZT 401	35 wt% B62 : 65 wt% powder
PZT 401	50 wt% B62 : 50 wt% powder
PZT 401	66 wt% B62 : 34 wt% powder

After casting, one-inch squares cut from the tapes were pressed at loads ranging from 1500 lbs- 40,000 lbs on a Carver Press. Thickness change was measured using a sheet thickness guage and the data are shown in Figures 10-14.

The graphs show a rapid decrease in thickness up to pressures ~10,000 lbs/sq in. then a leveling off. The measured changes in green density up to the maximum pressure were:

PZT 401	26 : 74 wt%	4.1 - 5.3 gm/cc
Jet Milled	26 : 74 wt%	3.7 - 5.3 gm/cc
	35 : 65 wt%	4.05 - 5.2 gm/cc
	50 : 50 wt%	3.5 - 4.3 gm/cc
	66 : 34 wt%	2.7 - 3.3 gm/cc

It was also found that additional pressings could further increase density by a few percent.

Micrographs of the PZT 401 - 74 wt% powder tapes after pressing to different pressures are shown in Figure 15, and clearly indicate the compaction of the microstructure.

The effects of pre-pressing on the final sintering are now being studied. Preliminary data (Figure 16) with the PZT 401 - 74 wt% powder indicate that densification lowers the required firing temperature so that satisfactory final density can be achieved at 1220°C compared to 1300 - 1340°C for normal pressed powder samples.

2.4. Multilayer Configurations

For the initial study of the heterogeneous multilayer preparation, the configurations listed in Table 5 were fabricated. Green tape was cut into one-inch square blanks, stacked in the appropriate sequence in a one-inch square die mounted

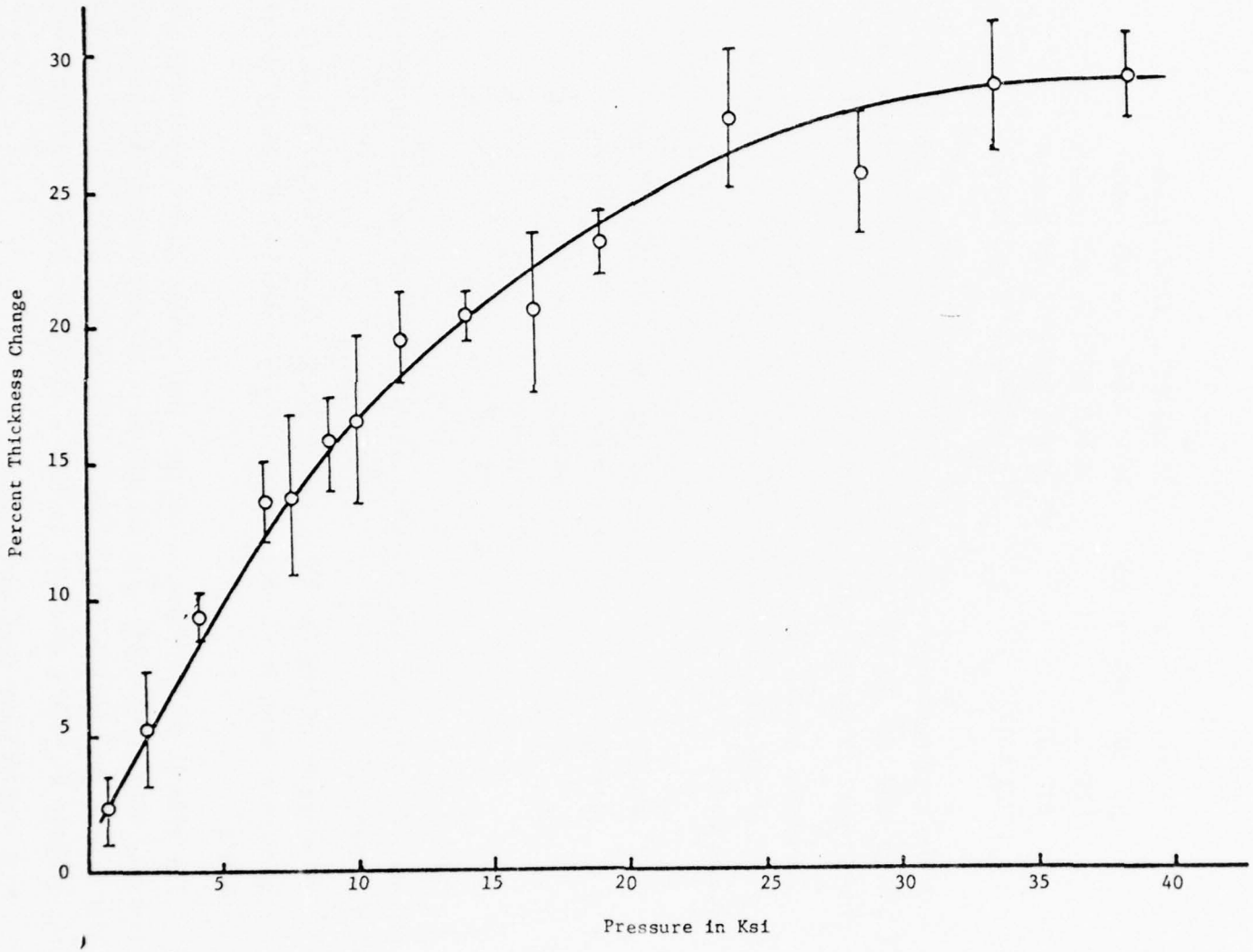

Figure 10. Percent thickness change vs pressure for PZT 401 - 26 wt% B62:74 wt% powder.

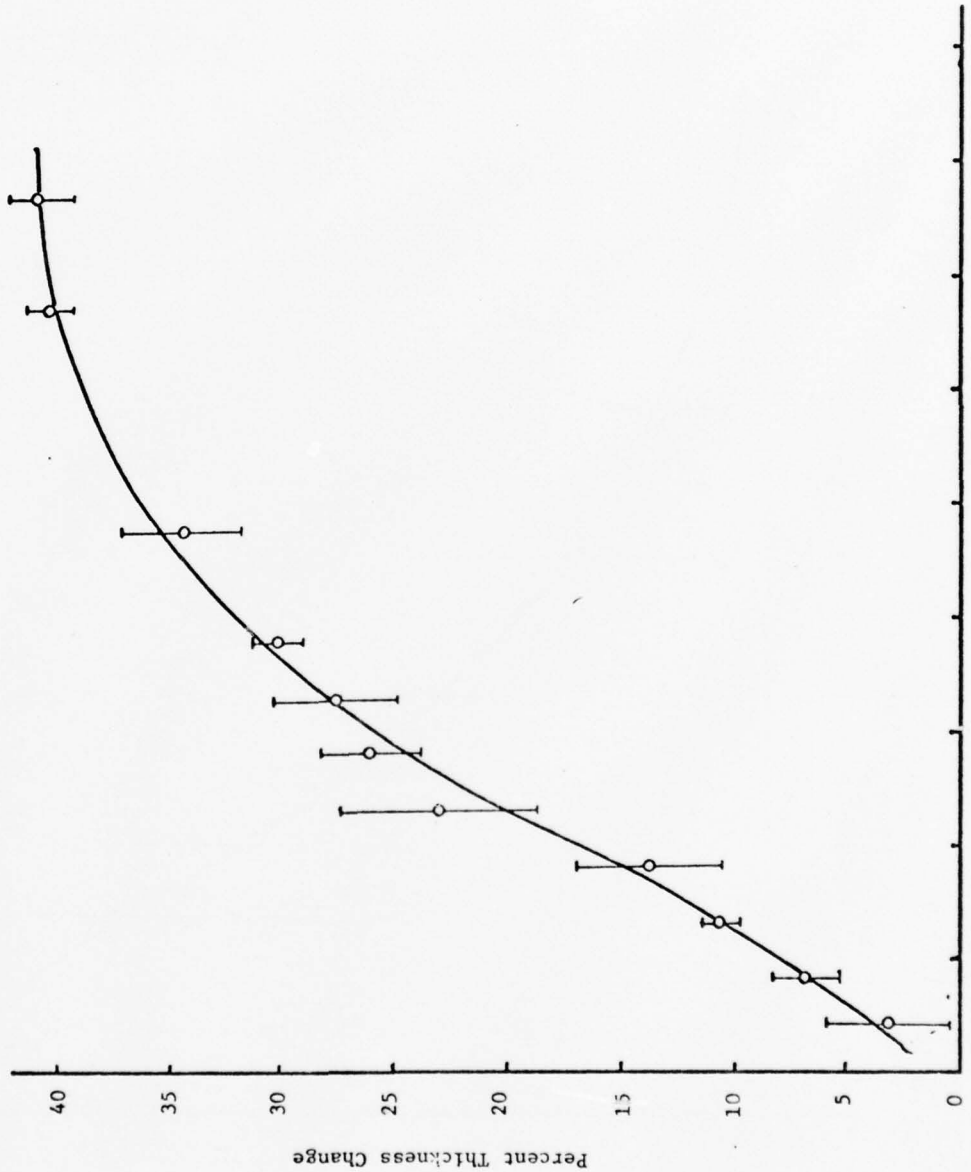

Figure 11. Percent thickness change vs pressure for PZT 401 (jet milled) 26 wt% B62:74 wt% powder.

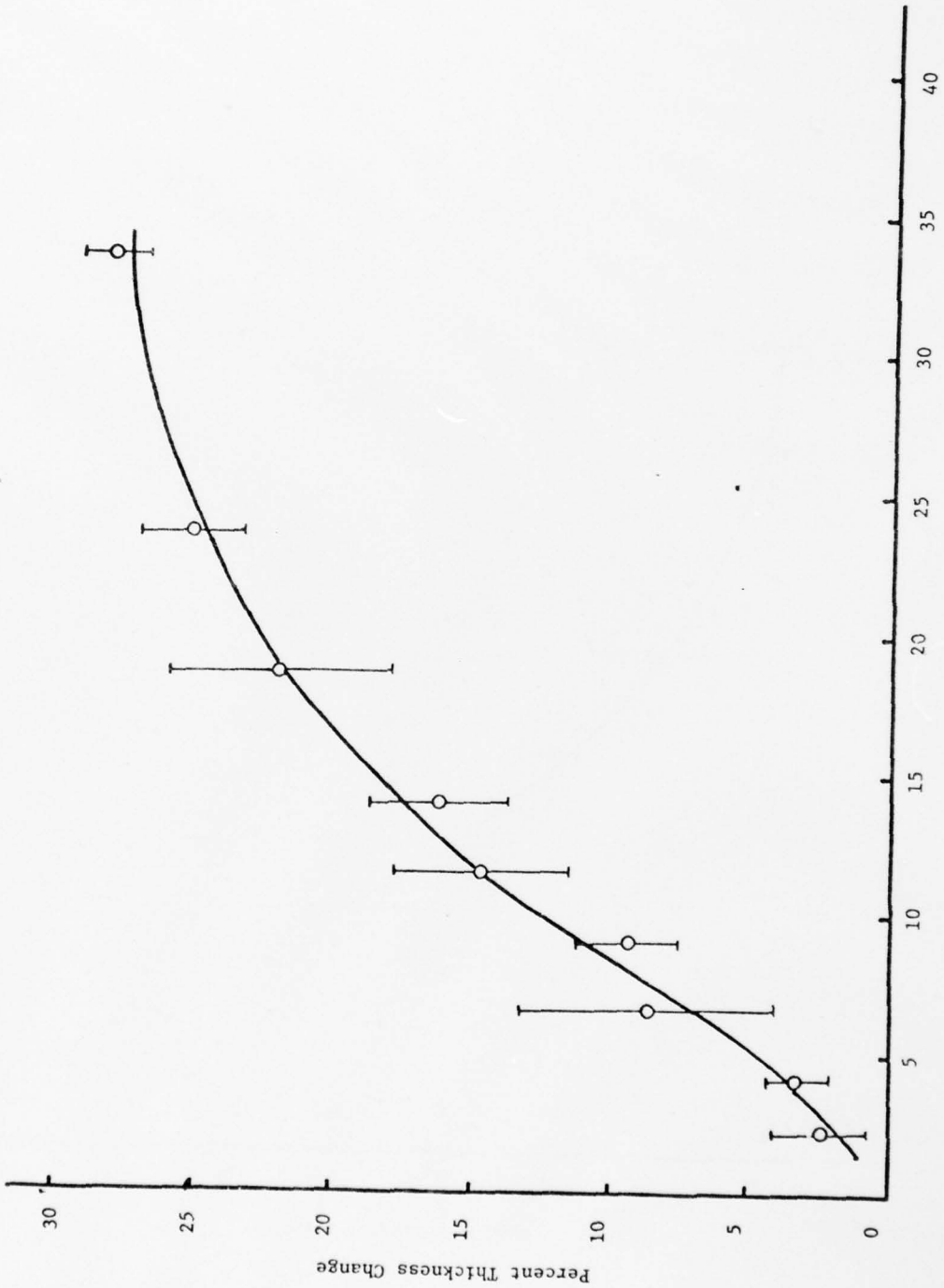

Figure 12. Percent thickness change vs pressure for PZT 401 - 35 wt% B62:65 wt% powder.

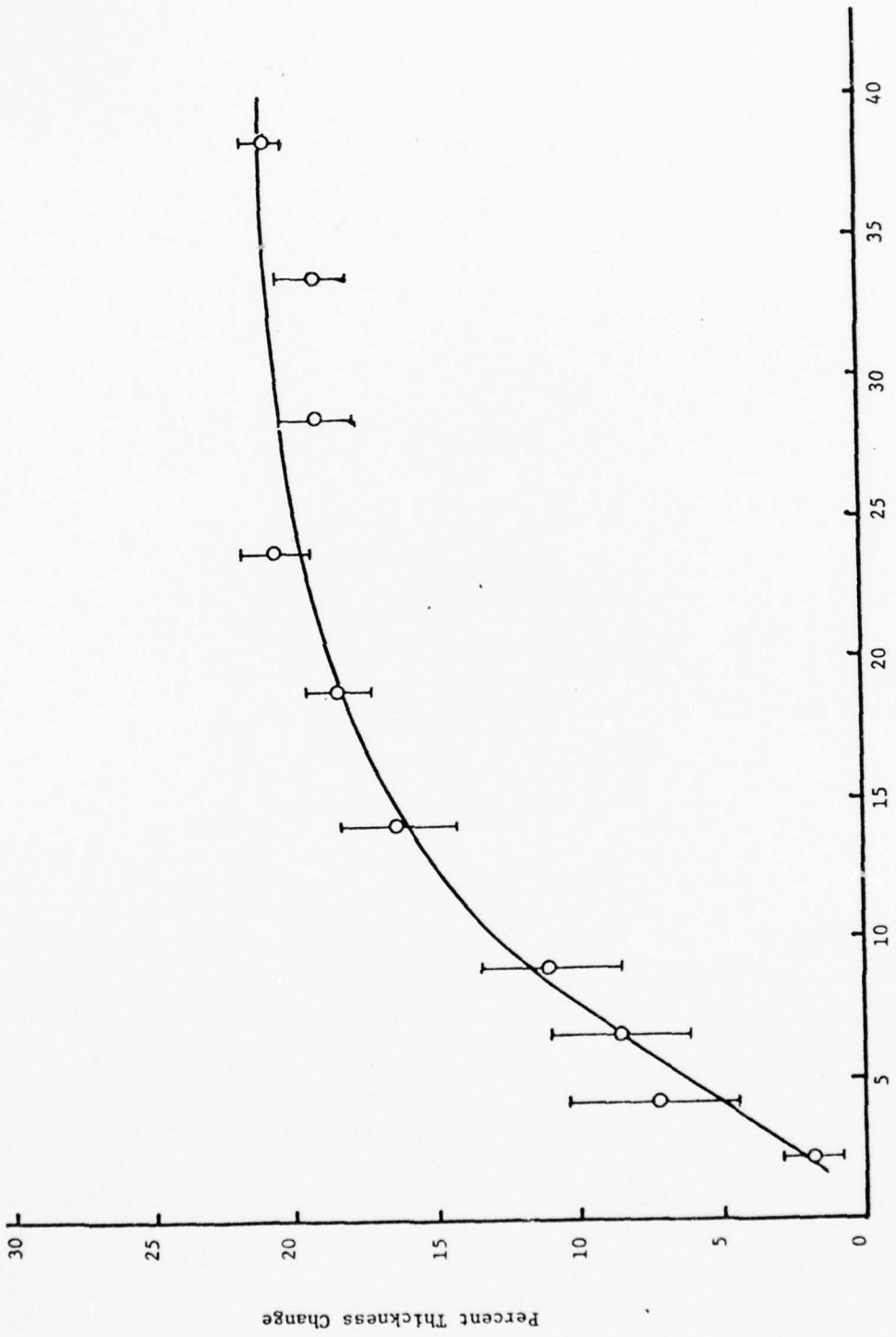

Figure 13. Percent thickness change vs pressure for PZT 401 - 50 wt% B62:50 wt% powder.

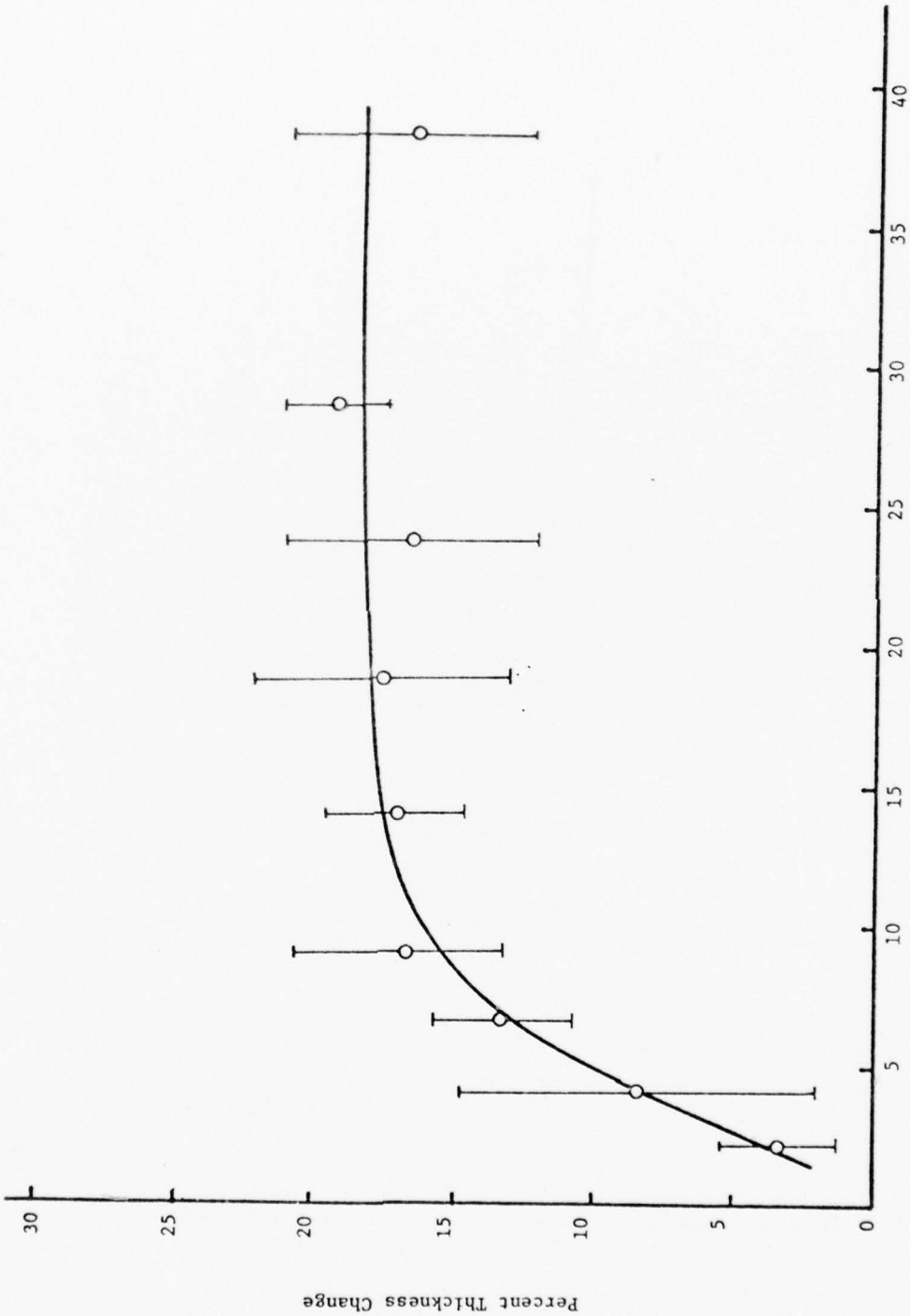

Figure 14. Percent thickness change vs pressure for PZT 401 - 66 wt% B62:34 wt% powder

Figure 15a. Micrograph of PZT 401 - 74 wt% unpressed.

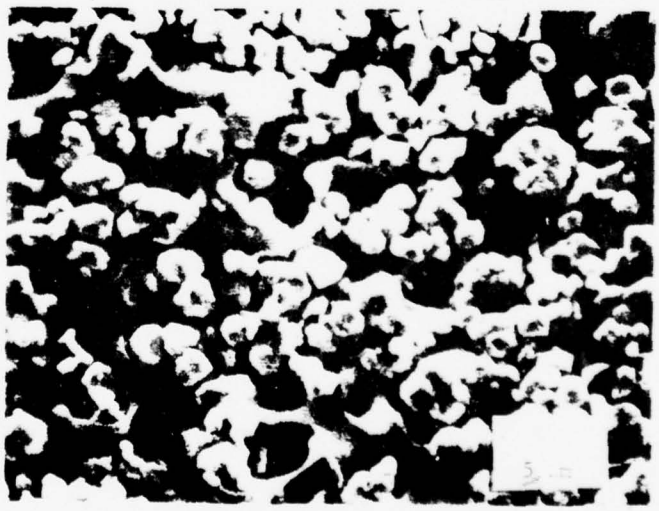

Figure 15b. Micrograph of PZT 401 - 74 wt% pressed at ~4300 psi.

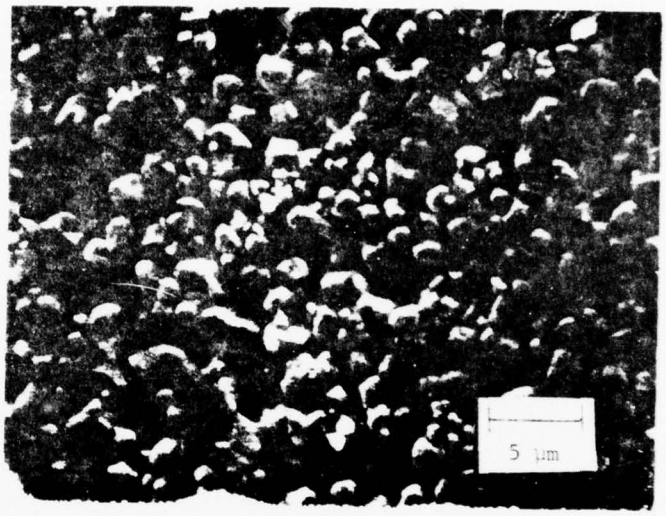

Figure 15 c. Micrograph of PZT 401 - 74 wt% pressed at ∿16500 psi.

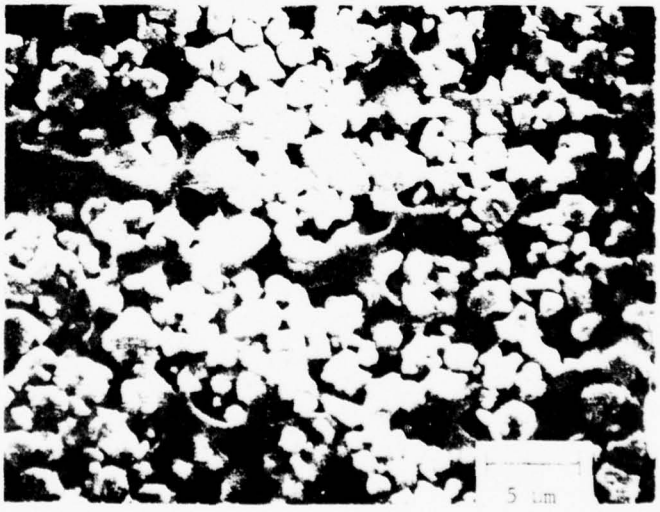

Figure 15d. Micrograph of PZT 401 - 74 wt% pressed at ∿ 33560 psi.

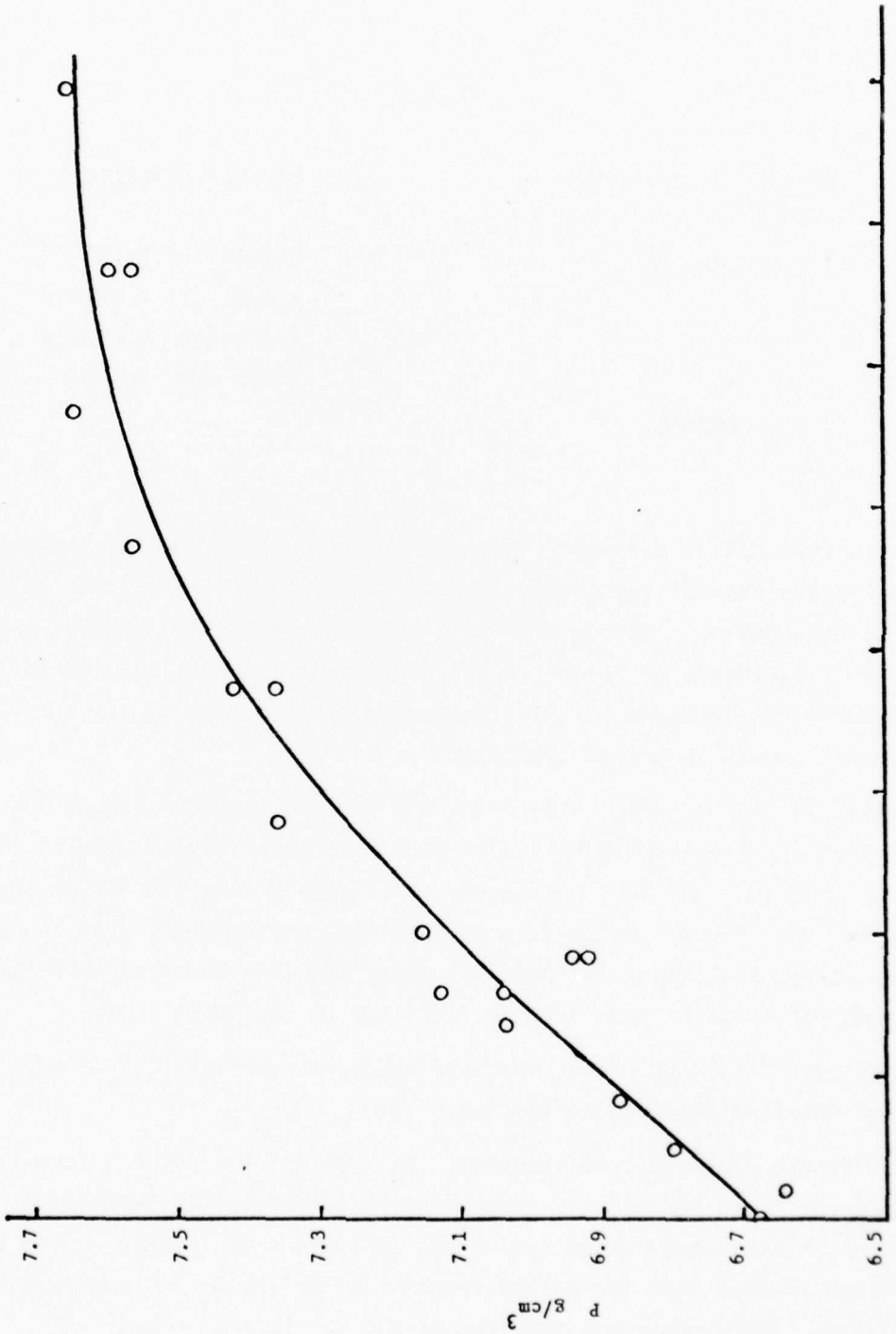

Figure 16. Density vs pressure of PZT 401 - 74 wt% powder tapes fired at 1220°C at 1-1/2 hrs.

on two large hot plates. For adequate adhesion between the green sheets a pressure of 5 - 10,000 psi was required with a temperature ∿50°C.

Table 5

Layer Configurations	PZT Formulations	
(1) ...AAA, BBB...	A-501A	B-401
	A-401	B-USH-32
	A-401-888	B-USH-32
	A-401-888	B-501A
(2) ...ABABAB...		

The current binder burn-out temperature:time profiles were determined from TGA and DTA analysis of the green structures. Final firing was in a closed alumina vessel using a suitable source of PbO to prevent excess lead loss or gain. The samples were supported on ceramic discs of similar composition, and to avoid warping due to differences in the firing conditions a disc of similar composition was placed on top of the sample.

Initial microstructures taken using the SEM are shown in Figure 17. It is evident from these and similar studies that for these initial samples the PZT tape layers of type 501A and type USH-32 are considerably less dense than the type 401 and 401-888 layers. We believe that this stems primarily from the difference in green densities between the original tapes and this was a major reason for initiating the study of pressure densification in the green state.

Additional multilayer structures are now being fabricated from the pre-pressed tapes for detailed property evaluation.

Preliminary dielectric measurements on the PZT 501:PZT 401 lamellar composite are shown in Figure 18. It is evident that the harder 401 composition, which gives the characteristic constructed hysteresis loop at 6 Hz (Figure 19) is beginning to exercise control over the poling process in the softer 501 composition (Figure 20). The rather poor density of the 501 layers, however, limit the utility of further experimental study. This will be taken up when denser samples have been fabricated.

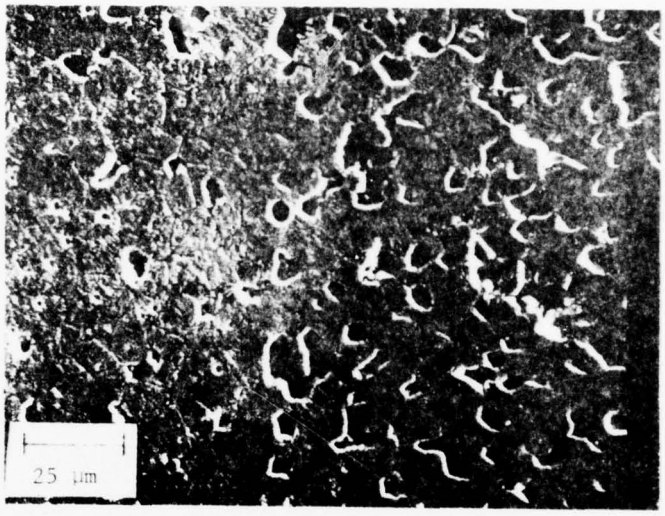

Figure 17. Microstructure of layer configuration... AAA, BBB...A-501A (right), B-401 (left).

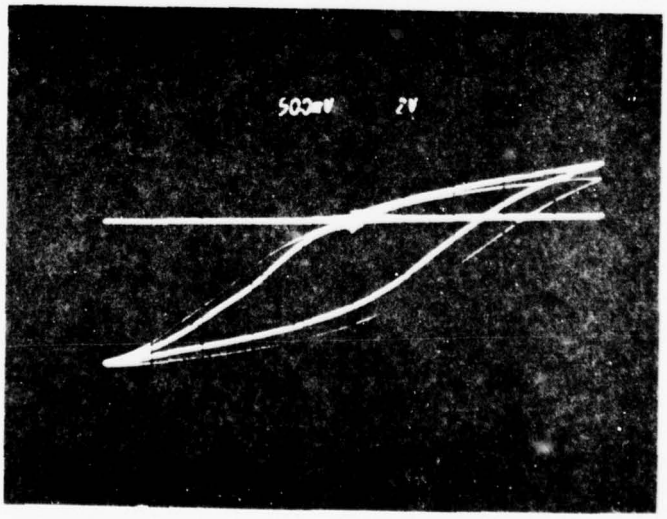

Figure 18. Hysteresis loop at 0.06, .6, and 6 Hz of PZT 501:PZT 401 lamellar composite.

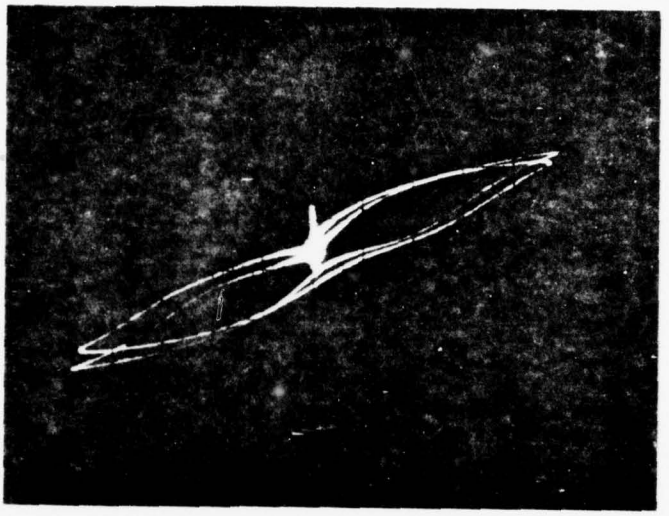

Figure 19. Hysteresis loop at .06 and 6 Hz of PZT 401.

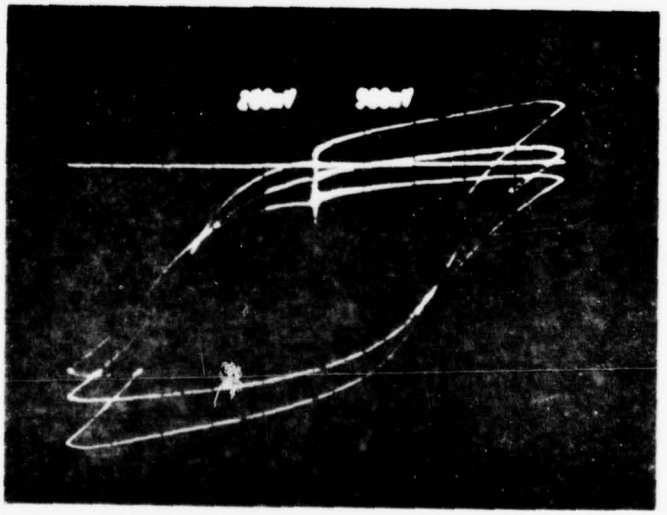

Figure 20. Hysteresis loop at .06 and 6 Hz for PZT 501A.

2.5 Preparation of High Surface Area Powders

2.5.1 Introduction

In the conventional processing of PZT ceramics, the starting material is often a mixture of the oxide of lead (PbO designated P), titanium (TiO_2 designated T) and zirconium (ZrO_2 designated Z). The intimately mixed oxides are subjected to a calcining step and go through a sequence of reactions

$$P + T + Z \xrightarrow{500\text{-}600^\circ C} PT + P + T + Z \xrightarrow{600\text{-}700^\circ C} PZT + PT + P + Z \xrightarrow{700\text{-}800^\circ C} PZT + PT$$

Lead titanate is the first product to form, then there are subsequent reactions eventually forming PZT and lead titanate. It is very difficult with commercial oxides to obtain a single phase PZT for calcining temperatures below the melting temperature of PbO (880°C).

In the first of these studies, the role of a chemically prepared ZrO_2, generated from the hydrolysis of zirconium alkoxide, in modifying the calcining behavior has been examined. In the second short study, the preparation from lead acetate or lead oxide and zirconium and titanium tetra-n-butoxides has been examined.

2.5.2 Preparation of PZT from Chemically Prepared ZrO_2

The zirconia powder was prepared by the hydrolysis of zirconium-n-butoxide (28.66 wt% ZrO_2) in the liquid phase. In this study 200 ml batches of the butoxide was added in a very slow stream to 500 ml of deionized water which was kept agitated in a Waring blender using a stainless steel paddle in a polypropylene vessel. An exothermic reaction occurs producing a very fine precipitate of hydrated ZrO_2, in a thick slurry. After drying at 120°C for 12 hours, the dried cake was ball milled in a polyurethene jar using zirconia balls (1:2 by weight) in ethanol. The milled powder was again dried and was then ready for use (flow sheet, Fig. 21).

Semiquantitative spectroscopic analysis, Table 6, revealed that the major impurities were TiO_2 and SiO_2 (100 ppm). The powder was amorphous to x-rays, but after heating to 500°C for 2 hours the diffraction spectra revealed a mixture of monoclinic and pseudocubic phases. BET method showed a surface area of 154 m^2/gm. Table 7 gives the surface area data of the different zirconia prepared and the Harshaw ZrO_2 lot 6-76. SEM pictures of the virgin powder showed strong agglomeration, but after ultrasonic dispersion in ethanol TEM studies showed a particle size ~100A in good agreement with the surface area values obtained.

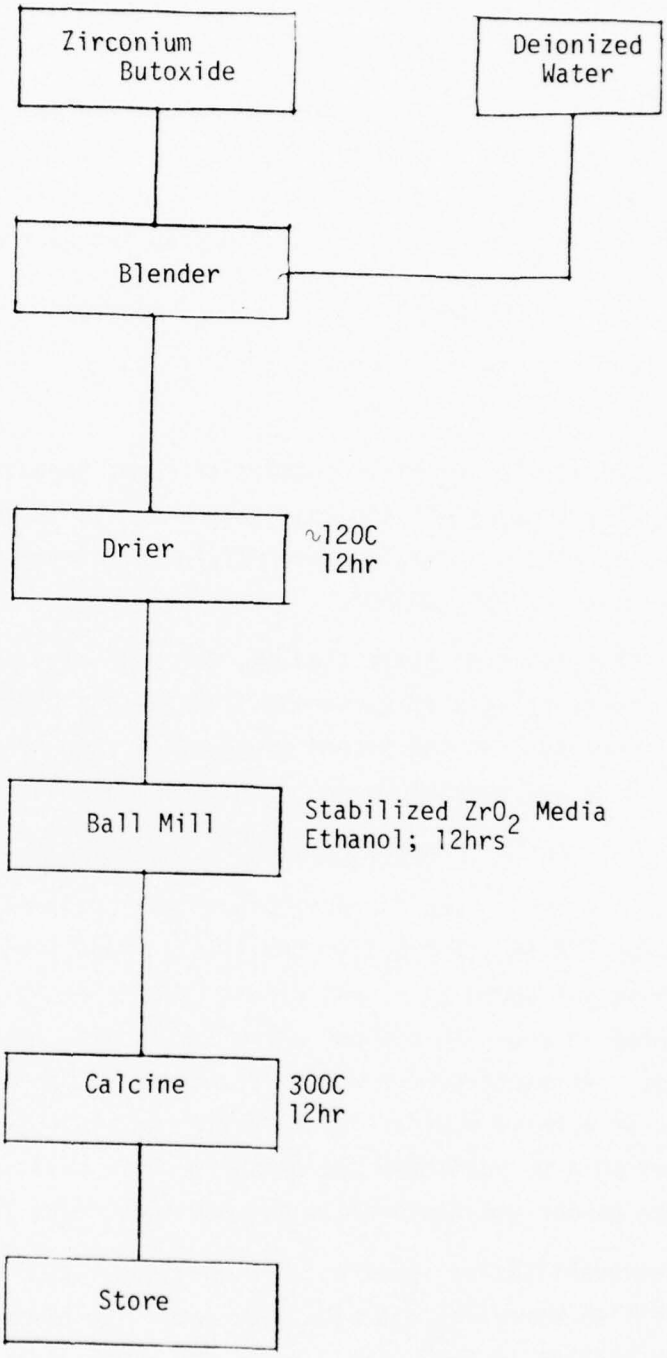

Fig. 21. Flow Sheet - Preparation of Alkoxy Derived Zirconia

Table 6

Sample No.	Z1.1	Z1.2 (Z.6)
Ti	100	100
Al	20	20
Si	100	100
Ca	∿5	∿5

Not detected in both: Fe, V, Mg, Mn, B, Be, Sr, Ba, Mo

Table 7

Sample No.	Process Detail	Surface Area M^2/gm
Z 1.1	$2(ZBT)^{*}\rightarrow 5(H_2O)$	188.0
Z 1.2	Z 1.1 calcined 500/2 hr	162.0
Z 2.1	$1(ZBT)^{*}\rightarrow 3(H_2O)$	148.0
Z 2.2	2.1 calcined 500/2 hr	142.0
Z 4.1	$5(H_2O)^{*}\rightarrow 2(ZBT)$	115.0
Z 6	$2(ZBT)^{*}\rightarrow 5(H_2O)$	154.0
Z.H	Harshaw. Lot 6/76	15.0

*Sequence of addition

Differential thermal analysis (Fig.22) showed a strong exothermic peak at 385° which has been identified as the development of the crystallized ZrO_2 phase in agreement with earlier studies by Cypres et al. (17), Bhattacharya et al(12) and Komissarova et al. (13). Based on the DTA data, the as-prepared powder was calcined at 300°C for 12 hours before use in the calcining studies.

2.5.3 Calcining Studies

Four compositions of PZT with zirconia/titania ratios of 40/60, 52/48, 60/40 and 90/10 were studied. The oxides were mixed in a polyethylene jar in ethanol and milled for 12 hours with zirconia media, then dried at 120°C for 12 hours and stored for use. For comparison purposes similar batches were made using the same PbO and TiO_2 powders and ZrO_2 from a Harshaw Batch 6-76. This Harshaw zirconia was monoclinic and was found by BET to have a surface area of 15 m^2/gm.

Calcination studies were done on both types of PZTs. The temperatures were 500, 600 and 800°C, for 3, 6 and 9 hours. The powders were calcined in a muffle furnace in closed sintered alumina crucibles. The percent weight loss was recorded in each case and x-ray diffraction analysis was done for phase identification (Fig.23).

Chemical analysis for the uncombined PbO was done by leaching out the free lead oxide as acetate with 6N acetic acid and titrating the solution against standard EDTA. The procedure is similar to that described by Robinson (8). A 1 gm sample was weighed accurately into a volumetric flask and 10 cc of 1:3 glacial acetic acid (6N) was added. The flask was kept for digestion for half an hour with occassional stirring. The slurry was then filtered and the filtrate washed with distilled water. The filtrant solution was then made up to 250 cc in a volumetric flask. Twenty-five ml of the solution was then titrated against a standard EDTA (0.01 M) solution with xylenol orange as the indicator. The pH of the solution was adjusted between 5-6 by the addition of NH_4Cl - NH_4OH buffer so that the color of the solution before is deep red which turned to straw yellow at the end point. The amount of uncombined lead oxide was calculated as:

$$\% \text{ PbO} = \text{vol. of EDTA} \times \frac{4.1386}{1000} \times \frac{250}{25} \times \frac{100}{\text{wt. of sample}} \times \frac{223.19}{207.19}$$

(1 ml of the standard EDTA = 4.1386 mgm Pb)

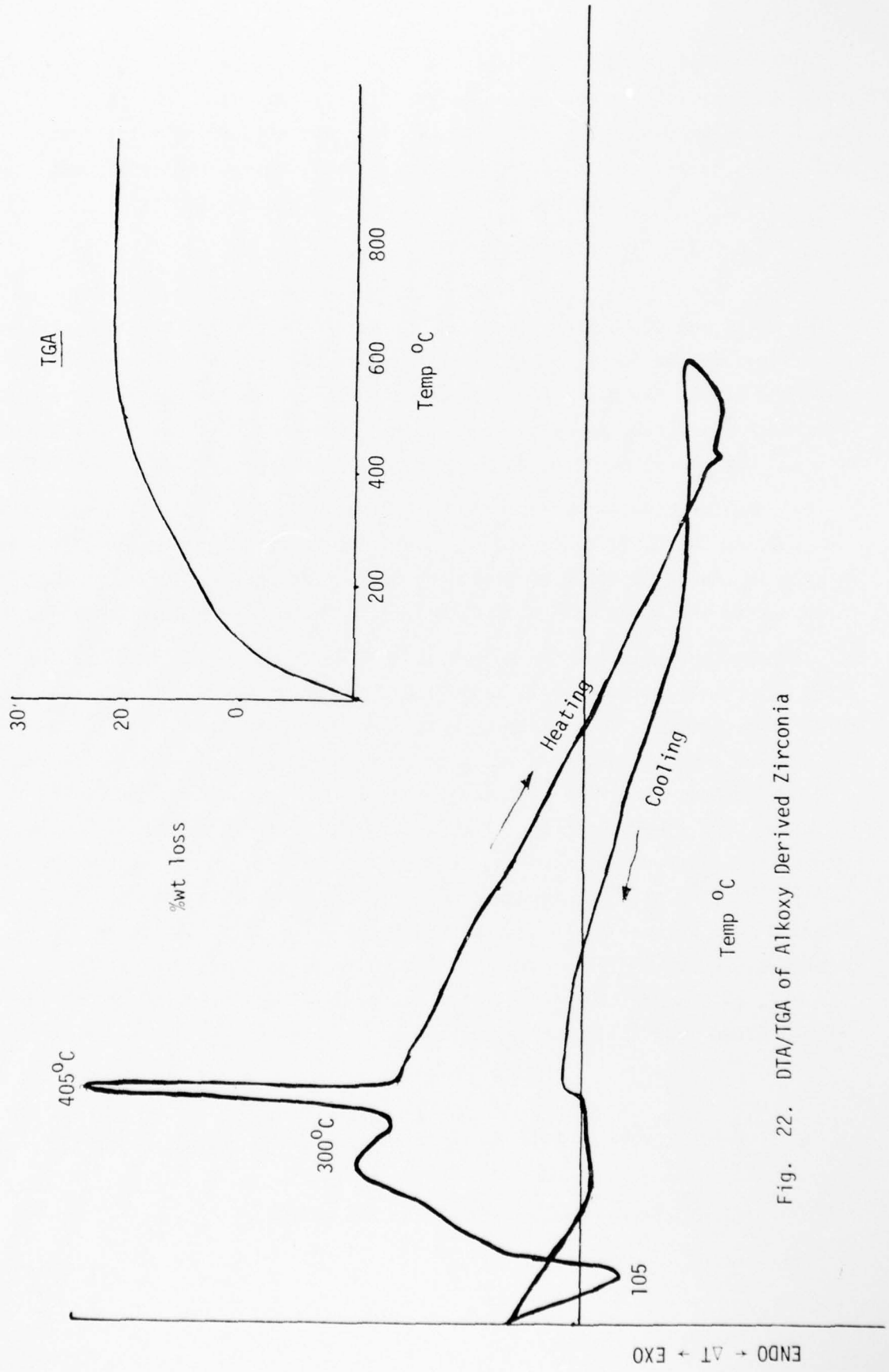

Fig. 22. DTA/TGA of Alkoxy Derived Zirconia

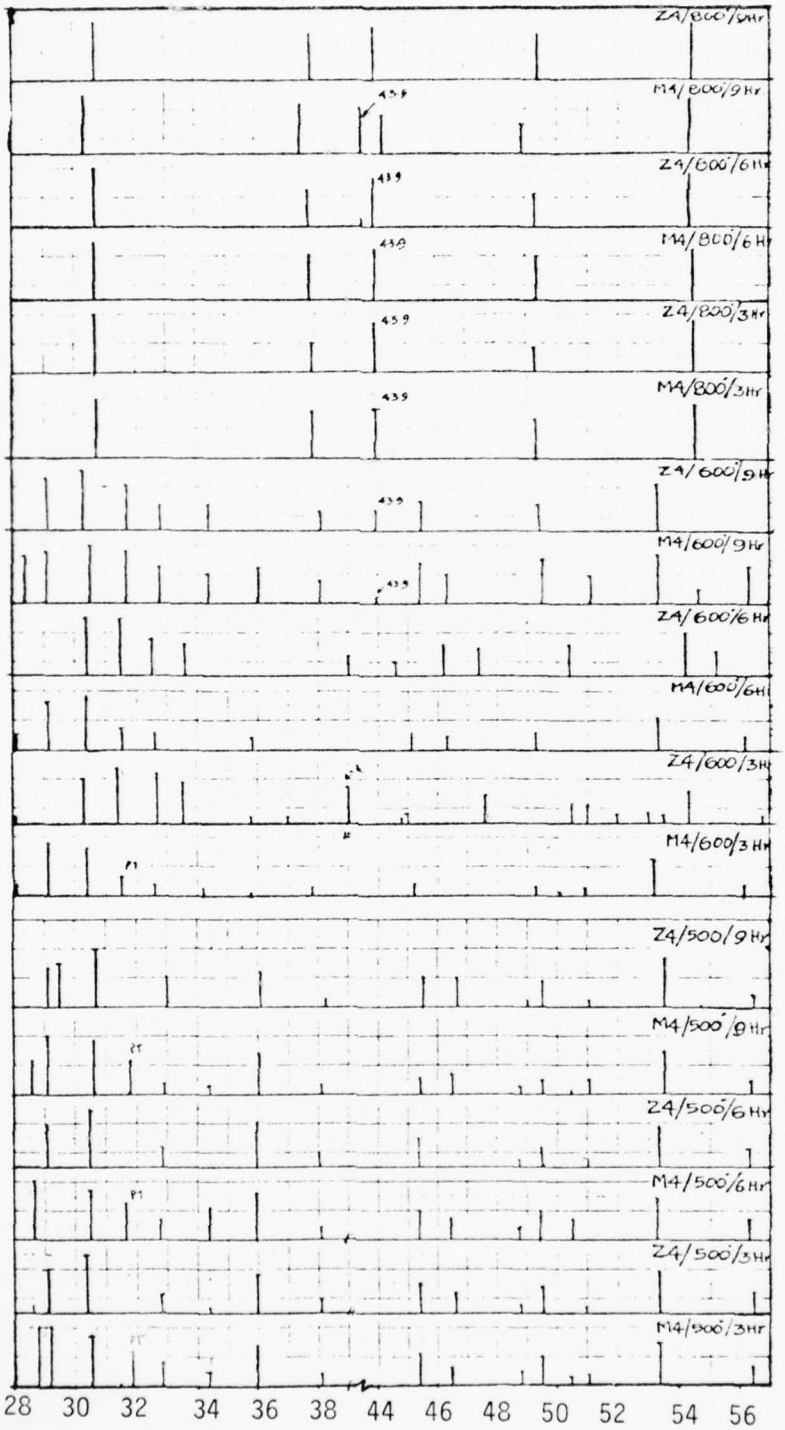

Fig. 23. X-ray diffraction map of reaction sequence of $PbZr_{0.9}Ti_{0.1}O_3$

M4 = Harshaw Lot 6/76-ZrO_2

Z4 = Alkoxy Derived ZrO_2

The weight losses on calcining revealed a 5-7 times higher weight loss in the material with chemically prepared zirconia, probably due to adsorbed ethanol and moisture on the large surface area powder. Some PbO loss was also recorded for the 800°C calcines. X-ray analysis gave consistently lower free PbO in all chemically prepared zirconia mixtures. For these samples only PZT and PT were detected after 600°C/6 hour calcine and only PZT for the 800°C/3 hour and 800°C/6 hour calcines, respectively. Chemical analysis after the 600°C/3 hour calcine gave values of 42% for Z-4 ($PZ_{0.9}T_{0.1}$ - chemically prepared ZrO_2) and 55% for MO-4 ($PZ_{0.9}Ti_{0.1}$ - Harshaw ZrO_2) (Fig. 24).

Clearly the high surface area fine powder character of the chemically prepared ZrO_2 greatly increases the reactivity with PT, P and T even at these low calcining temperatures.

2.5.4 Chemically Prepared PZTs

Starting materials for this study were lead acetate (or lead oxide), zirconium tetra-n-butoxide (28.66 wt% ZrO_2) and titanium tetra-n-butoxide (Tyzor TBT - 23.71 wt% TiO_2). In the preparation procedure used here, lead acetate corresponding to the required PbO content is dissolved in deionized water to a 25 wt% solution. This is then slowly added to the mixture of ZBT and TBT, and kept agitated in a Waring blender. The water of the acetate solution hydrolyses, the ZRT and TBT and the resulting precipitate is a complex PZT hydrate and acetate mixture. The total mixing time was about 20 minutes. The resulting viscous slip was dried overnight in an oven at ~120°C. The dried cake was then ball milled for 12 hours using an equal weight of ZrO_2 balls in ethanol in a polyethylene jar. The ball milled powder was then dried in an oven.

The different compositions had varying ZrO_2/TiO_2 ratios of 52/48, 60/40, 70/30, 80/20 and 40/60. Some of the compositions were also prepared by adding deionized water to an agitated mixture of PbO powder, ZBT and TBT solutions. The procedure was just the same as above. The flow sheet is given in Figure 25.

The compositions were calcined in alumina crucibles at 500, 600, 800 and 1000°C for 2, 4, 6, 8, 10, 12 and 16 hours as given in Table 8 . The weight losses during calcining were determined and XRD data were obtained to detect the major phases present. Figure 26 shows the DTA and TGA data for the 52/48 powder.

From Table 6 the percent weight losses at 500 and 600°C indicated that the co-precipitated gel is a mixture of lead acetate and zirconium titanium hydroxide complex. The DTA and TGA diagrams confirmed this; DTA giving an endothermic peak

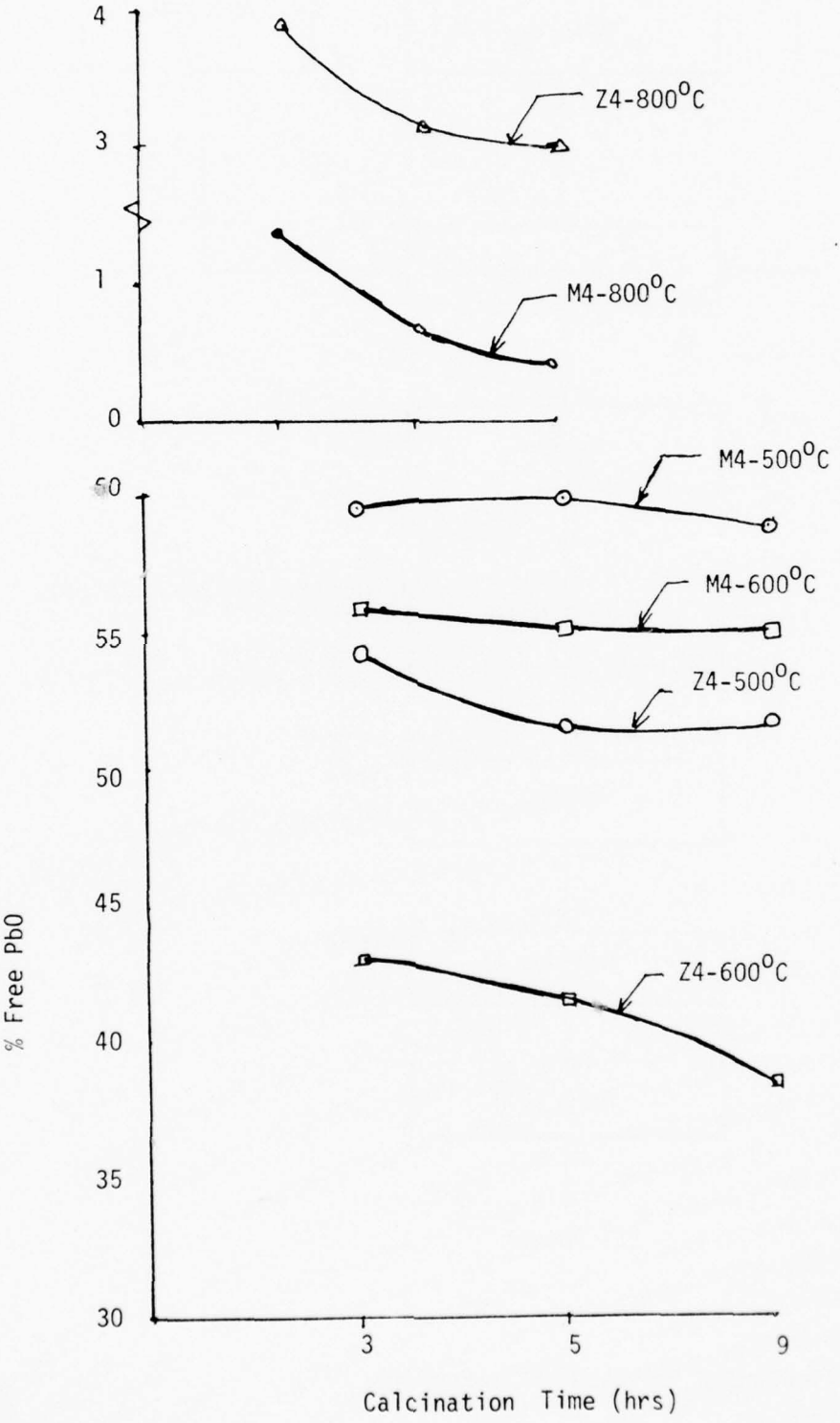

Fig. 24 Uncombined PbO

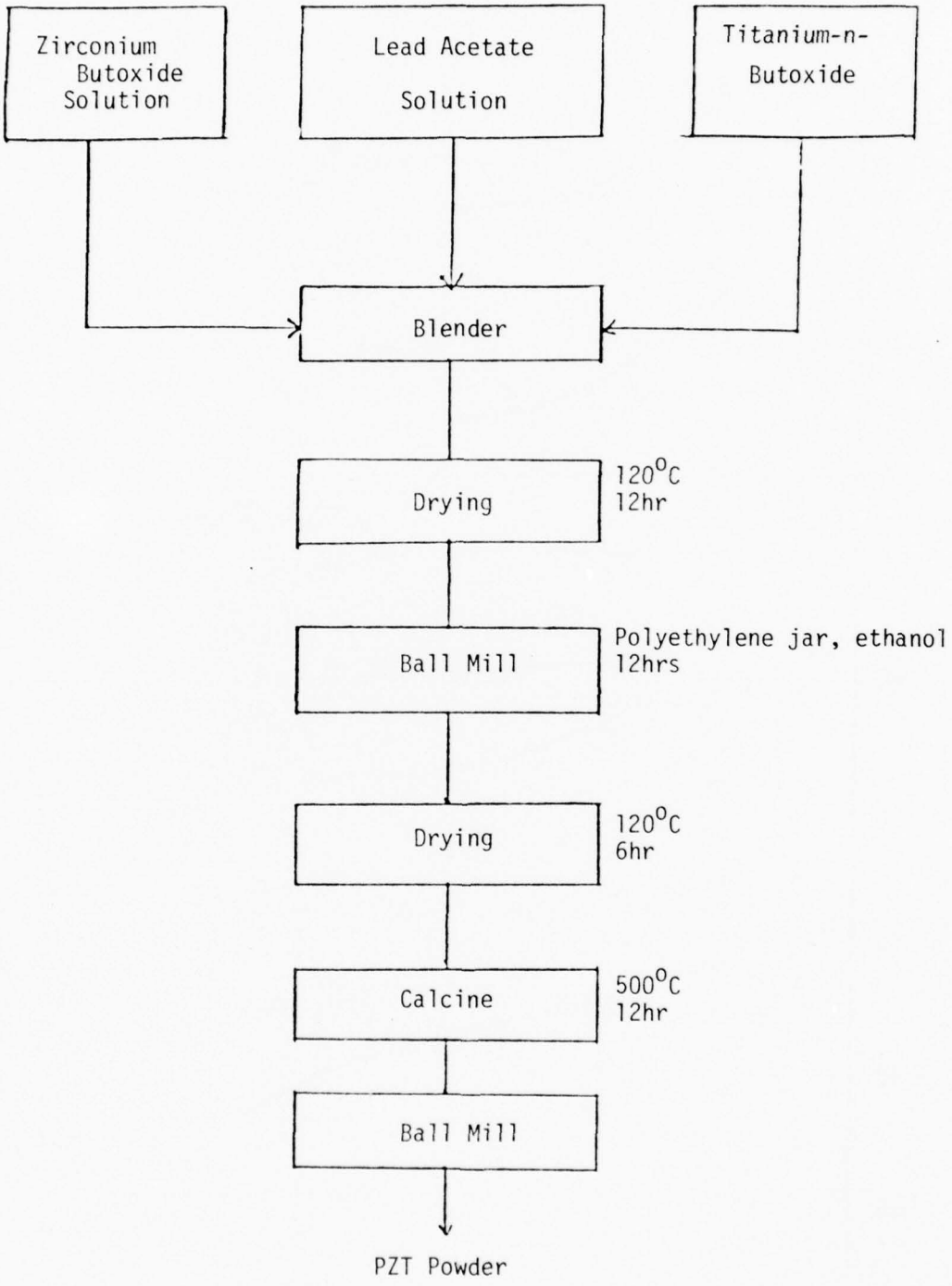

Fig. 25 Flow Sheet for Chemically Prepared PZT

Table 8

Composition	Calcination Temp/Time	Percent wt loss
$PbZr_{.52}Ti_{.48}O_3$	500°C/2hr	20.44
	500°C/4hr	20.61
	500°C/6hr	21.33
	500°C/8hr	22.02
	500°C/10hr	---
	500°C/12hr	21.81
	500°C/16hr	21.85
	600°C/2hr	22.73
	600°C/8hr	22.74
	800°C/2hr	22.62
	1000°C/2hr	22.47
$PbZr_{.52}Ti_4O_{83}$ (PbO+ZBT+TBT+H_2O)	800°C/2hr	6.67
$PbZr_{.6}Ti_{.4}O_3$	600°C/2hr	19.35
$PbZr_{.6}Ti_{.4}O_3$	1000°C/2hr	17.53
(PbO+ZBT+TBT+H_2O)	600°C/2hr	4.43
$PbZr_{.7}Ti_{.3}O_3$	1000°C/2hr	17.62
$PbZr_{.8}Ti_{.2}O_3$	1000°C/2hr	18.18

at 290°C corresponding to lead acetate to lead oxide conversion. TGA showed that major weight loss continued up until 500°C. The loss due to lead oxide evaporation occurs around 800°C.

The x-ray data showed the sequence of reactions occurring at various calcination cycles. Figure 27 gives the XRD data for the $PbZr_{.52}Ti_{.48}O_3$.

In the 500°C calcination the amount of lead oxide decreased and that of PZT increased as the time of soak was increased from 2 to 16 hours. The amount of $PbTiO_3$ also decreased.

The final product after 16 hours at 500°C and 2 hours at 800 and 1000°C consisted of PZT and PT as the major phases. There was no evidence of PbO in the XRD patterns. $PbZrO_3$ showed up distinctly only at the 800°C/2 hour calcine.

The initial 52/48 PZTs on calcining at 500°C for 2, 4 and 6 hours became green on the surface probably due to formation of lead.

The as-prepared and dried samples were amorphous to x-rays. The BET surface area of the PZT (52/48) was found to be 28.5 m^2/gm and the SEM pictures revealed particle sizes of the order of 0.5 μm.

It has been shown by several workers(3,18)that PZT forms only at temperatures greater than 700°C from mixed oxides whereas the alkoxy derived precipitates reacted at 500°C to form PZT and the reaction was complete at 600°C for a soaking period of 8 hours. Brown (19) and Haertling and Land (20) showed that PLZTs from akoxides reacted at 500°C to form a single phase PLZT. In fact, Brown had found that the co-precipitate is a single compound of PLZT.

In this work we have shown that by the hydrolysis of the alkoxides of zirconium and titanium with an aqueous solution of a lead salt, a chemically homogeneous submicron powder could be prepared which would react at the low temperatures of 600°C to form PZT.

2.6 Hot Isostatic Pressing

Gas isostatic hot pressing has been used in a wide variety of technologies to enhance densification. The parts may be formed to or near the final shape from either the powder state using a crushable container (21) or from a presintered state (22) with closed porosity acting as the gas seal to transmit pressure to the bulk.

In this study we are interested in the densification of oxide ceramics, particularly ones based on PZT and $BaTiO_3$. Because of the high sintering range (1200 - 1400°C) and the reactivity of the ceramic with most container materials, the primary thrust of this study will be to enhance the density of presintered parts. The initial objective will be to achieve near theoretical density in the PZT based composites and the honeycomb structured $BaTiO_3$ supplied by Corning.

In both these materials reduced density greatly limits the electric field levels and mechanical strength in their present form. Additional densification to near theoretical density should allow complete evaluation of these materials without expending the time necessary to optimize conventional sintering procedures for each trial composition. HIP also should allow densification of composites composed of materials that sinter together although they do not achieve maximum density under the same conditions.

The advantage of HIP is illustrated in Figure 28 for a typical oxide material of 1 micron particle size at 0 and 5000 psi. This figure shows the variation of different chemical potential gradients (driving force) as a function of relative density for conventional and HIP sintering. The driving force decreases very rapidly in the initial stage of sintering. At low densities, the surface free energy contribution dominates; but with increasing density this term becomes extremely low, which is why the final stage of sintering always requires a long time in the solid state. At even 90% theoretical density, the sintering rate is extremely low due to the weak driving force. To obtain near theoretical density a long time would be required which would favor grain growth. At this stage the porosity should be closed which would allow the application of gas pressure to the bulk. If the sample is subjected to 5000 psi at the same temperature, the driving force is raised about an order of magnitude and densification proceeds toward theoretical at a much higher rate (comparable to the initial stages of sintering).

Construction of a gas isostatic hot press has proceeded along the design outlined in the initial proposal. The pressure vessel is a relatively inexpensive (material and machining less than $1500) construction utilizing steel pipe with bolted end plates. During the furnace development work which we are just completing, this construction has proven to be versatile and easy to gain access to the hot zone.

Application of gas pressure is accomplished by using normal and high pressure gas tanks rather than expensive intensifiers. The use of tanks establishes a

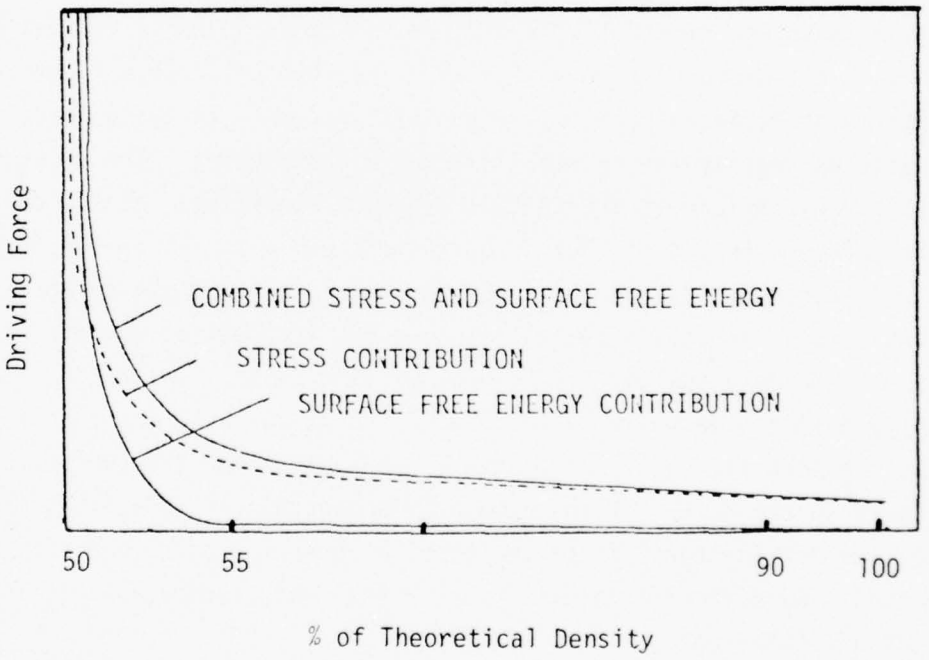

Figure 28. Driving Forces Involved in Pressure Sintering.

working maximum pressure of about 5000 psi (6000 psi maximum tank pressure). About 6 normal HIP runs of 3000 psi can be obtained from each high pressure tank when the chamber is first charged from a standard tank to about 1500 psi.

The actual furnace design has consumed a major portion of the in-house effort on HIP to date. Industrial sources familiar with the HIP process warn of "convection controlled heat transfer" and "hurricaning". These terms received additional emphasis when our first design, a conventional tube furnace which could run easily to 1400°C with 1 KVA at 1 atmosphere of argon, could not make 900°C with 6 KVA at 3000 psi. Industrial units normally utilize concentric molybdenum cans to break convection currents. This was initially tried, but lack of proper fabrication techniques made these systems very lossy and the danger of shorting furnace leads was always present. During the initial trials it also become evident that convection caused layering of the hot gas in the sample tube with gradients of several hundred degrees per inch.

In the present furnace design (Figure 29) we have returned to ceramic tubes which can be sealed with cement and do not require special techniques to protect furnace leads. We have also installed a hearth heater which utilizes the convection to transfer heat within the sample chamber and to stir the dense gas to reduce the gradients.

Reduction of the overall density of the gas has shown to be a significant factor in reducing the heat loss from the hot zone. Table 9 shows the relation between the gas pressure, power consumption and temperature distribution (thermocouple location given in Figure 29). The first column shows what little power is needed to drive a basic two inch tube furnace at one atmosphere. The earlier design was without winding C which is fixed at about 1 KVA and add additional convection sealing. Winding A is powered from the controller through a variac and can be used to adjust the temperature profile. For most of the runs, this small (1-1/4 inch diameter x 4 inch length) tube was driven between 2 and 2.5 KVA. Without winding A the temperature profile becomes very steep and more power is required to maintain temperature. The decrease in heat loss with gas mixing may be seen at 2500 psig. For all argon it requires 6.8 KVA to maintain a portion of the zone at 1300°C and not enough power was available to raise TC 2 to 1300°C. But using 1500 psig helium and enough argon to make 2500 psig, the power consumption was reduced to 5.4 KVA to stabilize TC 2 at 1300°C.

POWER REQUIREMENTS AS A FUNCTION OF GAS PRESSURE

		Tube Furnace with Small Hearth Heater			Design Shown in Figure 29							
Gas Pressure in PSIG:	Argon	0	1100	2000	2500	3000	----	----	500	1000	1500	2000
	Helium	----	----	----	----	----	1500	2000	1500	1500	1500	1500
Power in KVA		1.1	5.0	6.7	6.8	7.2	2.0	2.8	3.5	5.4	6.7	7.0
Temperature in ^{o}C:	TC 1	1285	1130	920	1345	1210	1290	1335	1295	1334	1305	1195
	TC 2	1300	1180	970	1280	1120	1300	1300	1300	1300	1265	1150
	TC 3	1290	1180	950	1235	1170	1305	1265	1325	1300	1270	1140
	TC 4	1260	1290	1085	1260	1100	1320	1260	1290	1270	1242	1115

Table 7: Gas Pressure, Power Consumption and Temperature Distribution.

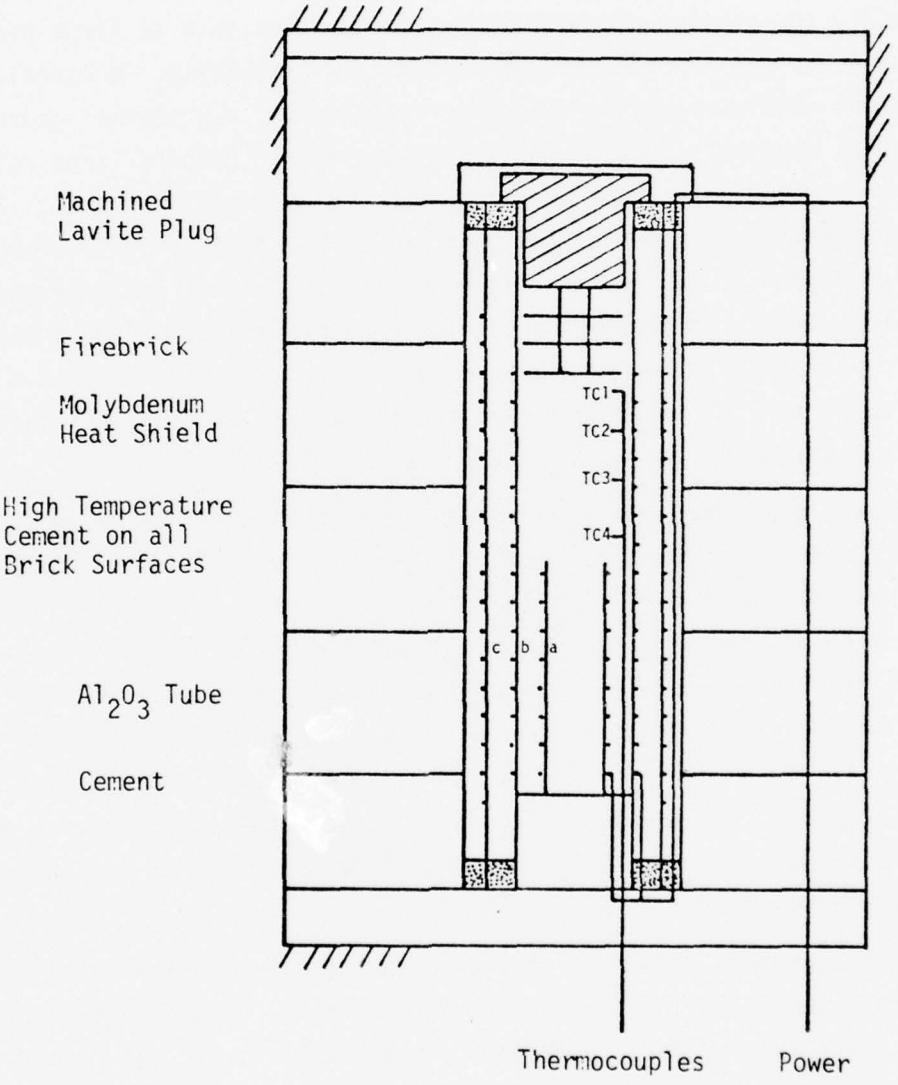

Figure 29. Gas Isostatic Hot Press Furnace.

3. COMPOSITE MATERIALS FOR ELECTRONIC COMPONENTS

3.1. General

If one considers, in the most general way, an operating electronic device, there are usually several phases involved and a number of material parameters to be optimized. An electromechanical transducer for example may require for a specific application a combination of properties such as large piezoelectric coefficient (d or g), low density and mechanical flexibility. A pyroelectric detector might require large pyroelectric coefficient, low thermal capacity, and low dielectric constant. Acousto-optic devices should require large refractive index, large elastic compliance and large photo-elastic coefficients. In general, the task of the materials design may be considerably simplified if it is possible to devise a "figure of merit" which combines the most sensitive parameters in a form allowing simple intercomparison of the possible 'trade offs' in these different coefficients. In certain acousto-optic systems for example a useful figure of merit is $n^7\pi^2/\rho v^2$, where n is the refractive index, π the photo-elastic constant, v the acoustic velocity, and ρ the density.

In general, the figure of merit for an application involves several property coefficients which are sometimes conflicting in nature. To make a flexible electromechanical transducer it would be desirable to use the large piezoelectric effects in a poled ceramic piezoelectric, however, ceramics are brittle and stiff lacking the required flexibility whilst polymers which have the desired mechanical properties are very weak piezoelectrics. Thus, for such an application a composite material combining the desirable proportion of both separate phases may be vastly superior. The basic important problem is to effect the combination in such a manner as to exploit the desirable features of both components and thus maximize the required figure of merit.

Combining materials means not only choosing component phases with the right properties but also coupling them in the best manner. Connectivity of each individual phase is of major importance, since this controls the fluxes in each. Symmetry is a second important consideration, since symmetry and properties go 'hand in hand'. There are several levels of symmetry to be considered: the crystallographic symmetry of each phase, the symmetry after processing, the combined symmetry of the composite, and the environment impact on the total symmetry (electrodes, clamps, etc.).

The points of interest are schematically formalized in Figure 30, for a simple two-phase system. It is interesting to note that in some composites, as well as the initial modification of the individual properties of the separate phases (sum properties) the composite may exhibit completely new couplings (product properties) impossible in either separated phase. To illustrate, consider a composite of barium titanate and cobalt ferrite. The single crystal monodomain point symmetries are 4mm for $BaTiO_3$ and $\frac{4}{m}$ m'm' for $CoFe_2O_3$. When prepared as polycrystals the symmetries revert to spherical $\infty\infty$m. If poled, however, the ferroelectric ceramic becomes ∞m and the ferrimagnetic ceramic $\frac{\infty}{m}$ m'. If the poling fields are applied in the same direction, the net symmetry of the composite is ∞. This point symmetry exhibits the magnetoelectric effect, even though neither $BaTiO_3$ nor $CoFe_2O_4$ alone are magnetoelectric!

To illustrate the major modifications in ensemble properties which can be effected even in simple linear systems, one dimensional solution has been obtained for the piezoelectric and pyroelectric properties of lamellar heterogeneous two-phase structures.

3.2. Lamellar Diphasic Composites

3.2.1. Piezoelectric Properties

(a) Series Connection: The longitudinal piezoelectric response $\bar{d}_{33}$ has been derived for a diphasic piezoelectric with the constituent phases arranged in alternating layers normal to the 3-direction (Figure (31)).

Designating phase 1 with a superscript 1, and phase 2 with superscript 2, the phase 1 has a volume fraction ^1v, piezoelectric $^1d_{33}$ and permittivity $^1\varepsilon_{33}$, and phase 2 has ^2v, $^2d_{33}$ and $^2\varepsilon_{33}$, respectively.

Solving for the converse effect given by

$$\bar{S}_3 = \bar{d}_{33}\,\bar{E}_3 \tag{1}$$

and as a check, for the direct effect which is given by

$$\bar{P}_3 = \bar{d}_{33}\,\bar{T}_3 \tag{2}$$

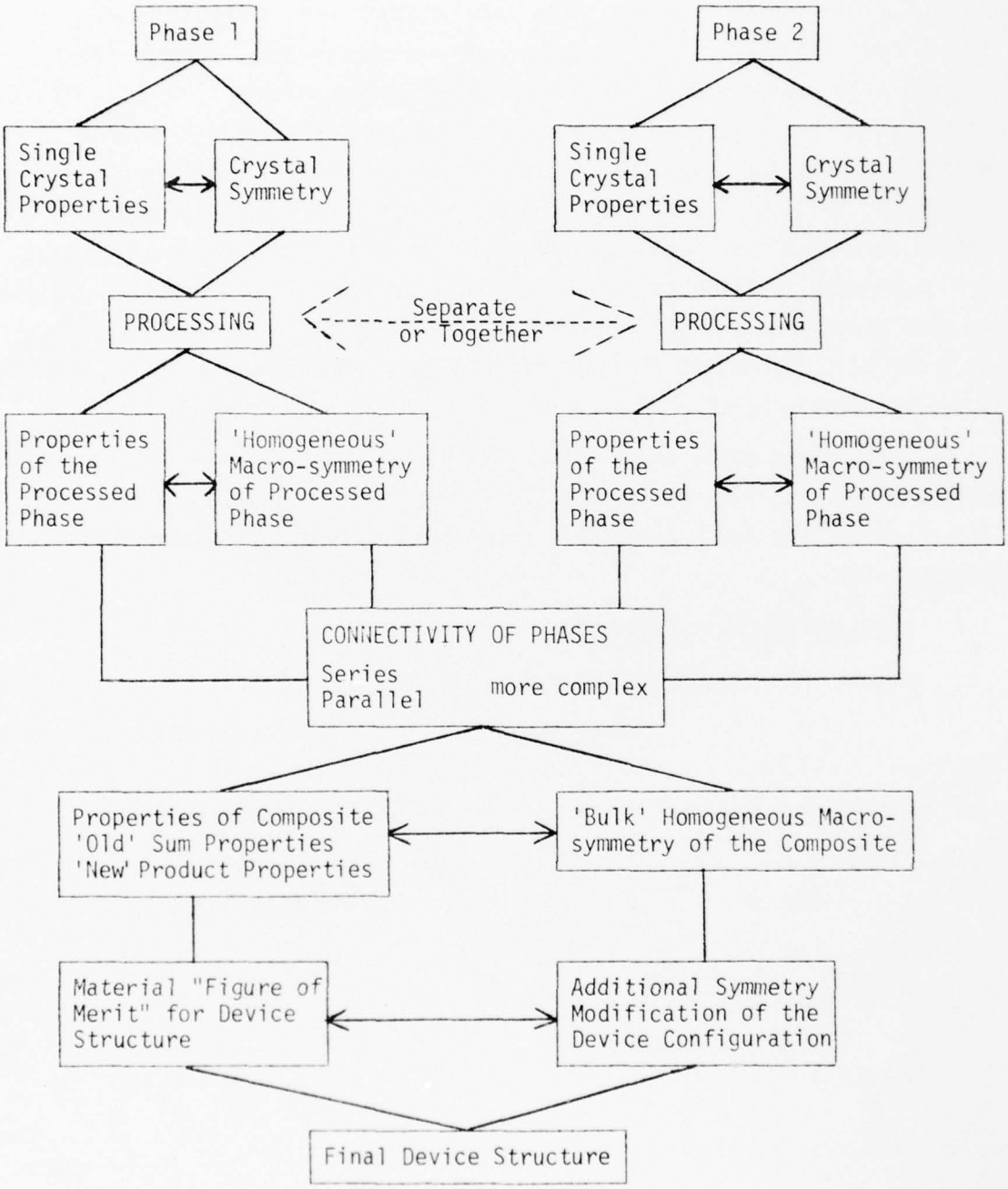
Phase 1
Phase 2
Single Crystal Properties
Crystal Symmetry
Single Crystal Properties
Crystal Symmetry
PROCESSING
Separate or Together
PROCESSING
Properties of the Processed Phase
'Homogeneous' Macro-symmetry of Processed Phase
Properties of the Processed Phase
'Homogeneous' Macro-symmetry of Processed Phase
CONNECTIVITY OF PHASES
Series
Parallel
more complex
Properties of Composite
'Old' Sum Properties
'New' Product Properties
'Bulk' Homogeneous Macro-symmetry of the Composite
Material "Figure of Merit" for Device Structure
Additional Symmetry Modification of the Device Configuration
Final Device Structure

Figure 30

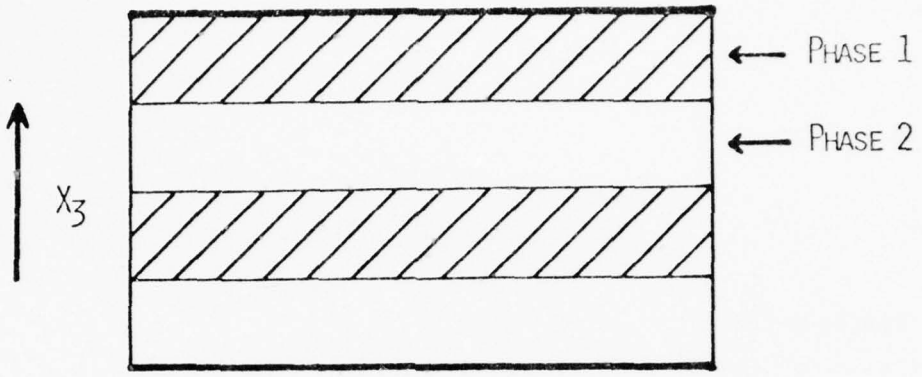

SERIES MODEL

Figure 31

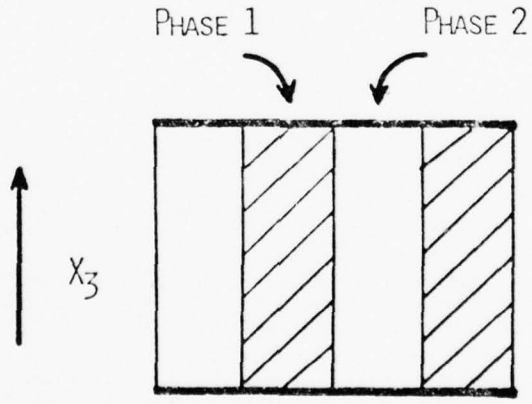

PARALLEL MODEL

Figure 32

gives

$$\bar{d}_{33} = \frac{{}^1v\,{}^1d_{33}\,{}^2\varepsilon_{33} + {}^2v\,{}^2d_{33}\,{}^1\varepsilon_{33}}{{}^1v\,{}^2\varepsilon_{33} + {}^2v\,{}^1\varepsilon_{33}} \tag{3}$$

and using the relation

$$\bar{g}_{33} = \bar{d}_{33}/\bar{\varepsilon}_{33} \tag{4}$$

yields the simple relation

$$g_{33} = \frac{{}^1v\,{}^1d_{33}}{{}^1\varepsilon_{33}} + \frac{{}^2v\,{}^2d_{33}}{{}^2\varepsilon_{33}} = {}^1v\,{}^1g_{33} + {}^2v\,{}^2g_{33} \tag{5}$$

It is interesting to note that for this case (neglecting transverse coupling) the elastic constants do not enter equations (3) or (5). To obtain some 'feel' for what the equations mean consider two simple extreme examples.

A strong piezoelectric e.g., PZT, interleaved with a small volume fraction of a low permittivity non-piezoelectric polymer or glass dielectric.

Taking ${}^1d_{33} = 3 \times 10^{-10}$ m/V, ${}^2d_{33} = 0$, ${}^1\varepsilon_{33} = 2000\varepsilon_o$, ${}^2\varepsilon_{33} = {}^2\varepsilon_o$. ${}^1v = 0.99$, ${}^2v = 0.01$ gives

$$\begin{aligned} \bar{d}_{33} &\simeq 0.09\, d_{33} \\ \bar{g}_{33} &\simeq g_{33} \end{aligned} \tag{6}$$

Thus even a very thin low permittivity layer rapidly lowers the d-coefficient but has little effect upon the corresponding g-coefficient.

As an opposite extreme example, consider a normal low permittivity piezoelectric such as quartz, interleaved with a high permittivity non-piezoelectric antiferroelectric like $NaNbO_3$.

Taking ${}^1\varepsilon_{33} = 5\varepsilon_o$, ${}^2\varepsilon_{33} = 5{,}000\varepsilon_o$, ${}^2d_{33} = 0$ and ${}^1v = {}^2v = \frac{1}{2}$ gives

$$\begin{aligned} \bar{d}_{33} &\simeq {}^1d_{33} \\ \bar{g}_{33} &\simeq {}^1g_{33}/2 \end{aligned} \tag{7}$$

In this case, the d-coefficient is not significantly changed, whilst the g-coefficient has been significantly reduced.

It may also be shown in general from equation (3) if ${}^1d_{33} \simeq {}^2d_{33}$ then $\bar{d}_{33} \simeq {}^1d_{33}$ and if ${}^1d_{33} >> {}^2d_{33}$

$$\bar{d}_{33} = {}^1d_{33} \left(\frac{{}^1v\,{}^2\varepsilon_{33}}{{}^1v\,{}^2\varepsilon_{33} + {}^2v\,{}^1\varepsilon_{33}}\right) \tag{8}$$

Thus since the expression in parentheses is always less than 1 it is not possible WITH LINEAR MATERIALS to obtain $\bar{d}_{33}$ greater than ${}^1d_{33}$ by this mode of mixing.

(b) Parallel Connection: If the two phases run in stripes perpendicular to the electrode (Figure 32), again for the one-dimensional case (neglecting transverse coupling)

$$\bar{d}_{33} = \frac{{}^1v\,{}^1d_{33}\,{}^2s_{33} + {}^2v\,{}^2d_{33}\,{}^1s_{33}}{{}^1v\,{}^2s_{33} + {}^2v\,{}^1s_{33}} \tag{9}$$

where ${}^1s_{33}$ and ${}^2s_{33}$ are the elastic compliances for stresses normal to the electrodes (in the 3-direction), and for the voltage coefficient

$$\bar{g}_{33} = \frac{{}^1v_1\,{}^1d_{33}\,{}^2s_{33} + {}^2v\,{}^2d_{33}\,{}^1s_{33}}{({}^1v\,{}^2s_{33} + {}^2v\,{}^1s_{33})({}^1v\,{}^1\varepsilon_{33} + {}^2v\,{}^2\varepsilon_{33})} \tag{10}$$

The case which is of most interest here is that of an elastically compliant non-piezoelectric in parallel with a stiff piezoelectric

In this case
$$\begin{aligned} {}^1d_{33} &>> {}^2d_{33} = 0 \\ {}^1s_{33} &<< {}^2s_{33} \\ {}^1v &= {}^2v = 0.5 \end{aligned} \tag{11}$$

then $\bar{d}_{33} \simeq {}^{1}d_{33}$

if ${}^{1}\varepsilon_{33} >> {}^{2}\varepsilon_{33}$

then $\bar{g}_{33} \simeq 2^{1}g_{33}$ (12)

and for smaller volume fractions of the piezoelectric phase, the g-coefficient is correspondingly amplified.

It is this case which accounts for the very highly successful performance of the replamineform transducer structure.

To evaluate the effective hydrostatic sensitivity for the series connection, it is necessary to evaluate the transverse piezoelectric coefficient d_{31} since

$$P_3 = - (\bar{d}_{33} + 2\bar{d}_{31})\,\sigma \tag{13}$$

where σ is the applied hydrostatic pressure. It can be shown that

$$\bar{d}_{31} = {}^{1}v\,{}^{1}d_{31} + {}^{2}v\,{}^{2}d_{31} \tag{14}$$

so that

$$\bar{d}_h = \bar{d}_{33} + 2\bar{d}_{31} = \frac{{}^{1}v\,{}^{1}d_{33}\,{}^{2}s_{33} + {}^{2}v\,{}^{2}d_{33}\,{}^{1}s_{11}}{{}^{1}v\,{}^{2}s_{33} + {}^{2}v\,{}^{1}s_{33}} + 2({}^{1}v\,{}^{1}d_{31} + {}^{2}v\,{}^{2}d_{31}) \tag{15}$$

A problem for using PZT type materials in single phase macro-homogeneous hydrostatic sensors is that $d_{33} \simeq -2d_{31}$ yielding a very low value for hydrostatic sensitivity.

Suppose for the composite we chose equal volumes of a piezoelectric PZT and a soft elastomer ${}^{2}v = {}^{1}v = 0.5$, ${}^{1}d_{33} >> {}^{2}d_{33}$, ${}^{1}s_{33} << {}^{2}s_{33}$ and ${}^{1}d_{33} \simeq -2{}^{1}d_{31}$.

Then for the composite $\bar{d}_{31} \simeq \frac{1}{2}d_{31}$ $\bar{d}_{33} \simeq d_{33}$

$$\therefore \quad \bar{d}_h \simeq \frac{1}{2}\,{}^{1}d_{33} \tag{16}$$

which is a very considerable improvement over the single phase performance. Since also the hydrophones used under hydrostatic conditions are voltage generators then the further favorable enhancement of the $\bar{g}_h$ can be exploited.

3.2.2. Pyroelectrics

The corresponding series and parallel connected diphasic systems have also been studied for their pure pyroelectric response. In this case the results of themselves are not of very special interest, however, the comparison to the corresponding piezoelectric solutions is quite informative. What is of much more practical interest is the next step which is to include the elastic interactions due to thermal expansion.

It is well known that all pyroelectric crystals are also piezoelectric. That the thermal expansion generated on heating gives rise to a strain which operates through the piezoelectric coefficients to give an additional secondary pyroelectric effect. If the crystal is free to expand, what is normally measured is the sum of primary and secondary effects, and in many materials both components are of the same order of magnitude.

It must be remembered, however, that in many crystals (poled PZT is a good example) the hydrostatic piezoelectric effect is small, due to cancellation between coefficients with opposite sign. Clearly if the negative part of the piezoelectric response could be removed by suitable clamping, the secondary contribution to the pyroelectric effect could be strongly enhanced. For this reason it is important to begin the study of connectivity in diphasic pyroelectrics.

(a) Simple Series Connection: Consider the response of a multilayer 2-phase pyroelectric (Figure 31) made up from a volume fraction ${}^{1}v$ of phase with permittivity ${}^{1}\varepsilon_{33}$ and pyroelectric coefficient ${}^{1}p_3$, interleaved along the 3-direction with a phase of volume fraction ${}^{2}v$, permittivity ${}^{2}\varepsilon_{33}$ and pyroelectric coefficient ${}^{2}p_3$.

Subjected to a uniform temperature change, the mean pyroelectric coefficient $\bar{p}_3$ is given by

$$\bar{p}_3 = \frac{{}^1v\,{}^1p_3\,{}^2\varepsilon_{33} + {}^2v\,{}^2p_3\,{}^1\varepsilon_{33}}{{}^1v\,{}^2\varepsilon_{33} + {}^2v\,{}^1\varepsilon_{33}} \tag{17}$$

Identical in form to Equation (3) for the piezo-response in series connection.

A crude figure of merit for a pyroelectric is given by $\frac{\bar{p}_3}{\bar{\varepsilon}_{33}}$ (comparable to the piezoelectric $\bar{g}_{33}$) which yields

$$\bar{A} = \frac{\bar{p}_3}{\bar{\varepsilon}_{33}} + {}^1v\,\frac{{}^1p_3}{{}^1\varepsilon_{33}} + {}^2v\,\frac{{}^2p_3}{{}^2\varepsilon_{33}} = {}^1v\,{}^1A + {}^2v\,{}^2A \tag{18}$$

Clearly though the pyroelectric coefficient itself will be rapidly reduced by interleaving a phase of lower permittivity, the figure of merit is little affected.

(b) Parallel Connection: For the arrangement shown in Figure (32), using again the same symbols

$$\bar{p}_3 = {}^1v\,{}^1p_3 + {}^2v\,{}^2p_3 \tag{19}$$

which is very much different from equation (9) for the corresponding parallel connection in the piezoelectric.

For this case

$$\bar{A} = \frac{\bar{p}_3}{\bar{\varepsilon}_{33}} = \frac{{}^1v\,{}^1p_3 + {}^2v\,{}^2p_3}{{}^1v\,{}^1\varepsilon_{33} + {}^2v\,{}^2\varepsilon_{33}} \tag{20}$$

Now one notes that the figure of merit cannot be raised above the figure of merit for the single phase (contrary to the $\bar{g}_{33}$ in the piezoelectric case).

3.2.2.1. Piezoelectric Contributions

(a) Series Connection: To simplify the calculation we assume again the structure of Figure 31, but now each phase is presumed to have conical symmetry (∞m) with the polar 3-axis perpendicular to the plane of the interleaving sheets.

Taking close transverse connection of thin sheets

$$^1s_1 = {}^2s_1 = {}^1s_2 = {}^2s_2$$

and assuming no surface tractions so that

$$^1\sigma_3 = {}^2\sigma_3 = 0$$

For a uniform temperature change ΔT.

$$\bar{p}_3 = \frac{^1v\,{}^1p_3\,{}^2\varepsilon_{33} + {}^2v\,{}^2p_3\,{}^1\varepsilon_{33}}{^1v\,{}^2\varepsilon_{33} + {}^2v\,{}^1\varepsilon_{33}} +$$

$$\frac{2\,{}^1v\,{}^2v({}^2\varepsilon_{33}\,{}^1d_{31} - {}^1\varepsilon_{33}\,{}^2d_{31})({}^2\alpha_1 - {}^1\alpha_1)}{({}^1v\,{}^2\varepsilon_{33} + {}^2v\,{}^1\varepsilon_{33})[{}^1v({}^2s_{11} + {}^2s_{12}) + {}^2v({}^1s_{11} + {}^1s_{12})]} \qquad (21)$$

and for the figure of merit

$$\frac{\bar{p}_3}{\bar{\varepsilon}_{33}} = \frac{^1v\,{}^1p_3}{^1\varepsilon_{33}} + \frac{^2v\,{}^2p_3}{^2\varepsilon_{33}} + \frac{2\,{}^1v\,{}^2v({}^2\alpha_1 - {}^1\alpha_1)}{[{}^1v({}^2s_{11} + {}^2s_{12}) + {}^2v({}^1s_{11} + {}^1s_{12})]}\left(\frac{^1d_{31}}{^1\varepsilon_{33}} - \frac{^2d_{31}}{^2\varepsilon_{33}}\right) \qquad (22)$$

(b) Parallel Connection: For the system shown in Figure (32) assuming that the only constraint is in the x_3 direction and that the material is free to expand in x_1 and x_2

$$\bar{p}_3 = {}^1p_3\,{}^1v + {}^2p_3\,{}^2v + \frac{({}^1d_{33} - {}^2d_{33})\,{}^1v\,{}^2v\,({}^2\alpha_3 - {}^1\alpha_3)}{{}^1v\,{}^2s_{33} + {}^2v\,{}^1s_{33}} \qquad (23)$$

3.3. Replamineform Transducers

3.3.1. Replication on a Natural Coral Template

The replamineform process has been used to produce diphasic PZT:silicone rubber composite transducers. This process which was originally developed in the Materials Research Laboratory at Penn State for prosthetic materials utilizes the calcium carbonate skeleton structure of natural coral as a microstructural template with complete connectivity (3:3) i.e., in coral both the carbonate phase and the pore space are continuously connected between each surface.

The advantage in duplicating a PZT with the coral microstructure is that the three-dimensional connectivity ensures a continuous dielectric flux path between surfaces, so that the PZT phase can be electrically poled to a saturation remanence by normal external electrodes.

The first step of the replamine process is to shape the coral, which is quite easily machinable, to the desired geometry. The coral is then vacuum impregnated with casting wax and the wax allowed to harden. The calcium carbonate skeleton of the coral is then leached away in weak hydrochloric acid leaving a wax negative of the original template structure.

This negative is then re-impregnated with a PZT slip of suitable composition, which contains a small addition of a PVA binder. The impregnated wax template is then subjected to heat treatment to burn out the wax. After burnout, the PZT positive is then sintered under proper atmosphere control to yield a porous PZT replica of the original coral structure. The replica is then again back-filled under vacuum with a silicone rubber or another suitable polymer. The surfaces are then cleaned and polished to expose the ceramic phase, electroded and poled under normal poling conditions.

Replication experiments have been carried through using coral of the species porites goniopera which has very well developed 3:3 connectivity (Figure 33) in the microstructure and using the species porites-porites (Figure 34) which has the connectivity better developed in one dimension.

From the linear models considered in the previous section it would appear that the ideal connectivity would be of the 3:1 type (Figure 35). Unfortunately, the porites-porites which most closely resembles this required structure, though of wide natural abundance, is at present in short supply at the laboratory, and most work has been carried through on the goniopera genus.

Figure 36 shows a typical microstructure developed in a replamine replica of goniopera using Ultrasonics PZT-501. It is evident by intercomparing Figures 33 and 36 that the original coral template has been quite faithfully reproduced in the PZT by the replamine processing.

The ceramic body has a solid surface area which averages 37% PZT. Samples impregnated with silicon rubber and poled electrically yield values of d_{33} as measured on the Berlincourt d_{33} meter $\sim 160 \times 10^{-12}$ C/N. The value obtained does not depend on the point of contact of the d-meter and similar values are measured if the sample is mounted between stiff metal plattens.

As poled, the replamine replica is still a rigid structure because of the 3:3 connection of the rigid ceramic phase. If, however, the body is 'crushed' to lower the transverse connectivity, an extremely flexible composite results (Figure 37). After crushing, the d-values are slightly degraded, but g_{33} now becomes large with values larger than 200 m^2/C ($\times 10^{-3}$) commonly occurring.

To further improve the g_{33} values, samples are now being fabricated using a softer PZT (Ultrasonics 1002). For improved poling we are also experimenting with a more rigid matrix polymer which may facilitate cleaning of the composite surface to be electroded.

Currently a flexible electrode material obtained from Technit Corp., is being used for measurements, but this is not entirely satisfactory and does show fatigue effects under elastic cycling. We are experimenting with a number of different approaches to produce a more satisfactory electrode for the highly flexible silicone rubber composites.

Currently experiments are being planned and carried forward to evaluate the coupling efficiency of these flexible transducers in water, and then obtain more precise measurements of the hydrostatic sensitivity.

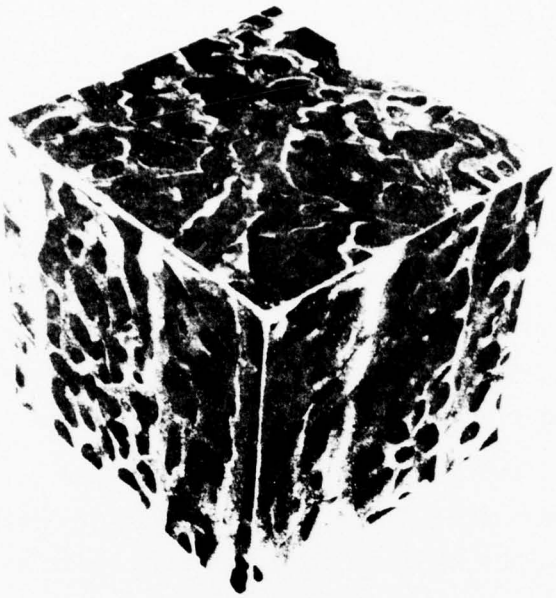

Microstructure of porites goniopera. (approx. 20X)

Figure 33

Microstructure of porites porites. (approx. 20X)

Figure 34

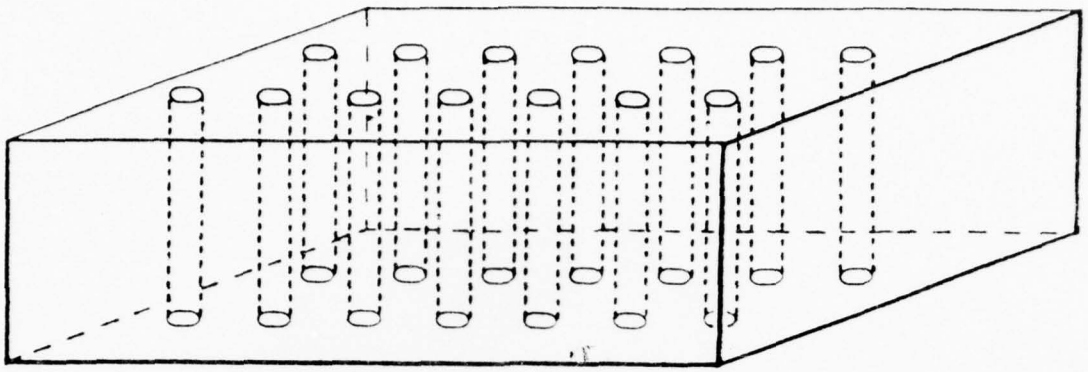

A 3-1 structure. One dimensionally connected columns in a three dimensionally coneected matrix.

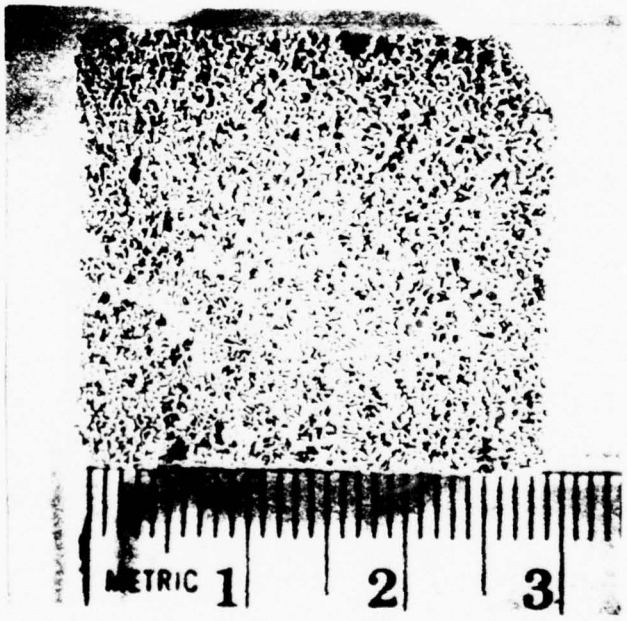

PZT replica of porites goniopera.

Figure 36

PZT : silicon rubber composite transducer showing the high degree of flexibility attainable.

Figure 37

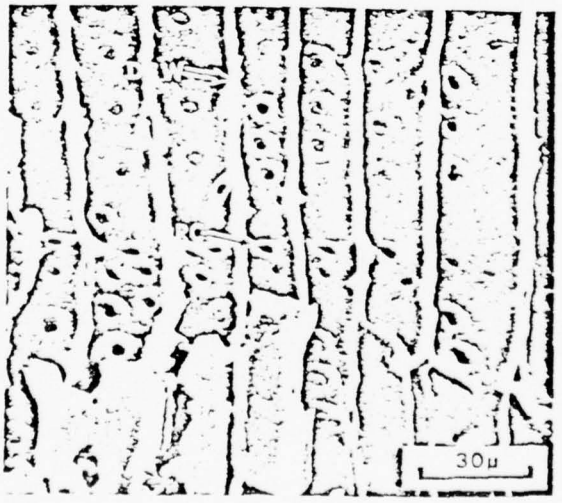

Microstructure of a hardwood charcoal showing large channels (vertically) and the small diameter interconnections.

Figure 38

3.3.2. Alternative Template Structures

Over the past three months some effort has been directed towards finding alternative template materials which might have the required connectivity.

Studies of polymer foams have shown somewhat similar pore structures, but, at the level when continuous porosity is well developed, the solid phase only occupies some 12 volume percent. Preliminary replication studies show that this is too small for effective transducer performance.

The microstructures of some monocotyledons appear promising and, in this family, corn stalks are being investigated. Various types of common hardwoods which have been partially charred are being studied. Of the pyrolized wood structures, red oak has the proper type and dimensions of channel structure (Figure 38).

The charcoal templates which have been invested with PZT slip have to date produced dominantly rod-like structures with very limited cross connection. The problem is felt to be probably associated with the very hygroscopic nature of the pyrolized wood, which appears to be affecting the PZT slip. Experiments are now proceeding to adjust the pH and constitution of the slip to combat these problems.

4. ELECTROSTRICTION TRANSDUCERS

4.1. Multilayer Monolithic Structures

In the 1976 contract year, the large electrostrictive deformations which could be realized in monolithic multilayer bodies fabricated from conventional high K capacitor dielectrics were documented. The electrostrictive origin for the observed behavior was confirmed and the concommitant absence of aging and deaging phenomena which occur when high amplitude DC fields are applied to conventional PZT ceramics documented.

Based on these studies, a joint program with Erie Technological Products was formulated be fabricate larger test samples which could be subjected to the more detailed testing required for application in commercial position control systems. This joint proposal was funded in June 1977 and the necessary fabrication of a range of larger multilayer structures is now proceeding under this contract.

To aid in the final choice of the precise composition to be chosen for initial fabrication, a series of pilot tests were run on small commercial elements fabricated from the K5,500 dielectric but with different minor phase additives which are used as "peak shifters" in fabricating the dielectric from commercial powders. The function of the 'peak shifters' is to trim the Curie temperature maximum to room temperature so as to satisfy dielectric specifications. Since experience had shown that the 'shifter' additive also modifies the grain size of the resultant ceramic quite markedly, it was thought desirable to ascertain the effect of additive doping upon the striction behavior before embarking upon large scale fabrication.

In Figure 39, 40 and 41 ε vs. T curves taken at 1 KHz, and static dilatation under field are compared for several doping levels. Clearly the proprietary additive trims T_C in the manner prescribed, however, this is at significant cost in the dilatation levels which can be achieved under field. It may be noted that the smaller additive level does reduce the minor hysteritic response on first poling and this may be useful for certain applications. On ballance, however, the improvement is not dramatic and it was decided to fabricate initial larger samples using the unmodified material.

It is anticipated that future studies on these systems will be carried foward on the new contract and thus will not be reported here.

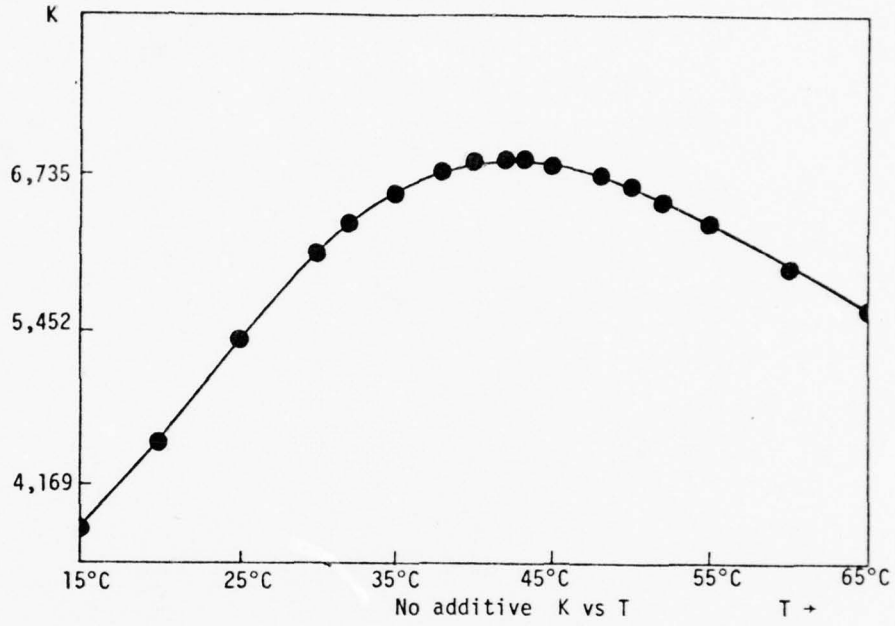

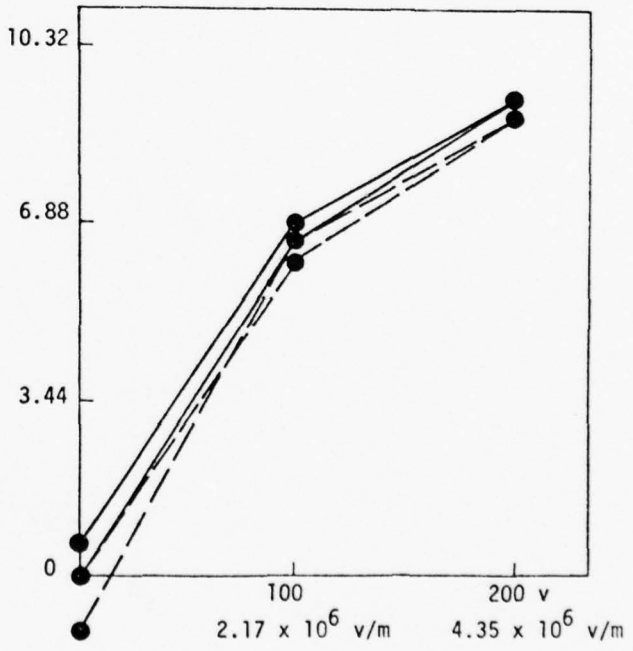

Fig. 39 Strain vs electric field

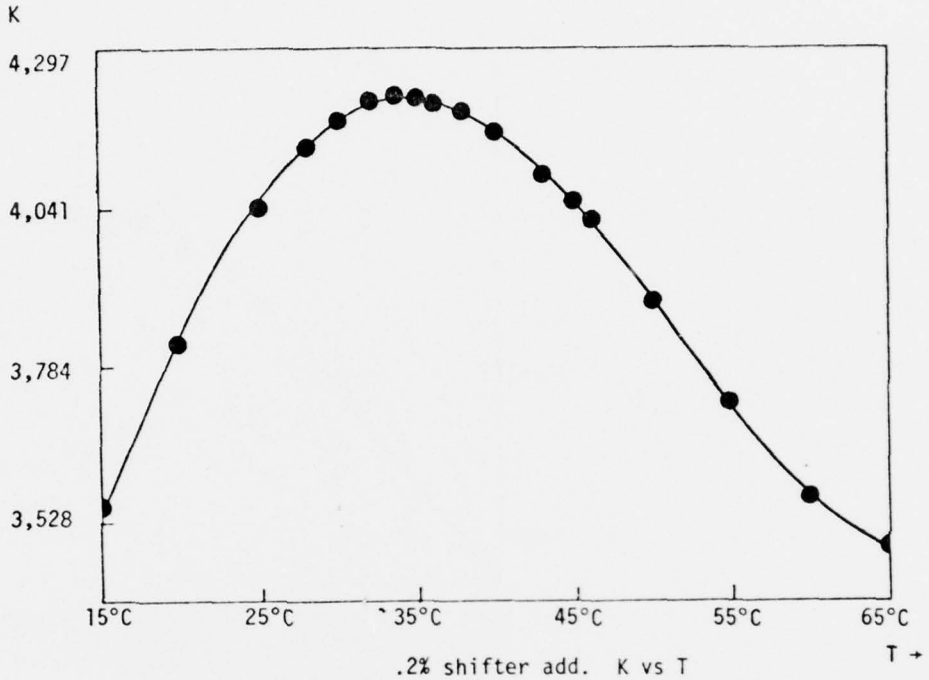

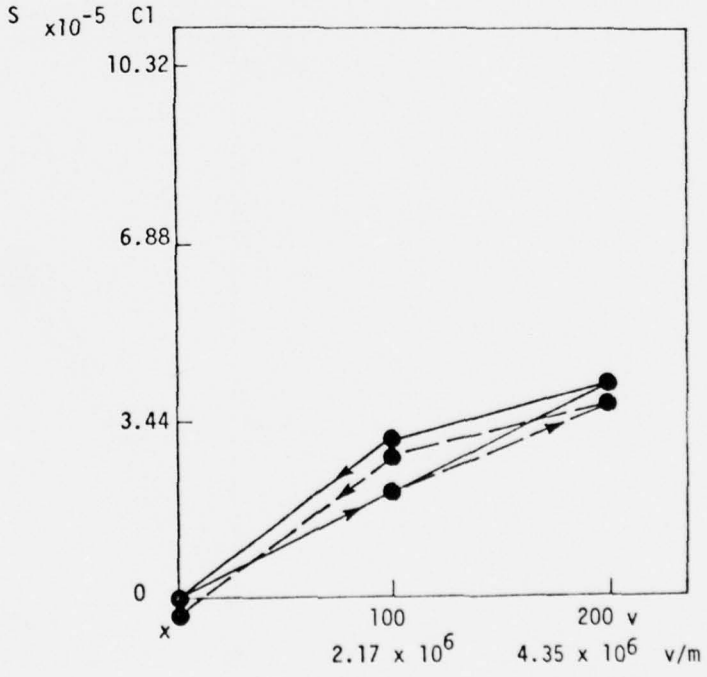

Fig. 40 Strain vs electric field

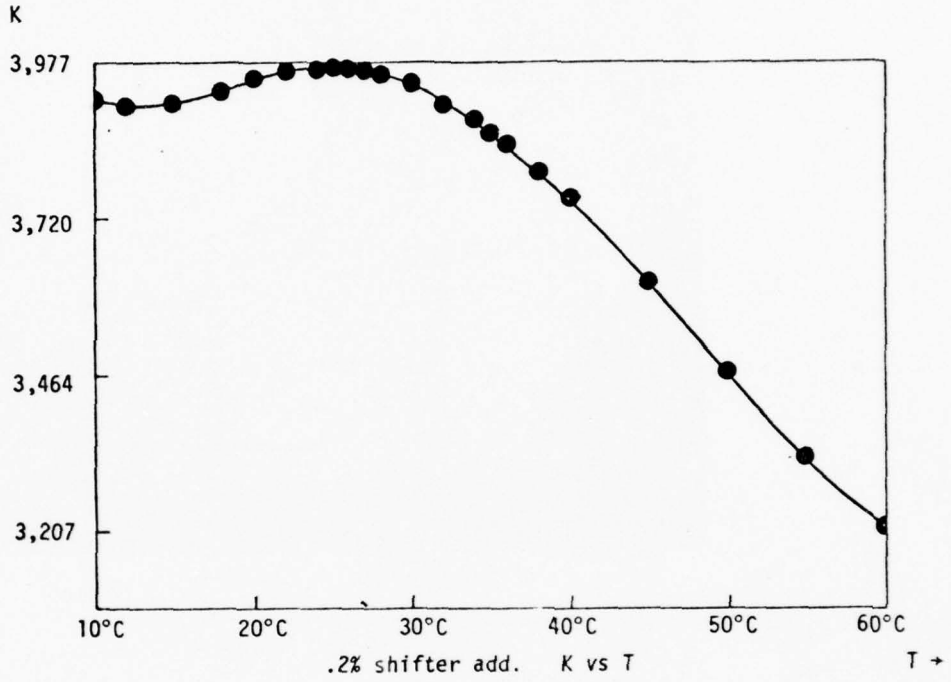

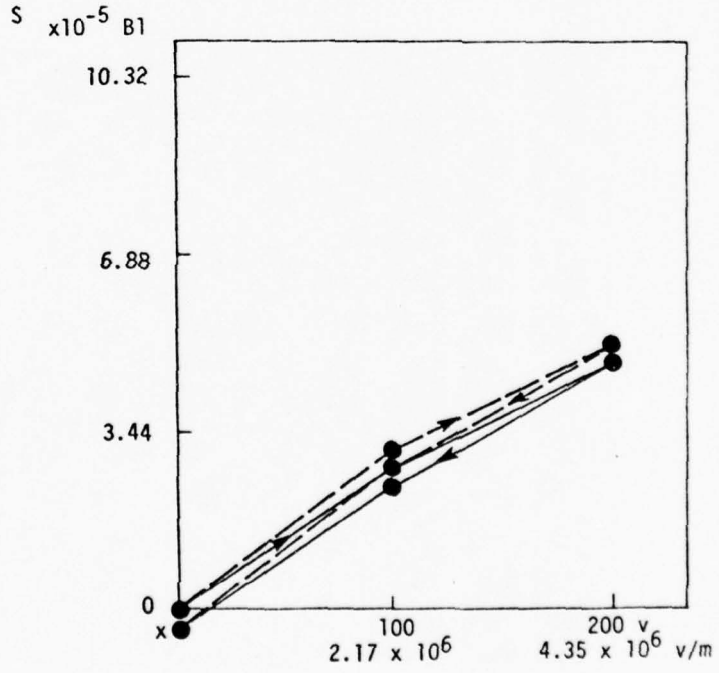

Fig. 41 Strain vs electric field

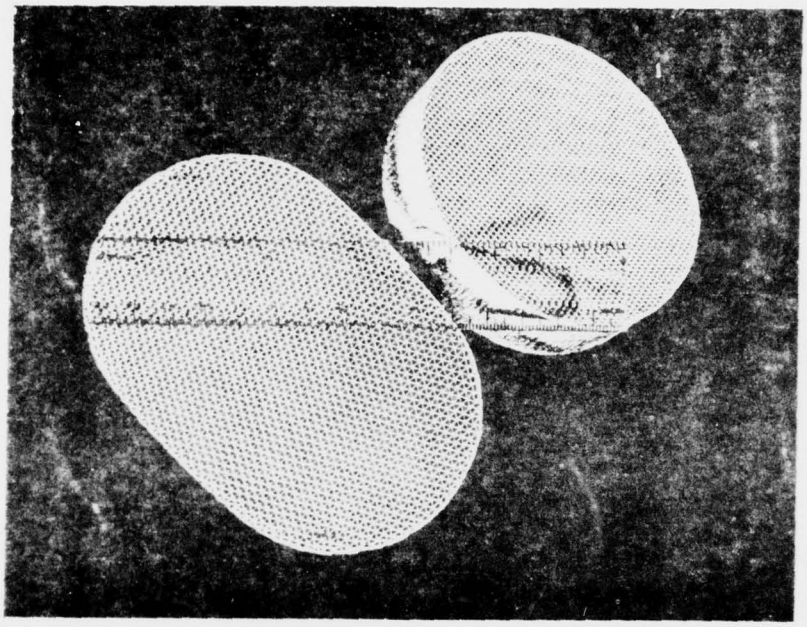

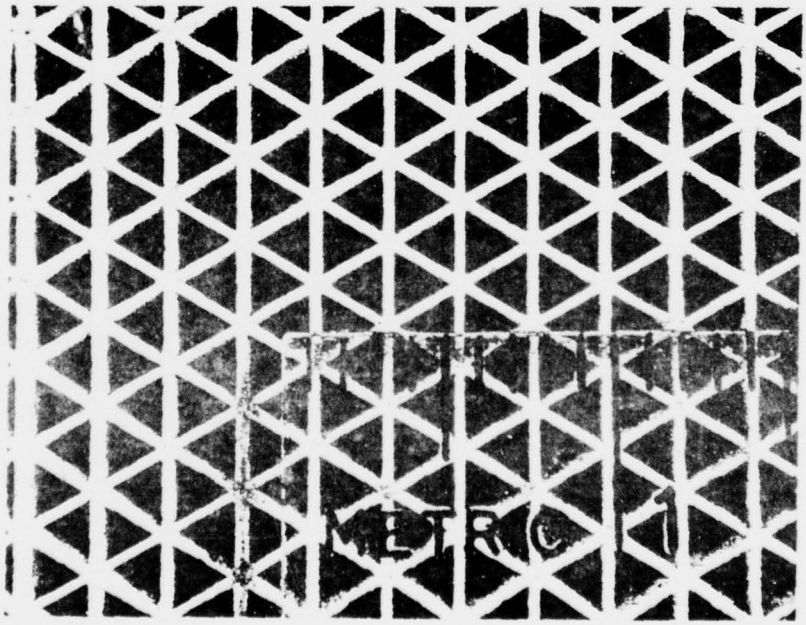

Figure 42

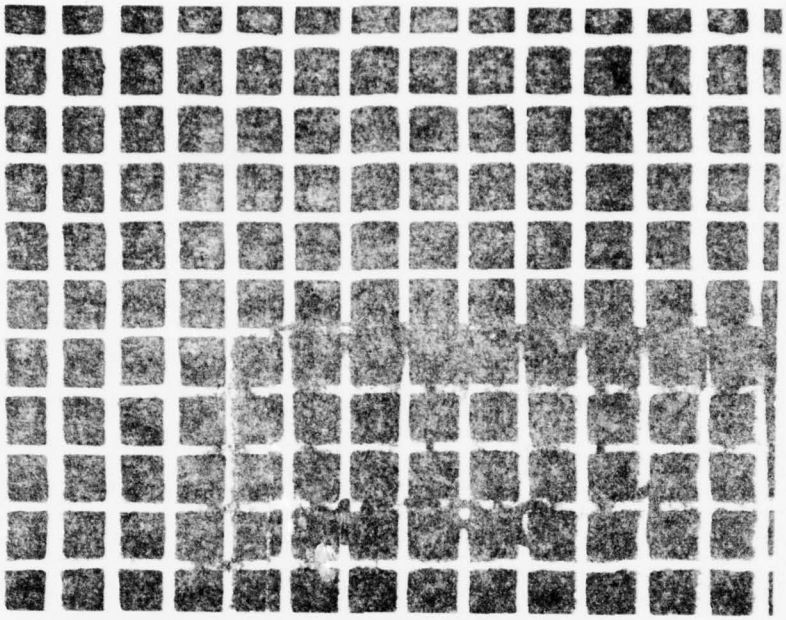

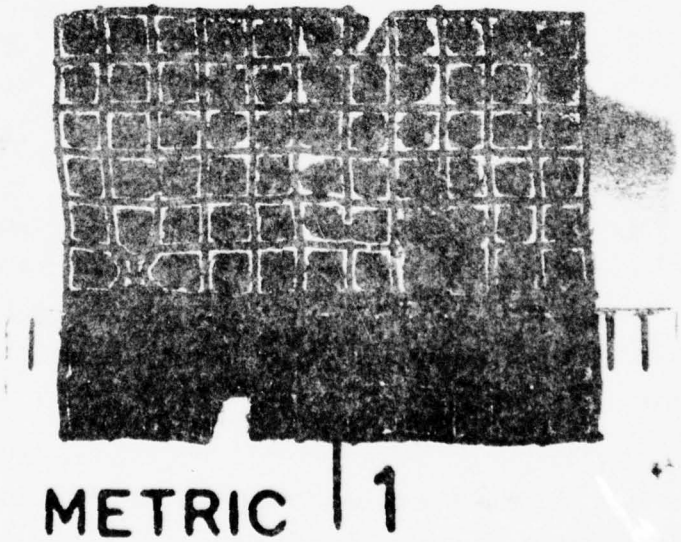

Figure 43

4.2. Extruded Multiply Connected Electrostriction Transducers

4.2.1. Introduction

During the early part of 1977, following contacts with ITEK, Boston and discussions upon some of the problems associated with the fabrication of multi-element mirror control systems based upon monolithic PZT transducers, contact was established with Corning Research Center, Corning, NY upon the possibility of fabricating extruded transducer arrays, based upon the technology which Corning has developed for the extruded exhaust catalyst structure.

By the Corning process, a tubular low expansion silicate based ceramic is extruded through a die set which establishes a closely space channel structure in the body. (Figure 42). The channels can have a square, hexagonal or triangular geometry and extent right through the tube. The channel size is of the order of 1.5 mm with a wall thickness down to 0.1 mm.

Clearly if the catalyst support structure could be duplicated in an electrostrictively active ceramic, by electroding the walls it should be possible by applying an electrical bias, to operate through the electrostrictive Q_{12} coefficient and change the length of the interconnected wall normal to the surface. For a thin membrane attached to the surface this should cause a puckering of the surface profile which could be regulated by the applied field.

Based on our original discussions, Corning Research Center agreed to fabricate several test specimens from their own K8,000 $BaTiO_3$ formulation, which is a Curie point suppressed ferroelectric.

4.2.2. Dielectric and Electrostriction Studies

Three sets of extruded samples have so far been supplied from Corning. The total circular cross-section was in each case $\sim$4 cm. The samples had a square grid channel structure with a wall spacing of $\sim$1.25 mm and a wall thickness of $\sim$0.25 mm. A typical cross section normal to the channel structure is shown in Figure 43.

For preliminary evaluation of the dielectric properties, several of the less well formed pieces were diamond sawed longitudinally parallel to one wall orientation and a flat plate sample of one wall thickness and of area suitable for capacitance measurement prepared. After polishing to a flat surface and cleaning, gold electrodes were evaporated onto the surfaces through a suitable masking system.

To evaluate the electrostrictive response, several short test sections of the best quality extrusions were sawed normal to the tube length, and polished to flat square grid surfaces. Silver electrodes were deposited down the length of the channels using long, thin wire type wooden bars and the end surfaces were cleaned and repolished. Electrical contact was made to the internal electrodes down each square channel using air drying silver. To investigate the bulk longitudinal electrostriction, contact was made to alternate diagonal rows of channels so that the E field could be applied to all inside walls simultaneously.

The first results for the dielectric permittivity as a function of temperature for sections from batches 1 and 2 are summarized in Figures 44 and 45 and the DC dilation behavior in Figure 46. Obviously, the dielectric permittivity in the batch 1 samples is much reduced from the level which should be realized in the formulation used.

Two factors appear to contribute to this undesirable

1. The density of the fired extruded samples was lower than the normal densities achieved with the dielectric formulation.

2. SEM pictures revealed what appears to be a silicate rich phase at the grain boundaries in the extruded samples.

It would appear from slow sweep Sawyer and Tower measurements taken on the dielectric samples that the resistivity of the grain boundary phase is lower than that of the bulk grain and larger polarization values could be induced than would be expected from the 1 KHz dielectric data.

The samples from batch 2 exhibit higher permittivity, but values which are still inferior to the expected response for this composition. For these samples, the bulk density has been improved, but is still too low, though the silica rich boundary phase has now been eliminated, and the Sawyer and Tower measurements show no enhancement of low frequency response.

In the DC dilatation measurements, Figure 46 the batch 1 samples show better sensitivity probably due to the Maxwell-Wagner polarization. Clearly, however, to achieve full response the fabrication procedure must be further improved. Additional work is now in progress.

4.3. New Materials for Electrostriction Transducers

The thrust of our current studies is to develop materials with larger electrostrictive response for static of low frequency position control and to explore some of the materials systems in which an electric field induced phase change may

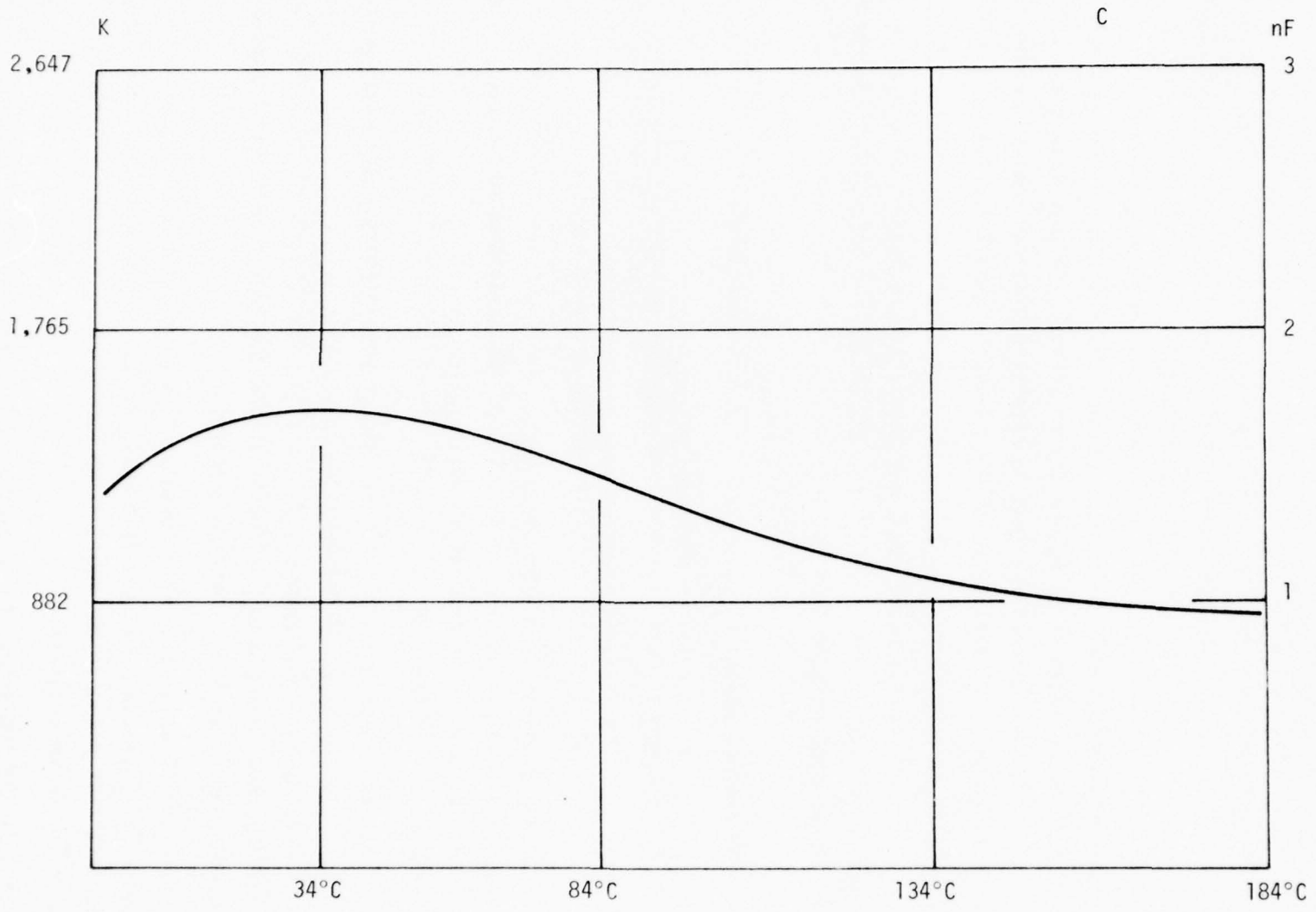

Batch 1 sample. KVS temp

Figure 44

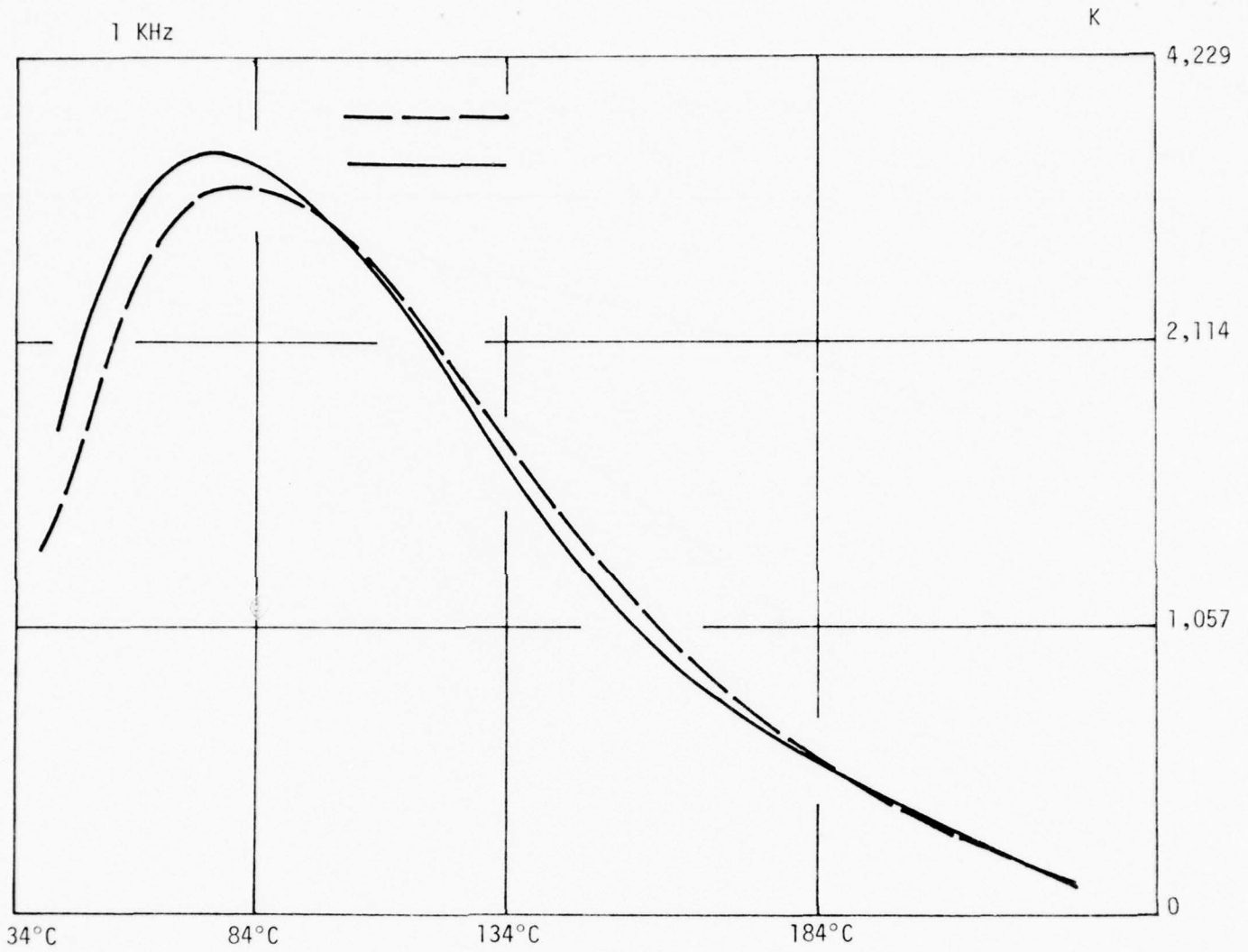

Extruded $BaTiO_3$ (K = 3,700 at rm temp) DT-100 5/10/77 Batch 2 Red - No bias
Green - with 50 v bias

Batch 2 sample KVS temp

Figure 45

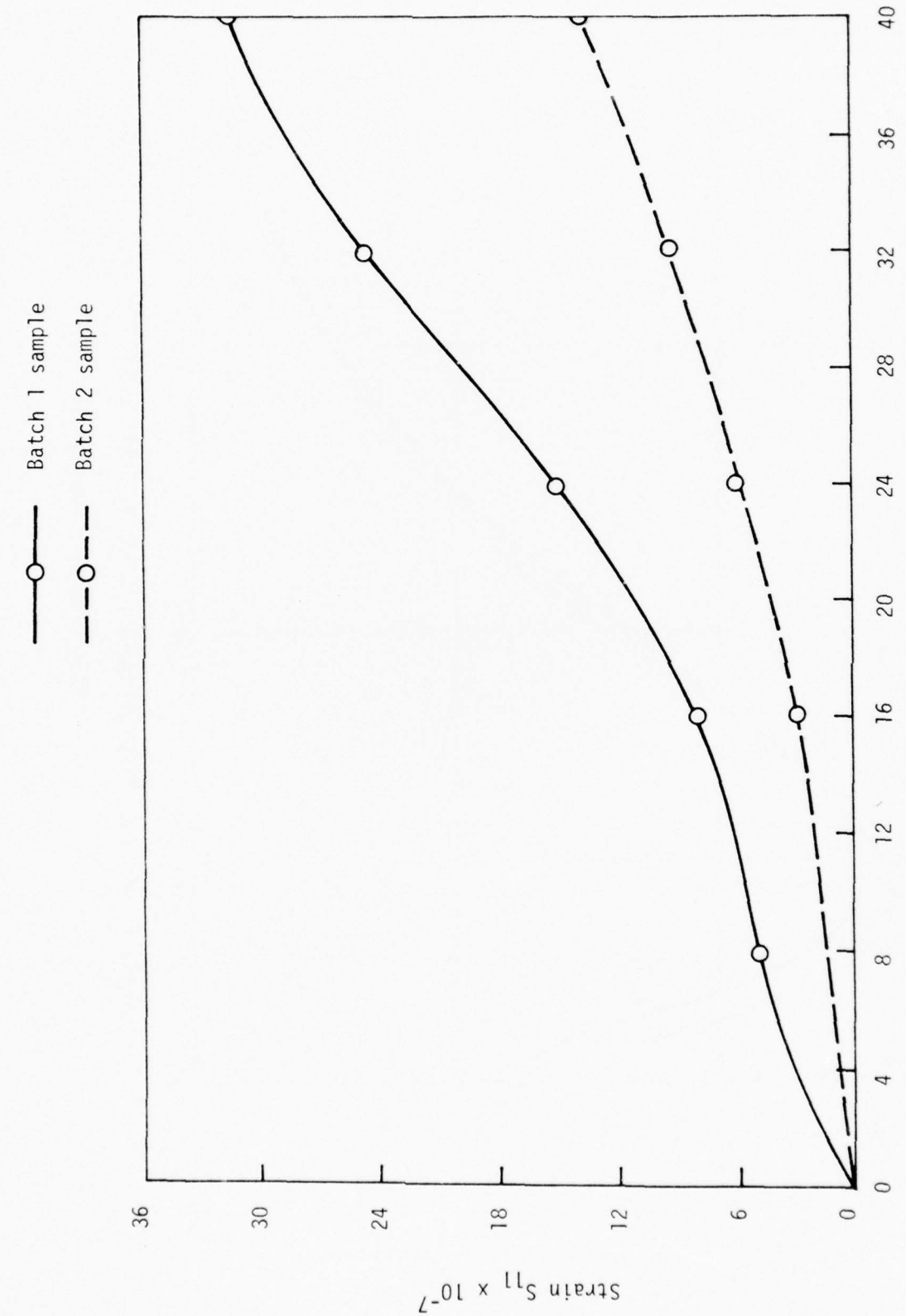

Figure 46

extruded thin wall $BaTiO_3$ sample

be used to generate and control a highly non-linear strain response.

Two areas of approach which suggest the possibility for major modification of the 'normal' paraelectric electrostrictive response involve systems which exhibit unusual time dependent dielectric response to electric field which has pronounced relaxation character.

4.3.1. Ferroelectric Relaxors

Considerable information is available, mostly in the Soviet literature, upon a large family of ferroelectrics which exhibit strong relaxation character in their dielectric response near to the ferroelectric Curie temperature (23, 24, 25). Lead-magnesium niobate ($Pb_3MgNb_2O_9$) is perhaps the best example, for which a wide spectrum of properties has been measured in both single and polycrystal samples. In this crystal, the unusual response has been traced to a statistical inhomogeneity in the distribution of the Mg^{2+} and Nb^{5+} ions upon the B-sites of the ABO_3 perovskite structure. This inhomogeneous distribution leads to a distribution of micro-volumes within the sample which drove widely different Curie temperature. Thus a cooling from high temperature, there is a Curie range rather than a distinct Curie point and within this Curie range the crystal exists as an intimate mixture of paraelectric and of ferroelectric volume elements.

The point which is of major interest for potential electrostriction applications is that for temperatures within this Curie range, the crystal can be poled into a strongly ferroelectric form, but, on removal of the poling field reverts back to a random arrangement of microdomain volumes with no net remanent moment. It is the growth, reorientation and subsequent decay of the microdomains which gives rise to the time dependent dispersive dielectric response over the Curie region.

High field dielectric measurements of 60 Hz for temperatures just below the Curie range show an apparant normal hysteritic response with large levels of induced polarization (26). However, low frequency pyroelectric studies clearly indicate that the apparent remanence is spurious (27) and is associated with the more slowly decaying domain component of the total polarization i.e., the pyroelectric measurement shows only an S-shaped saturation curve without remanence.

Clearly, then in the ferroelectric relaxors the possibility exists for utilizing the major poling strain for position control and for generating a high strain device which would be a close dielectric analogue of the magnetostrictive systems.

A critical initial datum required is a measure of the simple electrostriction in a relaxor ferroelectric for some temperature above the Curie range. If the magnitudes

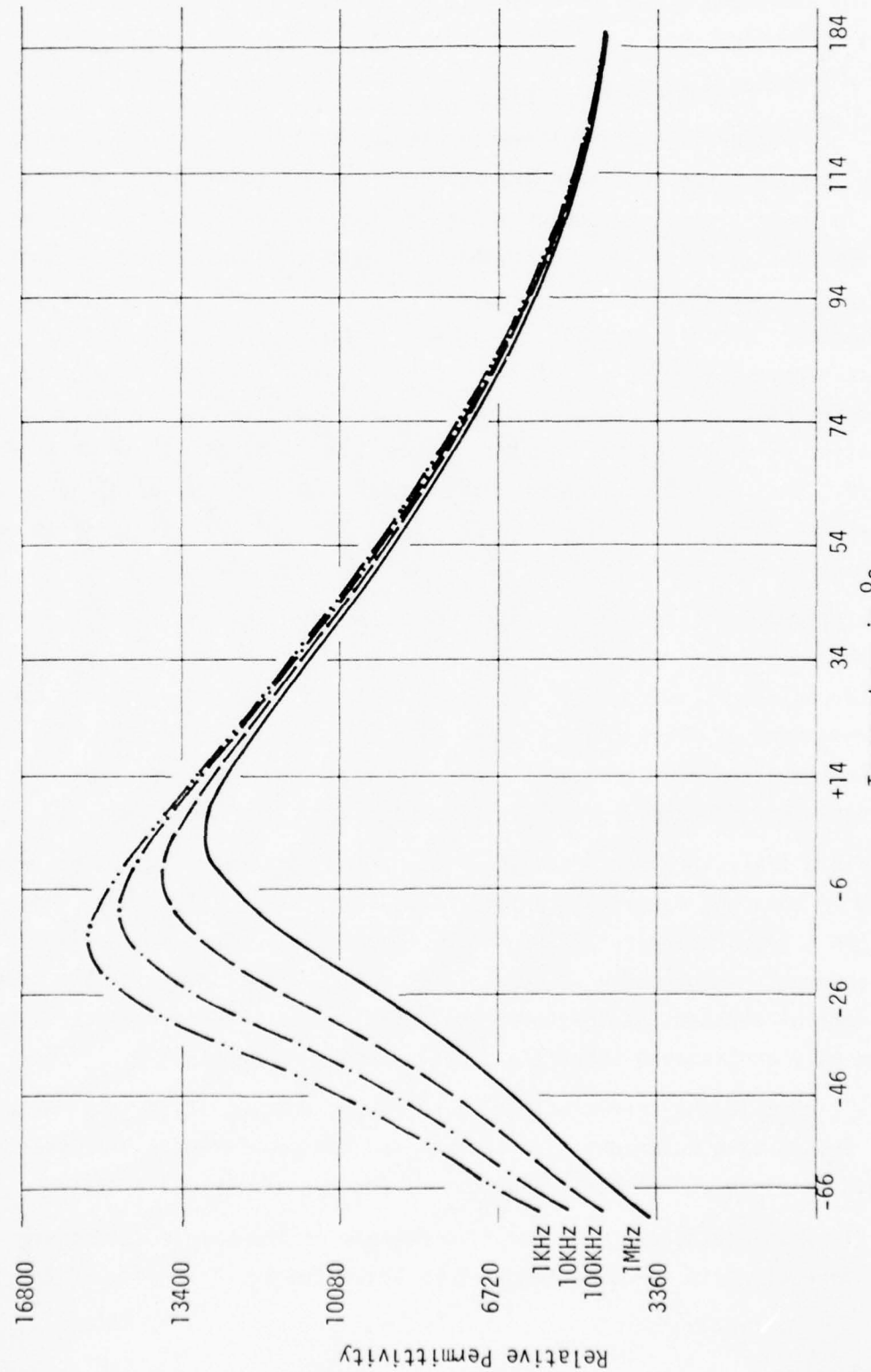

Fig. 47 Weak field dielectric permittivity as a function of frequency and temperature in ceramic $Pb_3MgNb_2O_9$

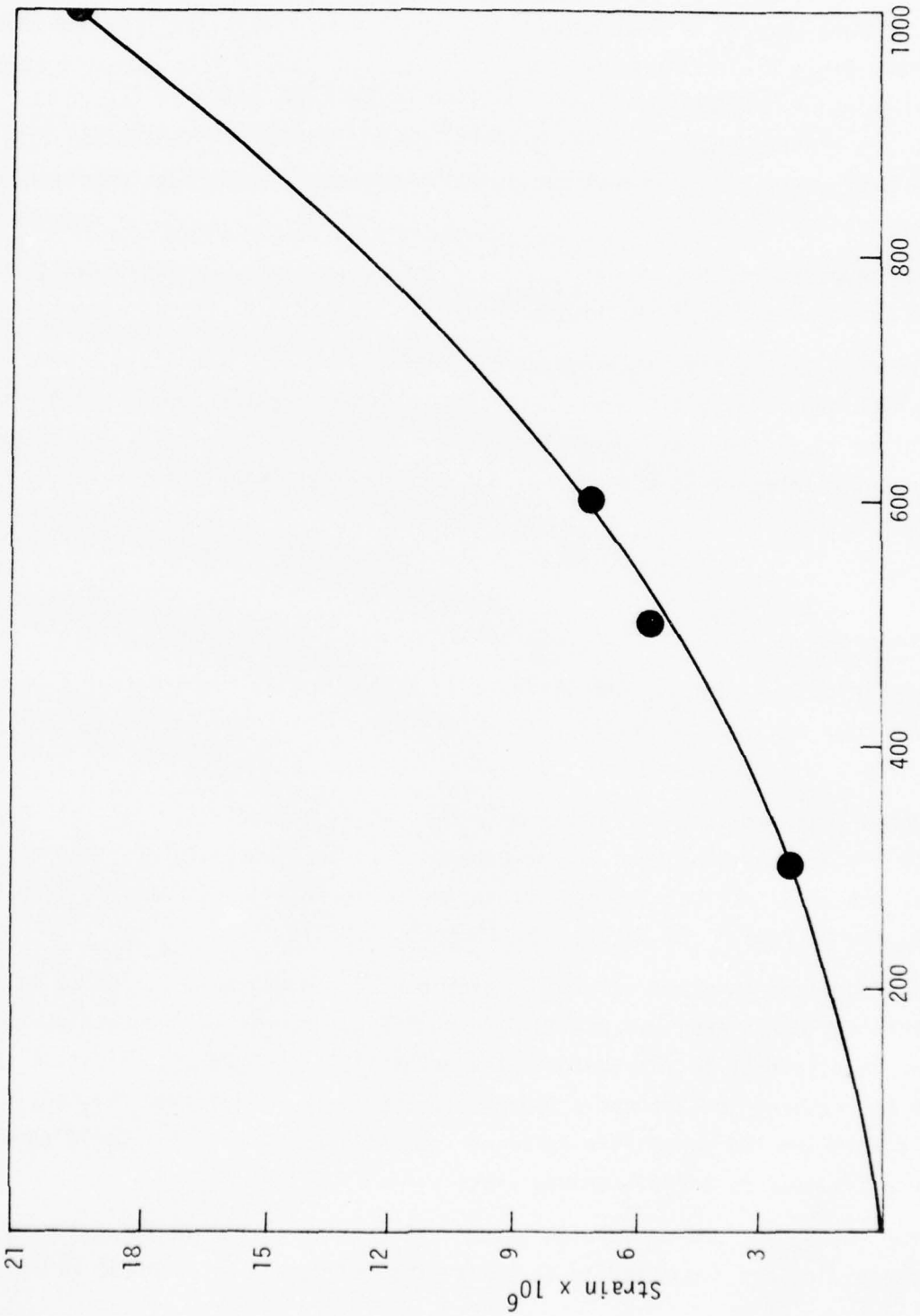

Fig. 48 Strain vs DC field in ceramic $Pb_3MgNb_2O_9$

of the Q_{ij} constants are similar to those in more normal perovskites (e.g., $BaTiO_3$), then the high induced polarizations in the Curie range must give rise to very high strain levels and these systems are obviously of considerable interest for further study.

Dense ceramic samples of lead magnesium niobate were fabricated from the mixed oxides. Weak field dielectric measurements taken using the HP 427A automatic bridge and a model Delta Design 2300 environment control chamber are shown in Figure 47. These data are closely similar to the original data published by Smolenskii (23), though the peak permittivity values are slightly higher probably due to better ceramic preparation.

At room temperature, the ceramic is above the Curie range, so that static dilatation measurements under DC fields should be dominated by the paraelectric phase.

Measurements of the electrostrictive constant Q_{12} at room temperature were made using the high sensitivity dilatometer described in our earlier report. These data are summarized in Figure 48. Over the whole range of applied fields the quadratic electrostrictive behavior is clearly evident and the measurement yield a value

$$Q_{12} = 1.3 \times 10^{-2} \quad \text{MKS}$$

of the same order as the Q constants for other simple perovskites.

Clearly in pure $Pb_3MgNb_2O_9$ the Curie range is too low in temperature to enable a practical room temperature device which could utilize a large fraction of the poling strain.

In present studies pure $Pb_3MgNb_2O_9$ will be used as a model material and our dilatometer is now being adapted for measurements at low temperatures. For practical systems we are also fabricating ceramics in the solid solution systems $Pb_3MgNb_2O_9$: $Pb_3ZnNb_2O_9$ and $Pb_3MgNb_2O_9$:$Pb_2(MgW)O_6$ and $Pb_3MgNb_2O_9$:PbTiO.

The Mg:Zn system is known to give relaxor behavior over the whole solid solution range within the Curie range up to 140°C in pure $Pb_3ZnNb_2O_9$. Unfortunately, the Zn end member is difficult to fabricate in the perovskite form and high pressure synthesis is required to suppress a pyrochlore structure derivative. $Pb_3MgNb_2O_9$, however, stabilizes the perovskite form and compositions with useful Curie range should be accessible by normal ceramic processing.

For the $Pb_2(MgW)O_6$ end member, an ordered perovskite structure has been reported and the properties are suggested to be antiferroelectric . The interest in

this system is to explore the dielectric and elastoelectric changes associated with the transition from a disordered (inhomogeneous) cation distribution to an ordered (homogeneous) phase.

Samples necessary for these studies are now being processed.

4.3.2. Defect Dipole Systems

Studies of the static electrostrictive effects in doped alkali halides (28,29) show a very large contribution to the electrostrictive response from the reorientation of polar defect centers. In these low temperature elastoelectric studies, it was postulated that the high local stress fields associated with the defect became oriented by the poling process leading to a large 'defect dipole' contribution to the measured electrostriction.

In alkali halides the dielectric polarizability is very low ($E_R \sim 10$), so that even though the measured electrostriction coefficients Q_{ij} are orders of magnitude larger than the corresponding coefficients in the perovskites, the total induced strains are still small.

To exploit this 'defect dipole' concept in any practical manner, clearly one should seek an 'orientable' defect system which occurs in a base lattice of much higher intrinsic polarizability. Skanavi et al. (30,31) have demonstrated the occurrence of a dipolar contribution to the dielectric response in $Bi^{3+}:SrTiO_3$ ceramics, which provides a very significant enhancement of the low frequency weak field permittivity. More recent work in this laboratory has confirmed the dipolar nature of the response in $(Bi_{2/3} \times Ti_{1-x})SrO_3$ solid solutions, and a similar even larger effect in $(La_{2/3} \times Sr_{1-x})TiO_3$ and in a number of rare earth $SrTiO_3$ ceramics.

We are presently fabricating samples of a number of the doped strontium titanate samples which will be used to examine the possibility of enhancing the basic electrostrictive response by the defect dipole mechanism.

5. POLING AND PROPERTY STUDIES

Work in this area over the first months of this contract period has been limited due to the need to focus effort onto the preparation and fabrication studies associated with developing the suites of samples required in each of the three major areas previously described.

For the initial poling studies under high hydrostatic pressure, a small externally heated pressure cell has been developed. This has been designed to accept samples up to one diameter, and is a liquid type pressure cell capable of maximum pressures over 7 Kbar at a safe operating temperature of 200°C. The cell is equipped with a compressed air intensifier and simple manual control system. Feed throughs are provided for electrical leads which can be used up to 1 Kvolt, and for an internal thermocouple for temperature measurement. This equipment has been assembled and tested over the whole temperature and pressure range, and work will now proceed with the poling studies.

To complement the high sensitivity dilatometer a new capacitance dilatometer has been built up, to cover the very low strain ranges projected for our studies on dimensional aging in poled piezoelectrics. The sensitive system components have all been constructed from super invar and the system is mounted on an air mounting table for vibration isolation in a thermostatically isolated room.

Preliminary studies have shown that the system can discriminate dimension changes of less than 10 Å in a sample 1 cm long. Though the system is assembled in a low pressure glove box in dry nitrogen, the major limitation upon the measured stability appears to come from pressure and humidity changes and it is now planned to put the whole system into a vacuum enclosure.

We are using the present equipment to complete the low strain data for electrostriction transducers at low field levels, and even in present form it will be most valuable for the initial characterization of the defect dipole electrostrictors. More complete details of these studies will be given in the Annual Report in December 1977.

6. BASIC PHENOMENOLOGY FOR PZT PEROVSKITES

Two topics have been the major subjects of study over the past six months

(1) The completion of the three-dimensional analysis for the polarization surfaces in a perovskite.

(2) Development of the graphics system to enable the automatic plotting of the ferroelectric phase diagram for any two component perovskite solid solution system.

Topic one above is now essentially completed. The programming has been completed to allow the three-dimensional presentation of the polarization surfaces for any proper perovskite ferroelectric for which the Elastic Gibbs Free Energy may be expressed as a power series in the polarization and allows for the inclusion of all symmetry allowed terms up to and including all allowed sixth power terms in P, i.e., if

$$\Delta G_1 = A(P_1^2 + P_2^2 + P_3^2) + B(P_1^4 + P_2^4 + P_3^4) + C(P_1^2P_2^2 + P_2^2P_3^2 + P_3^2P_1^2)$$

$$+ D(P_1^6 + P_2^6 + P_3^6) + E(P_1^2(P_2^4 + P_3^4) + P_2^2(P_1^4 + P_3^4) + P_3^2(P_1^4 + P_2^4))$$

$$+ F\, P_1^2P_2^2P_3^2$$

If the magnitudes of the A,B,C,D,E,F coefficients and their temperature dependence is known for the system of interest, the P may be plotted at any chosen values of ΔG, for temperatures anywhere within the known temperature field.

The usefulness of the chosen format has been demonstrated by modeling the cubic:tetragonal, the tetragonal:orthorhombic and the orthorhombic:rhombohedral phase transitions in $BaTiO_3$. Parameters were chosen to model the ΔG function for $BaTiO_3$, placing the phase changes at 120, 0 and -90°C respectively. The simple function was solved to give the ΔG, values at the transition points, and the polarization surfaces drawn for a small range of ΔG about the transition value, and for temperatures just above and just below the spontaneous transition temperatures.

Figure 49 reproduces several of the polarization surfaces of interest. Since the surfaces are quantitatively correct (for the chosen ΔG parameters) behavior in the immediate vicinity of the transitions can be correctly modeled.

The focus of the second task was to develop first the parameters in the ΔG function which would enable the description of a morphotropic phase boundary between tetragonal and rhombohedral phases of the type known to occur in the PZT family of compositions and this was described in the previous report. Working from this basis, the task was then to chose the mode in which the parameters in ΔG must change so as to model the known phase diagram for PZTs. For this purpose, the original program which placed the ΔG parameters under dial control through the analog feature of the Adage graphics system was modified so that under machine control, the parameters could be incremented over a prescribed range. In split screen mode the Adage has been arranged to plot for each set of ΔG parameters the full family of ΔG vs. T curves for all possible phases. To select the crossing points between the curves representing the lowest energy states (stable phases) and to plot corresponding points on a T vs composition diagram. Thus commencing with the values of ΔG corresponding to one end member phase the program builds up the full phase diagram up to the second end member phase plotting and labeling the stable phases and allowing direct inspection of the ΔG_1 vs. T diagram at each incremental composition.

Fixing the temperature and composition dependence of the A parameter from the known dielectric response in the cubic paraelectric phase, and from the known temperature dependence of the cubic ferroelectric phase change, experience has shown that only a very limited family of higher order parameters will effectively model the morphotropic tetragonal:rhombohedral phase. The best fitting so far obtained is shown in Figure 50.

Using the model parameters chosen in this study, the full family of polarization: temperature and permittivity:temperature curves is being developed for incremental compositions across the phase diagram. If the assumption is made that the spontaneous strain in the ferroelectric phases is electrostrictive in origin, which is most reasonable for a simple proper ferroelectric, the calculated P vs. T curves can be compared to the experimentally determined P vs. T curves to justify the machine calculations.

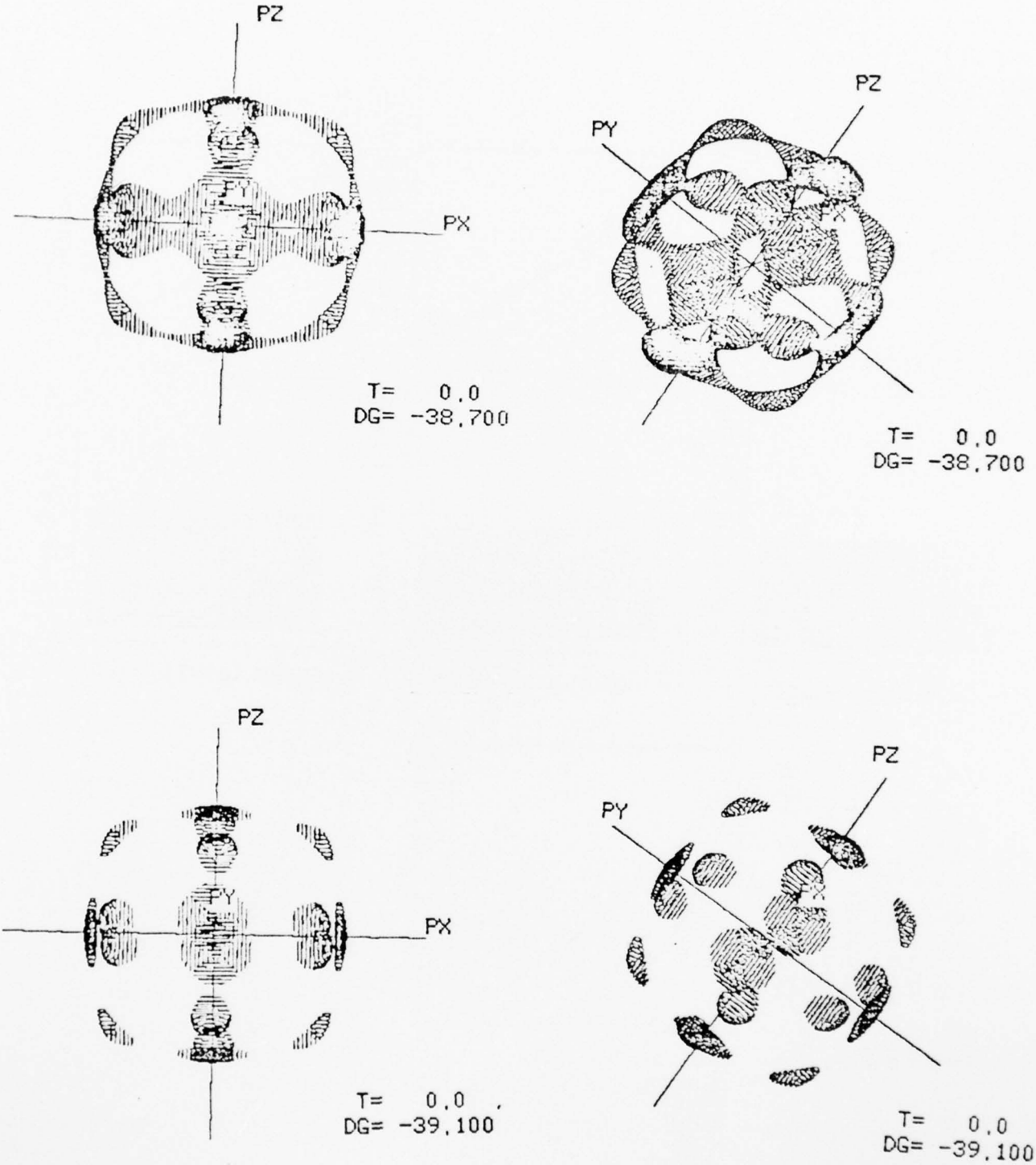

Fig. 49 Polarization Surfaces in $BaTiO_3$ Near the 0^oC Transition

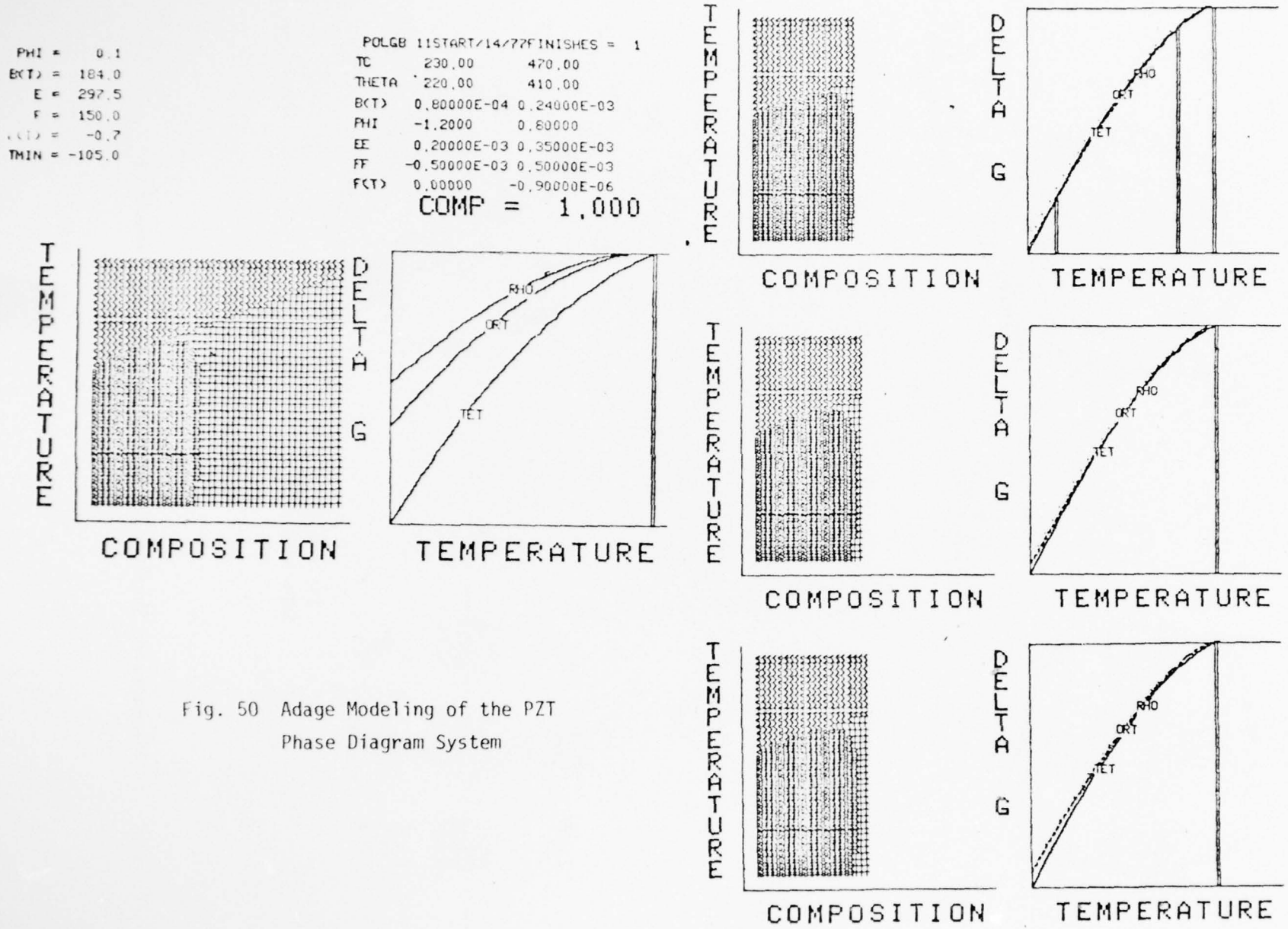

Fig. 50 Adage Modeling of the PZT Phase Diagram System

When the family of ΔG parameters has been checked in this manner, the intrinsic single domain dielectric, piezoelectric and elastic properties will be accessible for the unperturbed state. It is also then a relatively straight forward step to calculate the perturbation to the intrinsic properties from changes in the elastic or electric boundary conditions, such as those which will occur from the mutual contstraints between grains in the polycrystalline ceramic.

7. FUNDAMENTAL STUDIES OF AMORPHOUS AND MICROCRYSTALLINE HIGH T_c FERROELECTRICS.

These studies have been concentrated upon the development of amorphous films of the distorted pyrochlore ferroelectric $Si_2Nb_2O_7$. Sputtering pyrochlore ferroelectric $Si_2Nb_2O_7$. Sputtering was chosen as the method of preparation and an extensive exploratory study has been carried through to establish the conditions required to sputter uniform pinhole free films.

This work was carried out on an MRC Model 8502 commercial sputtering unit using argon, argon:oxygen mixtures and pure oxygen as the gas phase. The system can be diffusion pumped to a pressure of less than 10^{-7} torr before back filling with the carrier gas. So far about 100 sputtering runs have been carried through.

A number of different substrates were used including glass (microscope cover glasses), pure fused silica, Al_2O_3 (99.5% pure), ultra high purity alumina and ALSIMAG 614. To provide a base contact for electrical measurements, Al, Cu, Pd and Pt films were evaporated or sputtered onto the substrate before a number of the sputtering runs.

Before each experiment the substrates were cleaned with liquid Nox, acetone and alcohol.

The initial sputtering runs to establish deposition conditions were carried through using a target prepared from sintered stoichiometric mixed oxides of reagent grade purity.

In the Model 8502, the target substrate spacing is of order 3 cm and the RF frequency is 13.5 MHz. Some typical conditions and deposition rates onto fused silica are given in table 10.

Table 10. Deposition Conditions

		Watts			A^o/min		
Runs	Gas	R	F	Power P_w	Deposition Rate		
4	O_2	25	50	100	150	200	300
3	Ar	25	50	100	200	370	500
3	O_2:Ar	25	50	100	200	350	800

Excellent films, firmly adhering to the substrate could be sputtered onto all the oxides and onto aluminum, attempts to sputter onto Cu, Pd, Pr were unsuccessful apparently due to reaction or high surface strain breaking up the film into isolated islands upon formation.

Preliminary measurements of the capacitance using aluminum counter electrodes showed exerting properties, but these were traced back to a thin highly resistive Al_2O_3 film at the electrode interface.

A study of the oxide stoichiometry was made using the JSMSOA JOEL scanning electron microscope with energy dispersive secondary x-ray analysis. Probe data were corrected for backscatter, ionization, penetration, absorption and fluorescence using the MAGIC (microprobe analysis general intensity correction) program from J.W. Colby at Bell Telephone Laboratories, utilizing $LiNbO_3$ and $SrTiO_3$.

For the stoichiometric target, films sputtered in oxygen were found to be slightly niobium rich.

Using a compound target the correct target composition was found to be between stoichiometric and $2(SrO)_{1.05}(Nb_2O_5)$, and new targets in this stoichiometry region are being made up.

In one thick sputtered sample (1-week sputtering time) several large pieces of film about mm dimensions ~10 um thick were found to have parted from the substrate. Dielectric permittivity was increased using evaporated Pd electrodes and Delta Design environment control sample enclosure. Permittivity and tan δ measured at 1kHz, 10 kHz, 100 kHz and 1 MHz over the temperature range -60°C to +300°C are shown in Fig. 51 and Fig. 52.

The initial heating curves show some structure, but after this annealing, the data became reproducible. The dispersive high near 300°C is associated with a rapid rise in tan δ and may be associated with water condensation around the lead structure in the cooling chamber.

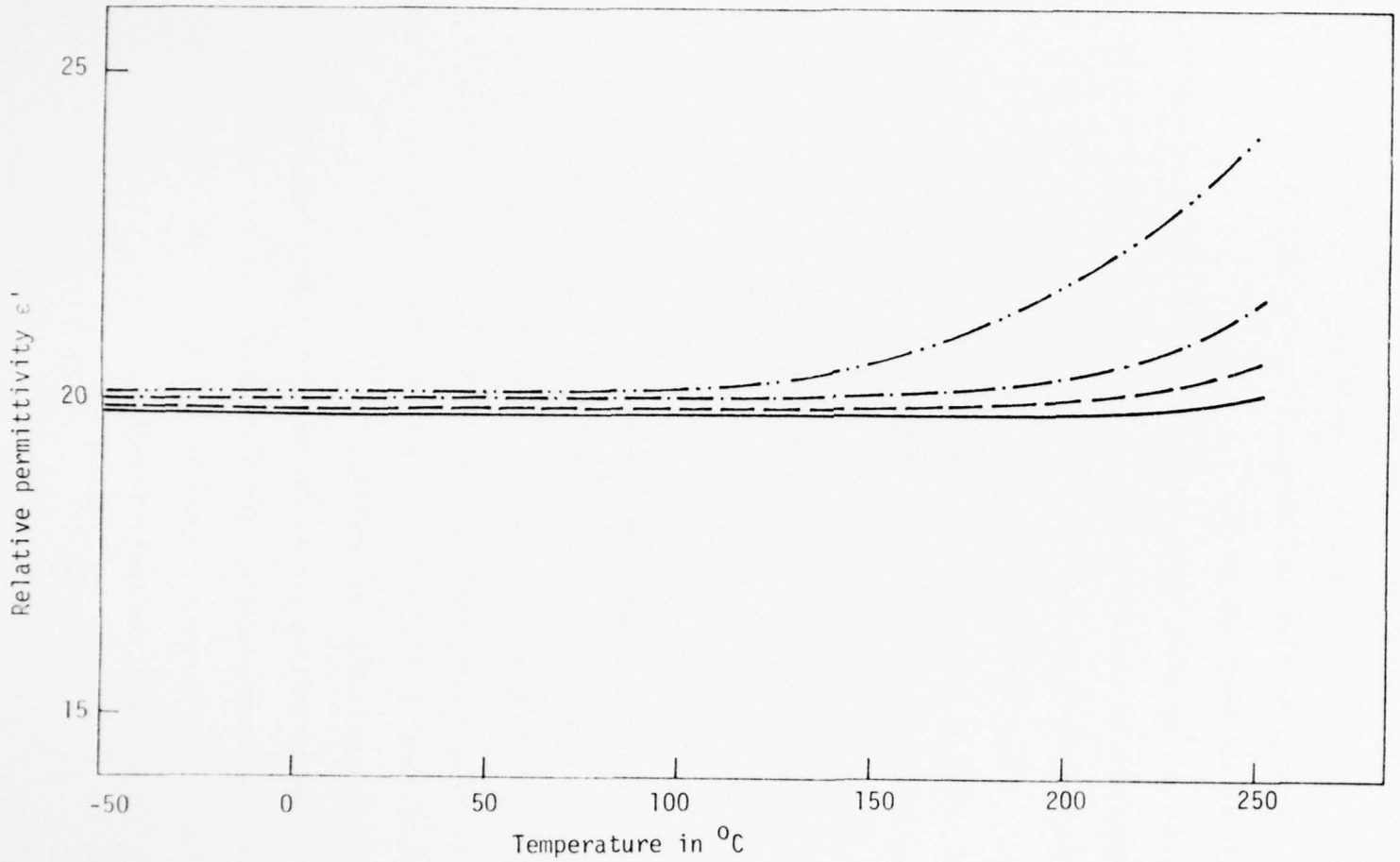

Figure 51. Dielectric permittivity as a function of temperature and frequency in amorphous $Sr_2Nb_2O_7$

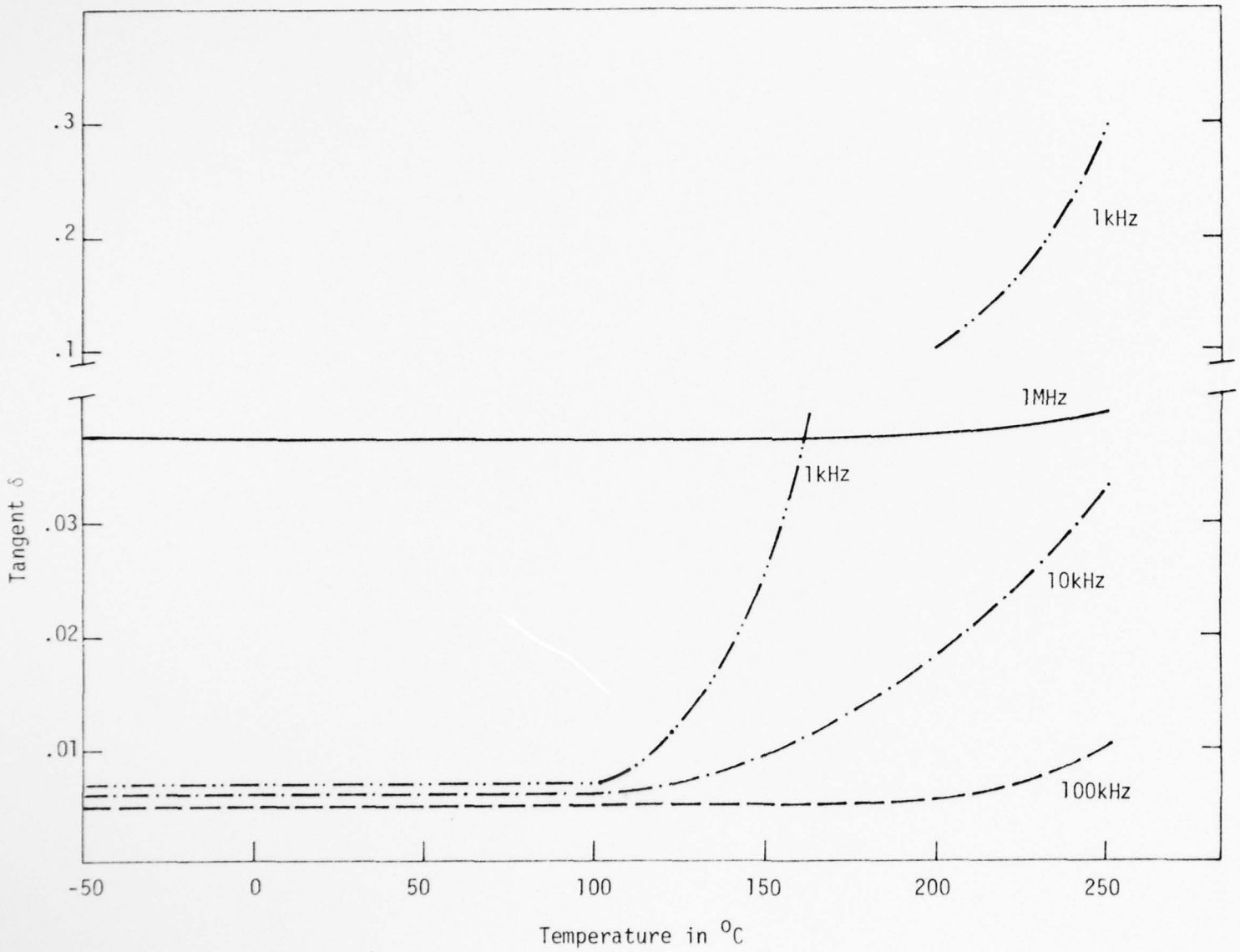

Fig. 49. Dielectric loss tangent δ as a function of temperature and frequency in amorphous $Sr_2Nb_2O_7$

Preliminary annealing studies suggest that the $Sr_2Nb_2O_7$ glass (even slightly off stoichiometry) is highly stable. Films annealed at 1000^oC for many hours exhibit no x-ray pattern. Studies to higher temperatures are now progressing.

References

1. T. Yamaguchi, S.H. Cho, M. Hankomori and H. Kuno, Effects of Raw Materials and Mixing Methods on the Solid State Reactions Involved in Fabrication of Electronic Ceramics. Ceramurgia Internationa, vol. 2(2), pp. 78-80 (1976).
2. D.A. Buckner and P.D. Wilcox, Effect of Calcining on Sintering of Lead Zirconate-Titanate Ceramics. The Amer. Cer. Soc. Bull. vol. 51(3), pp. 218-222 (1977).
3. Y. Matsuo and H. Sasaki, Formation of Lead Zirconate-Lead Titanate Solid Solutions. J. Amer. Cer. Soc. vol 48(6), pp. 289-291 (1965).
4. Personal communication, J.A. Kyonka, Honeywell, Inc., Minneapolis MN.
5. Personal communication, P.O. Wilcox, Sandia Laboratories, Albuquerque NM.
6. J.H. Rosolowsky, R.H. Arendt and J.W. Szymanszek. Lead Zirconate Titanate Ceramics. Annual Report, June 1977, G.E. Schenectady NY.
7. Stoichio Fushimi, Takuro Ikeda, Phase Equilibrium in the System PbO-TiO_2-ZrO_3. J. Am. Ceram. Soc. 50(3), pp. 129-132 (1967).
8. A.E. Robinson, T.A. Joyce, Preparation of Lead Zirconate-Titanate Composition. I. Determination of Unreacted Constituents. Trans. Brit. Cer. Soc. 61(2), pp. 85-93 (1962).
9. R.A. Gardner and R.W. Nuter, Properties of Multilayer Ceramic Green Sheets. Solid State Technol. 17(5), pp. 38-43 (1974).
10. R. Capek, Multilayer-Multicompositon Ceramic Capacitors for Hybrid Microcircuits. International Hybrid Microelectronics Symposium, pp. 87-97 (1969).
11. M. Bennett, W.E. Boyd and J.C. Noble, Fabrication of Multilevel Ceramic Microelectric Structures, U.S. Pat. 3,518,756.
12. J. Etloc and G.R. Costley, Pressure-Fusible Tapes for Multilayer Structures. Amer. Cer. Soc. Bull. 51(5), pp. 482-485 (1972).

13. B. Schwartz and D.L. Wilcox, Laminated Ceramics. Ceram. Age 83, pp. 40-55 (1967).

14. D.A. Chance and D.L. Wilcox, Metal-Ceramic Constraints for Multilayer Electronic Packages. IEEE 59(10) (1971).

15. R.B. Runk and M.J. Andrejco, A Precision Tape Casting Machine for Fabricating Thin, Organically Suspended Ceramic Tapes. Amer. Cer. Soc. Bull. 54(2) (1975).

16. R. Cypres, R. Wollast and J. Raucq, Ber. dt. keran. Ges. 40, pp. 527-532 (1963).

17. S.K. Bhattacharya and S. Kameswari, J. Chim. Phys. 56, pp. 823-829 (1959).

18. V.M. McNamara, A Wet Chemical Method for the Preparation of Oxide Mixtures Applicable to Electronic Ceramics. J. Can. Cer. Soc. vol. 33, pp. 102-119 (1964).

19. L.M. Brown and K.S. Macdigasni, Cold-Pressing and Low-Temperature Sintering of Alkoxy Derived PLZT. J. Am. Cer. Soc. 55(11), pp. 541-544 (1972).

20. G.H. Haertling and C.E. Land, Recent Improvements in the Optical and Electro-optical Properties of PLZT Ceramics. Ferroelectrics, vol. 3, pp. 269-280 (1972).

21. P.E. Price, R. Widmer and J.C. Runkle. Proc. 1976 Int. Pow. Met. Conf.

22. K.H. Hardtl, J. Am. Cer. Soc. 54(2), pp. 201-207 (1975).

23. G.A. Smolenskii, V.A. Isopov, Al. Agranovskaya, S.N. Popou, Soviet Phys.-Solid State 2, 2584 (1961).

24. V.A. Bokov, I.E. Mylnikova, Sov. Phys.-Solid State 3, 613 (1961).

25. G.A. Smolenskii, Suppl. J. Phys. Soc. Japan 28, 26 (1969).

26. R. Blinc, S. Detroni, I. Levstek, M. Pitas, S. Probesaj, M. Schara, J. Phys. Chem. Solids 20, 187 (1961).

27. J.W. Smith, Ph.D. Thesis, The Pennsylvania State University (July 1967).

AD-A046 010 PENNSYLVANIA STATE UNIV UNIVERSITY PARK MATERIALS RE--ETC F/G 9/1
CERAMIC PIEZOELECTRIC TRANSDUCERS.(U)
JUL 77 L E CROSS, J V BIGGERS, R E NEWNHAM N00014-76-C-0515

UNCLASSIFIED NL

2 OF 2
ADA
046010

END
DATE
FILMED
12-77
DDC

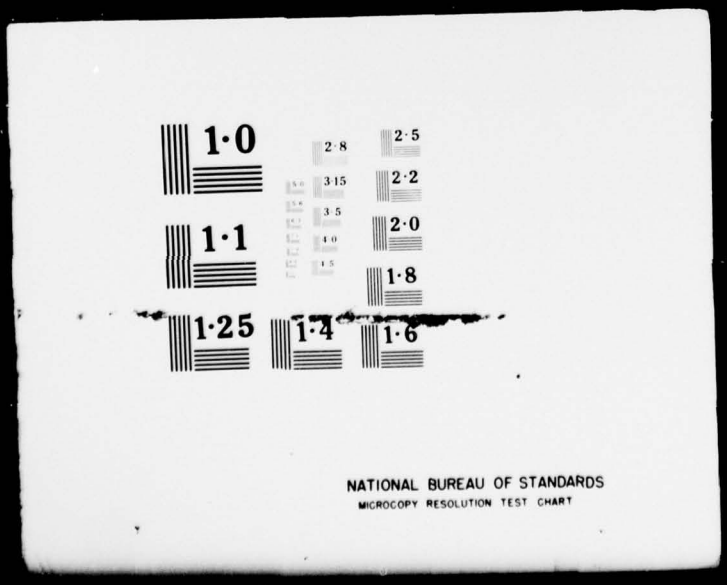

28. H. Burkhard, W. Kanzig, Appl. Phys. Letters 27, 423 (1975).

29. H. Burkhard, W. Kanzig, M. Rossinelli, Helv. Phys. Acta 49, 13 (1976).

30. G.I. Skanovi, E.N. Matveeva, Soviet Physics JETP 3, 195 (1957).

31. G.I. Skanavi, I.M. Ksendzov, V.I. Irigubenko, V.G. Prakhvatilov, Soviet Phys. JETP 6, 250 (1958).